P O L I T E C H N I K A G D A Ń S K A

Wydział Chemiczny

Katedra Chemii Nieorganicznej

Rozprawa doktorska

SILANETHIOLATES OF IRON

LUIS APARICI PLAZA

Promotor:

Prof. dr hab. inż. Barbara Becker, prof. nadzw. PG

Gdańsk 2009

La fragua de Vulcano by Diego Velázquez. Museo del Prado, Madrid.

"The best scientist is open to experience and begins with romance - the idea that anything is possible."

Ray Bradbury

Abbreviations and codes

MeOH – methanol
MeCN – acetonitrile
py – pyridine
pip – piperidine
morph – morpholine
pic – picoline (methylpyridine)
lut – lutidine (dimethylpyridine)
dmeda – dimethylethylenediamine
tmeda – Tetramethylethylenediamine
phen – 1,10-phenanthroline
N-meimid – N-methylimidazole
^{t}Bu – *tert*-butyl group
Ph – phenyl group
Me – methyl group
Et – ethyl group
Bmt – 4-*tert*-butyl-2,6-bis[(2,2”,6,6”-tetramethyl-*m*-terphenyl-2’-yl)methyl]phenyl
benz – benzoate
tcnq – 7,7',8,8' -tetracyano-*p*-quinodimethane
pmedta – *N*,*N*,*N*’,*N*’,*N*”-pentamethyldiethylenetriamine
Me_3tacn – 1,4,7-trimethyl-1,4,7-triazacyclononane
L^{tBu} – β-diketiminate

[I] – $[Fe\{SSi(O^{t}Bu)_3\}_2(MeOH)_4]$
[II] – $[Fe_4S_4\{SSi(O^{t}Bu)_3\}_4](Et_3NH)_2$
[III] – $[Fe\{SSi(O^{t}Bu)_3\}_2(py)_2]$
[IV] – $[Fe\{SSi(O^{t}Bu)_3\}_2(pip)_2]$
[V] – $[Fe\{SSi(O^{t}Bu)_3\}_2(morph)_2]$
[VI] – $[Fe\{SSi(O^{t}Bu)_3\}_2(\alpha\text{-pic})(MeOH)_2]$
[VII] – $[Fe\{SSi(O^{t}Bu)_3\}_2(\beta\text{-pic})]$
[VIII] – $[Fe\{SSi(O^{t}Bu)_3\}_2(\gamma\text{-pic})]$
[IX] – $[Fe\{SSi(O^{t}Bu)_3\}_2(3,5\text{-lut})]$
[X] – $[Fe\{SSi(O^{t}Bu)_3\}_2(tmeda)]$
[XI] – $[Fe(N\text{-meimid})_6]Cl_2.2H_2O$
[XII] – $[Fe(phen)_3]Cl_2.6MeOH$

Color code:

Fe		**H**		**I**	
S		**N**		**P**	
Si		**O**		**Ni**	
C		**Cl**		**Mo**	

INDEX

1 INTRODUCTION

Iron is one of the most abundant metals in nature and, therefore, also one of the most common elements. It is not a surprise then that humans have taken advantage of this availability and found several heterogeneous uses for this metal in its different oxidation states.

Human civilization has grown on par of our knowledge of iron and the development of the technologies that have allowed us to make use of this metal. Indeed, the relationship is so close, that it is easy to determine the exact moment in history when a radical discovery or development in iron technology took place since it generally led to similarly radical changes in a society or culture (often the discovery being adopted very fast and over a wide area). A few well-known examples are shown following.

Fig. 1. Hittite relief depicting a couple of Hittite warriors in battle. Museum of Ankara, Turkey.

The oldest archaeological findings of man-made iron objects date from 4000 BC in Egypt and Sumer. These remains consist of small objects such as pendants and tips of arrows and spears

obtained from the rudimentary crafting of metallic iron of – most probably – meteoritic origin.

The first examples of iron smelting appear in 3000 BC, when the Hittites in Asia Minor learned to heat ores with coal or charcoal to produce metallic iron[1,2]. This technique, although primitive, gave the Hittites a technological advantage over their rivals, which did not rely on such a sturdy metal to fabricate their weapons. Obviously, the Hittites kept their method a secret to retain their supremacy on the area, but after their demise in 1200 BC, the technique was finally revealed and spread fast all through Eurasia, giving start to the Iron Age.

In times of the Roman Empire, the province of Hispania[3] (currently, Spain) was known for its important iron manufacture. This industry produced weapons and armory for the Roman legions and contributed to the supremacy of the Empire for several years.

Fig. 2. The god Mars, by Diego Velázquez.

During the Middle Ages, the alchemists identified iron with Mars and correspondingly gave the element his symbol: the shield and spear of the god of war[4] (♂).This belligerent correspondence was not casual. On the one side, metallic iron oxidizes under aerobic conditions to red iron(III) oxides, which remind of the color of blood (caused by the heme group in the iron-containing hemoglobin) and the color of the planet Mars (also motivated by iron(III) minerals). On the other side, the possibility of making harder and sturdier weapons with this metal was clearly related with the god of war.

In the XIV century, the first blast furnaces appeared in Europe and the production of steel started[4,5]. It increased the demand of charcoal up to a point where most woods in Europe were severely damaged and the iron industry started to decline. In response to Europe's deforestation, A. Darby developed a method to use coke as a fuel at the beginning of the XVIII century. As a result, the production of steel increased[4,6].

More than a century after Darby's contribution, the next revolution in the iron/steel industry occurred. In the middle of the XIX century, the mass production of steel was considerably improved with the development of new methods such as the Bessemer converter or the Martin-Siemens open hearth furnace that allowed producing much cheaper steel and at the same time improved its quality, minimizing its impurities[7-9]. The new processes allowed steel to be readily available, so soon the railroads extended and several new buildings were

Fig.3. The Golden Gate Bridge. San Francisco, CA, USA

planned with steel as a structural material. Amongst these, some of the most impressive examples of the architecture of the XIX and XX centuries: the Eiffel Tower, the Statue of Liberty, the Golden Gate Bridge or the Empire State Building.

In the meantime, another decisive technology was being developed. At the beginning of the 20th century, the German scientist Fritz Haber developed a process to fix atmospheric nitrogen at high pressure and temperature with the use of an iron catalyst[10,11]. Shortly after, Carl Bosch[12] started to commercialize the idea which, consequently, boosted the efficiency of the production of fertilizers and explosives. Nowadays, it is estimated that 1-3% of the world energy is destined to the production of ammonia and about one third of the world population is sustained by the fertilizers derived from it[13].

Higher oxidation states of iron, the most common Fe(II) and Fe(III), have also found their niche and applications, specially within the pigment and ink industry. Iron oxides provide a wide range of colors[14] from yellow (α-FeOOH) to red (α-Fe_2O_3) and black (Fe_3O_4). These oxides are very stable and last long: they are known since ancient times, as the prehistoric cave paintings testify; and they can be used even at high temperatures, for instance to decorate ceramic materials. In some cases, the iron oxide is preferred to other metal oxides that give a more intense color, but present a higher toxicity (for example, Cd or Pb oxides used in glass and ceramic industries are nowadays substituted total or partially by iron oxides). Another kind of pigments, iron hexacyanates[15] (Prussian blue) can be often found in printer's inks or in automobile paints. $FeSO_4$, $FeCO_3$ and FeS are also demanded by the industry.

Fig.4. A ferritic audio tape.

Besides paints and colors, iron compounds have found diverse applications according to their chemical and physical properties. Iron oxides are used as prime matters for the production of iron. Owing to their hardness, calcined Fe_2O_3 has been used as a polishing material for glass or metals[16]. Magnetite (Fe_3O_4) makes a good material for manufacturing electrodes due to its resistance to acids, bases and chlorine. Due to their ferrimagnetic properties, the industrial processing[14] of magnetite and γ-Fe_2O_3 for their use in analogical audio and video tapes bloomed during the last three decades of the 20th century, until the digital revolution started in the 90s ren-

dered these technologies obsolete. More recently, there has been a certain interest in the field of nanotechnology for iron compounds with interesting results such as the synthesis of single crystalline magnetite nanotubes[17] or iron oxide nanoparticles[18] with magnetic activity.

Ferrimagnetism is one of the most characteristic properties of certain phases of iron oxides. Spinel ferrites[19,20] and hexagonal ferrites[21] account for some of the most economically viable sources of magnets[22] and are extensively used in electronics and electric equipment[23] (for example, in dynamos, DC motors, transformers, but also in radios, telephones, computers...).

Iron sulfides, present in nature as pyrite minerals, have also found their technological applications. Both FeS and FeS_2 can be used to produce highly efficient Li and Li-Al batteries[24]. The disulfide has also been postulated as an alternative solar cell material, although so far the results have not met the expectative[25].

From the biological point of view, the influence of iron compounds in living organisms is unquestionable. Two big groups of iron metalloproteins can be distinguished: hemoproteins and non-heme iron proteins.

Hemoproteins are composed of a porphine macrocyclic ring which is attached to an iron mononuclear center. Generally, they are bound to the rest of the protein through one of the nitrogen atoms of a histidine residue (*e.g.* hemoglobin, myoglobin). This kind of metalloproteins is found in most aerobic organisms accomplishing functions of oxygen transport and storage[26].

Amongst the non-heme iron proteins, Fe-S proteins account for the most numerous subset of proteins. They are very versatile from the biological point of view and are able to accomplish structural, electron storage and catalytic functions. Essential enzymes such as nitrogenase, hydrogenase and many others could not fulfill their roles were it not for the presence of some Fe-S centers. Likewise, some fundamental steps in the most basic mitochondrial respiration chain require of Fe-S proteins for the storage and delivery of electrons[27].

Traditionally, iron thiolates have been used in order to model these important biological centers. The electronic properties of thiolates as well as their stability can be fine-tuned by changing their substituents. This feature has been exploited to produce a wide range of compounds; from relatively simple alkyl or aryl thiolates to more complicated chelating or macrocyclic multidentate polythiolates[28].

Silanethiolates are homologue compounds to organic thiolates which have been studied for more than twenty years[29-31]. The presence of the Si-S bond significantly alters their elec-

tronic structure with respect to that of thiolates and makes them more vulnerable towards hydrolysis and temperature[32]. Some metal silanethiolates[33-43] have been thoroughly investigated but so far little attention has been paid to iron[44-51]. A quick preliminary search on the Cambridge CCDC database revealed that so far, only 9 silanethiolates of iron had been structurally characterized.

When I was first offered the possibility of choosing iron as the metal to base my PhD research on, I did not hesitate much. Actually, my first reaction was of perplexity, since I supposed that such an important metal as iron, with so many technological applications and such an influence in biology would have already been thoroughly studied. I was wrong.

Obviously, I accepted. The proposal was too interesting to be dismissed and quickly several questions arose: do iron silanethiolates behave much like organic thiolates or does the presence of silicon radically alter their chemistry? Will they provide new routes to model iron-sulfur clusters of biological significance or will they be a source of materials with technological applications? Why are there just a few examples of these compounds? Are they difficult to synthesize or are they too unstable? How are they related to other metal silanethiolates? The present text is the result of my investigations concerning iron silanethiolates and an attempt to answer these questions.

2 A REVIEW OF THE LITERATURE

2.1. IRON

2.1.1. Iron in nature

Iron is one of the final elements produced by stellar nucleosynthesis together with nickel. It is a relatively common element in the universe, with a cosmic abundance on pair with that of silicon. On Earth, iron is the most abundant element on the planet if we consider it as a whole, comprising 36.9 % wt. However, most of it is located in the core, where it accounts for about 86% wt of it and can be found in a molten liquid metal state – other main components of the core are Ni (7%), S (6%) and Co (1%). In the Earth's crust, metallic iron is not so readily available, since it is mainly found forming compounds in minerals such as oxides, sulfides or carbonates. Still, it is the second most abundant metal and the fourth most abundant element (4.7% wt) in the crust[5,52,53].

During the first stages of the evolution of life on Earth, the atmosphere had a more reductive composition, lacking free oxygen gas and, therefore, most iron could be found at that time in the +2 oxidation state. Thus, soluble Fe(II) was readily available for primitive life forms to fulfill their catalytic and structural roles – which explains the ubiquity of Fe(II) in today's metalloproteins. In contrast, copper could be found then in the insoluble, reduced Cu(I) form and therefore, was not bioavailable[54,55].

Natural occurring isotopes		**Synthetic nucleides**		
Isotope	Occurrence	Isotope	Radioactivity	$\tau_{1/2}$
$^{54}_{26}Fe$	5.8%	$^{52}_{26}Fe$	β^+ emitter	8.2 h
$^{56}_{26}Fe$	91.7%	$^{55}_{26}Fe$	e^- capturer	2.6 y
$^{57}_{26}Fe$	2.2%	$^{59}_{26}Fe$	β^- emitter	45.1 d
$^{58}_{26}Fe$	0.3%			

Table 1. Natural and synthetic isotopes of Fe. Occurrence and type of radioactivity

Fig. 5. Precambrian banded formations of iron oxides.

About 3000 million years ago cyanobacteria started to proliferate, delivering O_2 as one of the byproducts of their metabolism. Soon (in less than 500 million years, which is relatively fast – at least, from the point of view of geology), this oxygen oxidized the Fe(II) dissolved in the oceans to the insoluble Fe(III), as the layers of iron oxides present in Precambrian geologic deposits testify. At the same time, Cu(I) oxidized likewise to Cu(II), which is soluble and has been available since for organisms to form metalloproteins. Once the iron in the oceans had precipitated, molecular oxygen started to be released to the atmosphere about 2700 million years ago[53,55-57].

In nature, weathered rocks – exposed to the atmosphere for a long time – contain almost exclusively iron(III) compounds. Hematite (Fe_2O_3), goethite (FeO(OH)) or the mixed valence magnetite ($FeO.Fe_2O_3$) account for some of these minerals. Pure iron(II) compounds can be found in magmatic rocks such as siderite ($FeCO_3$), pyrite (FeS_2) or marcasite (FeS_2). Iron in the 0 oxidation state can be found in the mineral triolite (FeS) or in meteorites. The table on the next page displays some examples of iron minerals[58].

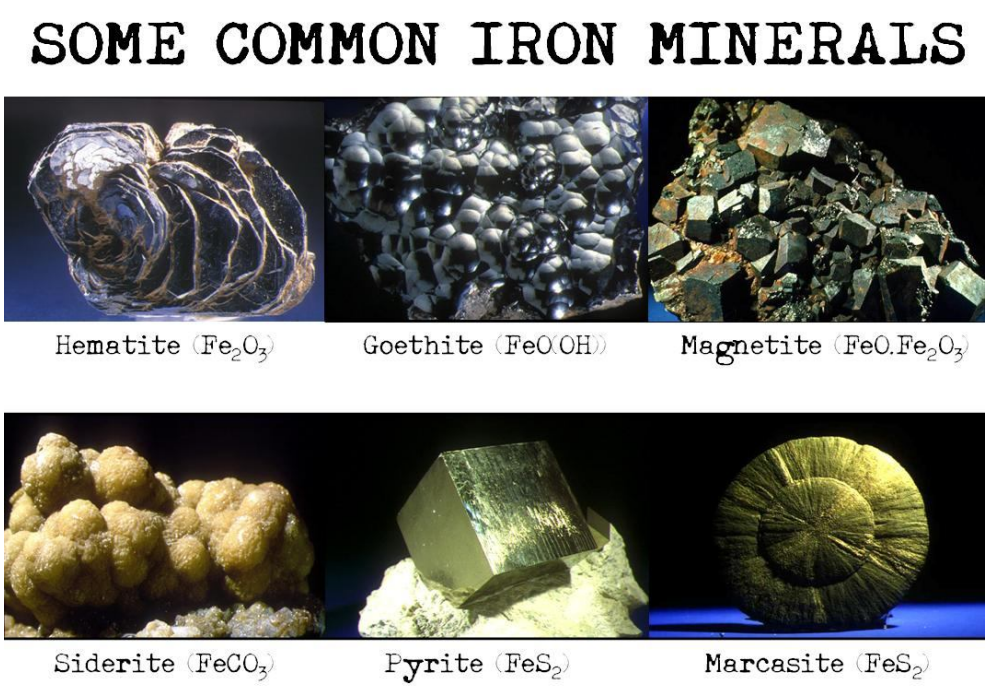

Fig 6. Photography by José Manuel Sanchís Calvete. Extracted from http://www.uned.es/cristamine/min_descr/busqueda/alf_mrc.htm. Printed with kind permission.

2.1.2. Iron – electronic structure and oxidation states

The electronic structure of a neutral Fe atom is: [Ar] $3d^6$ $4s^2$. As with other transition metals in the 4th period, iron can easily lose its two outermost shell electrons to give the Fe^{2+} cation. For iron, all the oxidation states from –2 to +6 have been reported, the most commonly found valences in nature being +2(d^6) and +3(d^5). Although theoretically its highest valence should be +8, as it has been reported for other elements of its group (Ru and Os); iron species in the VII or VIII oxidation states have never been isolated[59].

Both Fe^{2+} and Fe^{3+} are Lewis acids, although they differ in hardness. On the one hand, Fe^{3+} is classified as a hard acid due to its relative high charge and small size, which makes it difficult to polarize. As such, Fe^{3+} prefers hard bases which contain oxygen as the donor atom (*e.g.* hydroxyl, carboxyl…). On the other hand Fe^{2+} is considered a borderline acid and favors slightly softer bases[60,61] such as N- and S- donor ligands (*e.g.* histidine, protoporphyrine, cysteine…).

From the point of view of coordination chemistry, geometries attained by Fe(II) and Fe(III) complexes are similar. The most common coordination number is 6 for these cations, which accounts for octahedral geometry, but coordination numbers 5 (trigonal bipyramid) and 4 (tetrahedral) are likewise found often. Coordination number 3 is rare, but also possible for both coordination states[59].

Tetra- and pentacoordinated iron(II) complexes always present a low spin configuration (S=2). However, when dealing with octahedral geometry, we find that the metal can assume two different spin states depending on the ligands[62] attached to it (S=0 or 2). Thus, strong-field ligands (which have all their electrons paired, inducing high crystal field splitting, such as CO or CN^-) form very stable low-spin complexes, which are generally inert towards ligand exchange. On the other hand, weak field ligands (those that maximize the number of unpaired electrons and therefore induce low crystal field splitting, like F^- or OH^-) form kinetically labile high-spin complexes. Physically, this change in spin can be appreciated by the longer ionic radii[59] of the high spin Fe^{2+} cations when compared to their low spin counterparts.

For iron(III) complexes, there is also an orbital energy splitting when adopting an octahedral conformation (S=1/2 or 5/2), as well as for the pentacoordinated square pyramidal geometry (S=3/2 or 5/2). While high- and low-spin octahedral complexes are relatively easy to identify by measuring the ionic radius variation, the determination of the exact spin state in square pyramidal complexes may need more sophisticated methods, since the difference in ionic radius between the high- and low-spin is not significant in this case[62].

The more uncommon iron(IV) complexes generally adopt an octahedral geometry[62] with spin state S=1.

2.1.3. Iron metabolism

The average concentration of iron in the human body is approximately 60 mg/kg. The recommended daily intake of this metal is 5-9 mg for men and 14-28 mg for women, while a normal diet consists of 20 mg/day. Eggs, whole grains, nuts, spinach and meat, all with a medium iron content (3mg/100g) account for the main contributors of iron to our organism. In contrast, caviar, cocoa and leek are amongst the foods with highest Fe content (around 12mg/100g) while fats and milk products with their low iron content (0.3mg/100g) do not make any significant contributions to the iron intake[63].

The protein transferrin is in charge of iron transport and delivery through the organism (plasma iron). Plasma iron accounts only for less than 0.1% iron content in the human body. Most of it is concentrated in the bone marrow (75%), carrying out the synthesis of hemoglobin, and in the liver, bound to ferritin (16%). The rest of it is distributed amongst

myoglobin in the muscles (3%), cytochromes in mitochondria (0.1%), in the enzyme catalase (0.1%) and in other proteins and enzymes carrying out respiration and dioxygen transport processes[63].

In plants, Fe metalloproteins such as ferredoxins can be found[64,65], accomplishing functions of electron storage. Plant Fe metalloenzymes are mainly found carrying out functions such as photosynthesis or chlorophyll formation[63].

2.2. METALLOPROTEINS

The term metalloprotein is applied to any protein that includes a transition metal within its structure and their importance in biological chemistry stems from their ability to activate different biological reactions such as biomolecule transformation, oxidative metabolism or oxidative phosphorylation. Understanding the structures of active sites and reactive intermediates and deciphering the mechanistic details of the reactions involved is essential to the development of technologies based on their synthetic equivalents[66].

According to Frausto da Silva and Williams[67] and Ochiai[68] , the fundamental rules for the bioselection of elements are (in this order):

1) The abundance of the element in the environment
2) Its efficacy
3) Its basic fitness for a given task
4) The evolutionary pressure

Metalloproteins are often classified according to their function[62,69]:

Function	Examples
Transport of molecular oxygen	Hemoglobin (Hb) – Active site = Fe-porphine Myoglobin (Mb) – Active site = Fe-porphine Hemocyanine (Hc) – Active site =Cu_2O_2 cluster Hemeritrine (Hr) – Active site = Fe-O(OCO)-Fe cluster
Electron transfer	Redox reactions – FeS clusters, cytochromes
Structural	Proteins that regulate the expression of genes containing Zn^{2+} (DNA and RNA polymerases) or a metal ion that causes a polypeptide to adopt a tertiary structure.
Metal ion storage and transport	Ferritin
Catalysis (Metalloen-zymes)	Nitrogenase Hydrogenase Reductases

Table 2. Classification of metalloproteins according to their function.

A more detailed subdivision can be made for metalloenzymes[69,70]:

Function	Examples
Hydrolytic enzymes	Zn^{2+}, Mn^{2+}, Ni^{2+}, Ca^{2+}, Mg^{2+}
Dielectronic redox enzymes	Cytochrome P-450 (Fe) Tyrosinase (Cu_2) Sulfur oxidase (Mo) Dehydrogenase (Zn) Nitric reductase (Mo)
Multielectronic redox enzymes	Polynuclear Fe-Cu-Mo clusters
Grouping enzymes	Kinases (Mg^{2+}/Mn^{2+})

Table 3. Classification of metalloenzymes according to their function.

Metals also play a role in biological communications as magnetic compass or regulators of gene expression.

When modelling metalloprotein metal clusters, there are two approaches from which to start the research[71]: either the classical bottom-up point of view of chemists or the somehow opposed top-down approach of molecular biologists. The first one is based on the known metal ion chemistry. It builds the models with small ligands instead of using a huge macromolecular protein. Then, it extrapolates the model to a biological environment, arguing how the chemistry of the site can be altered. Inversely, the biological approach works from the top-down. It applies the analysis directly on the proteins and their mutants and discusses how the metal ion influences the function of the protein. Of course, both approaches are complementary and a complete knowledge of nature is impossible if any of them is missing.

2.2.1. Iron metalloproteins

On table 4, a summary of the classification of iron proteins is presented. Notice that hemoproteins are sub-classified according to their functions while Fe-S proteins are generally sub-classified according to their nature. Amongst the "other iron proteins" epigraph, we find proteins that have not been so extensively studied as the previous ones: lipoxygenases, monooxygenases, purple acid phosphatase, uteroferrin or catechol 2,3-dioxygenase[72].

Hemoproteins		Non-heme proteins		
Hemoproteins	Oxygen carriers	Fe-S proteins	Rubredoxins	Other iron proteins
	Activators of molecular oxygen		Ferredoxins	
	Electron transport proteins		Nitrogenases	

Table 4. General classification of Fe metalloproteins.

The extended use of iron in biological organisms may seem surprising nowadays, since iron(II) rapidly oxidizes under our atmosphere and the solubility of iron(III) is some orders of magnitude lower than that of iron(II). According to Ochiai[68] and others[73], the use of iron in metalloproteins started at the very beginning of evolution, when the Earth's atmosphere was still free of oxygen and iron(II) was the prevalent form of this metal.

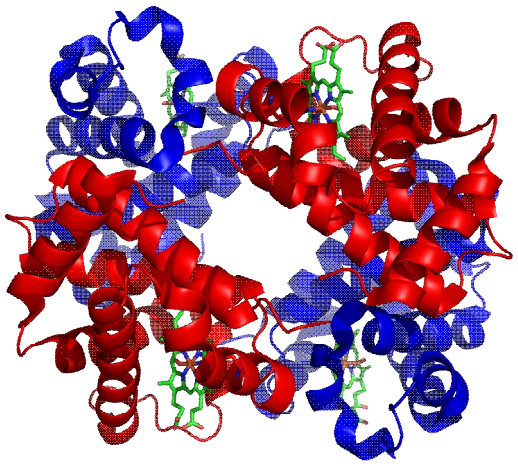

Fig. 7. 3D structure of hemoglobin. Observe the planar structure of the porphyrin rings.

Within iron metalloproteins, heme cofactors are the most ubiquitous in nature. They are comprised of a macrocyclic organic ring of the porphine type called porphyrin which immobilizes an iron cation at its center. Hemes fulfill a wide range of biological roles: electron transfer, oxygen binding and transport, oxygen activation and oxidation of organic molecules. Examples of hemes with an iron cation in the +2, +3 and +4 oxidation states have all been identified[26].

In nature, hemes are almost always bond to the backbone of the protein via an aminoacid ligand (proximal ligand) and the sixth coordination site can be occupied by a distal ligand or left open. Porphyrin is able to bind Fe either in high- or low- spin electronic state, but only high-spin Fe(II) is able to interact with paramagnetic molecules as O_2 to form bonds thanks to its unpaired electrons. Low-spin Fe(II) and both spin-states of Fe(III) are more apt for other functions such as electron transfer[26].

2.2.2. Iron-Sulfur proteins I. Mononuclear ferredoxins and rubredoxins.

Iron sulfur clusters are regarded as some of the most relevant fundamental cluster complexes in biology due to their abundance and versatility. They present a variety of nuclearities and geometries and accomplish several functions, *e.g.* electron transfer, catalytic and structural functions. R.H. Holm distinguishes five different basic site types according to their functions[62]:

(i) structural – configuration (in part) of protein tertiary and/or quaternary structure;
(ii) storage – uptake, binding, and release of metals in soluble form;
(iii) electron transfer – uptake, release, and storage of electrons;
(iv) dioxygen binding – metal-O_2 coordination and decoordination;
(v) catalytic – substrate binding, activation, and turnover.

Due to the frequency that such centers appear in biology, there has been much interest in developing working model complexes of these sites. Some of them have been successfully

synthesized and characterized[28,74-79]. This includes not only some of the most commonly found Fe-S centers in nature such as those of rubredoxins and ferredoxins[80-82]: FeS_4, Fe_2S_2, Fe_3S_4 and Fe_4S_4, but also clusters of higher nuclearities[83-87] (Fe_6S_6, Fe_8S_6, Fe_6S_9, and even[88] $Fe_{18}S_{30}$) as well as mixed-metal clusters[76,89-94] (mainly of the type MFe_3S_4, where M= Mo, V, Ni). However, it has not been possible to reproduce some of the most complicated (and interesting from the catalytical point of view) biological clusters (*e.g.*, the Fe-Mo cofactor of nitrogenase or the Fe-Fe and Fe-Ni cofactors of hydrogenases), which still remains as a challenge for the chemists of the 21st century. The synthesis of these iron-sulfur cluster complexes is generally accomplished by the use of simple arene- and aryl-thiolato ligands. Some of these clusters are shown in fig. 8.

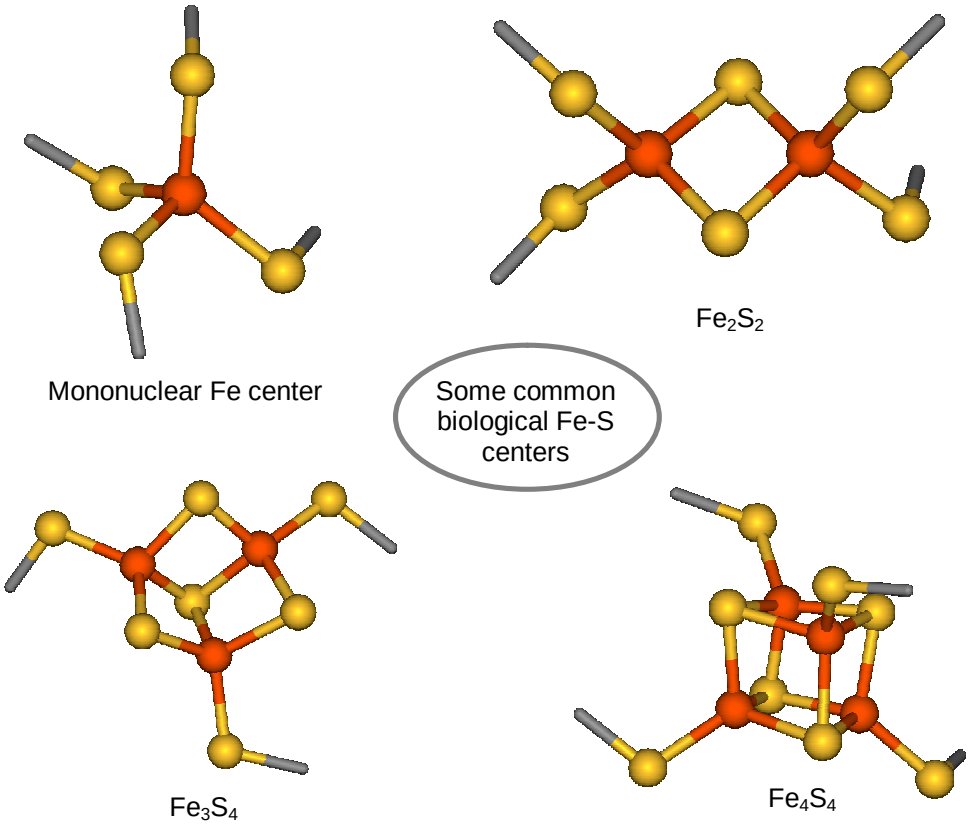

Fig 8. Some examples of Fe-S centers. In the image, the mononuclear Fe center of desulfoferrodoxin from *Desulfovibrio desulfuricans*, the Fe_2S_2 center of ferredoxin of the thermophyllic cyanobacterium *Mastigocladus laminosus* and the Fe_3S_4 and Fe_4S_4 clusters of the ferredoxin in *Acidianus ambivalens* are shown.
Structures obtained from the RCSB PDB, rendered with Accelrys Discovery Studio Visualizer 1.7. DOI: 10.2210/pdb1dfx/pdb , 10.2210/pdb1rfk/pdb, 10.2210/pdb2vkr/pdb .

Originally, ferredoxins were erroneously classified in two groups: bacterial ferredoxins, which contained a Fe_4S_4 cluster; and plant ferredoxins, which contained a Fe_2S_2 cluster. This classification was some time afterwards proved wrong and rendered obsolete, because it was discovered that both kind of clusters can be found in ferredoxins of plant, animal and bacterial origin[95].

Rubredoxins are essentially different from ferredoxins since the former are exclusively monometallic while the latter often contain polynuclear [2Fe-2S] or [4Fe-4S] clusters. Furthermore, ferredoxins contain an acid-labile sulfide which evolves to H_2S at low pHs, while the rubredoxins do not. Ferredoxins are also involved in a wider spectrum of functions: N_2 and CO_2 fixation, photosynthesis, mitochondrial respiration chain, etc. and the range of potentials covered by them is much broader than in the case of rubredoxins, as shown in Fig. 9.

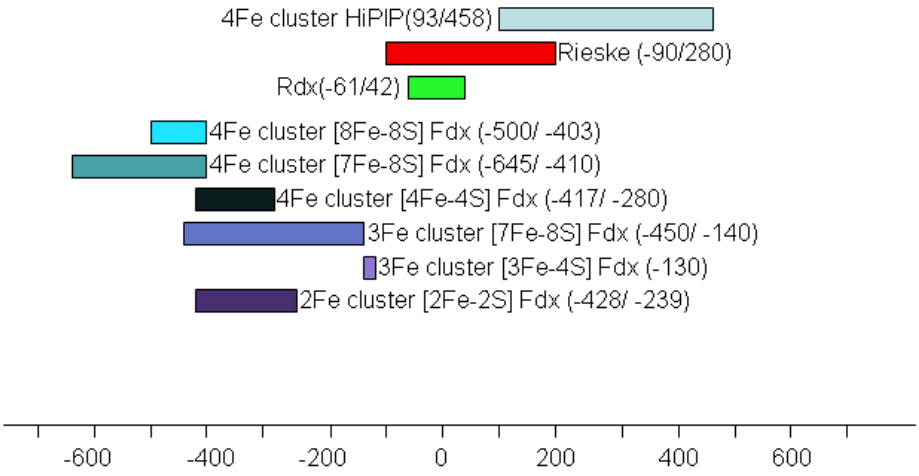

Fig 9. The redox potential of Fe-S centers compared to some other biologically relevant potentials. Adapted from Biological Inorganic Chemistry: Structure & Reactivity.

Despite these inherent differences, there are undeniable resemblances between mononuclear ferredoxins and rubredoxins. First, the iron centers are generally linked to the rest of the protein via the terminal sulfurs of cysteine residues. Second, both metalloproteins undergo extremely fast electron exchange since they do not suffer drastic structural changes during redox processes and therefore the energetic requirements to change the structure are minimal. This structural invariability of mononuclear ferredoxins contrasts with the major changes that Fe_4S_4 clusters suffer during redox processes. Anyhow, cubane clusters are considered amongst the fastest self-exchange clusters.

Extensive research concerning the modeling of [4Fe-4S] clusters amongst others has been performed by R. H. Holm, E. I. Solomon and others for more than 30 years, contemplating the problem from multiple points of view and offering an insight to the ubiquity of such clusters[96]. For example, the series $[(\mu_3\text{-}E)_4Fe_4(SR)_4]^{z-}$ (E=S or Se, z=2 or 3) has been thoroughly investigated as analogues of the [4Fe-4S] ferredoxins. These structures are composed of two slightly compressed and concentric tetrahedra, the first one composed of 4 E atoms while the 4 Fe atoms form the second one. The 4E tetrahedron is substantially larger, so E-Fe-E angles average 104º, while Fe-E-Fe angles average 74º. The Fe·····Fe and E·····E mean distances are correspondingly 2.75Å and 3.75Å.

The cubane shaped Fe_4S_4 is one of the most biologically relevant iron-sulfur clusters[97-99]. It is present in several non-heme proteins and high potential proteins (HiPIPs); for instance it has been identified in both oxidized and reduced forms of HiPIP in *Chromatium*[100], the ferredoxin I in *Azotobacter vinelandii*[101,102], the hydrogenase in *Clostridium pasteuranium*, the iron protein of nitrogenases or the [8Fe-8S] ferredoxin of *Peptococcus aerogenes*[103], which contains two independent $[Fe_4S_4]^{2+}$ clusters. In any case, the four iron atoms of the cubane cluster are usually bond to the rest of the protein through the sulfur atoms of four cysteine residues. Despite this kind of cluster has been thoroughly studied for twenty years; still many aspects of its chemistry are unknown. For instance, $[Fe_4S_4L_4]^{2-}$ clusters generally undergo reversible one electron reductions, but the relation and influence of the terminal ligand coordination in the redox properties of such clusters are not well understood.

Fe_4S_4 clusters are not only used as models for protein active sites, but also as precursors for mixed metal clusters where one iron atom is removed and substituted by another metal[91,93,104-111]. Furthermore, stable Fe-Se clusters of nuclearities[112-120] 2, 3, 4, and 6 which are structurally and electronically analogous to Fe-S clusters, can be readily prepared by similar methods. While there is no clear evidence of the inclusion of selenide in metal clusters in biology, artificially synthesized Fe_2Se_2 and Fe_4Se_4 clusters have proven to be instructive and interesting in determining the function of sulfide in native proteins[121,122]. What is more, some proteins with reconstituted Fe-Se clusters have demonstrated to be far more reactive than their native Fe-S clusters.

In biology, [4Fe-4S] clusters can be found in four different oxidation states. All of them have been successfully reproduced. These cores are usually found as redox couples as can be seen in the next table[28]:

Core oxidation state	$[Fe_4S_4]^0$	$[Fe_4S_4]^{1+}$	$[Fe_4S_4]^{2+}$	$[Fe_4S_4]^{3+}$
	4Fe(II)	3Fe(II)+Fe(III)	2Fe(II)+2Fe(III)	Fe(II)+3Fe(III)
Proteins		-0.3 to +0.1 to		
		Fe protein ⟷ Fd_{red} ⟷ Fd_{ox}/HP_{red} ⟷ HP_{ox}		
		-0.8 V -0.8 V +0.5 V		
Analogues	$[Fe_4S_4(SR)_4]^{4-}$ ⟷	$[Fe_4S_4(SR)_4]^{3-}$ ⟷	$[Fe_4S_4(SR)_4]^{2-}$ ⟷	$[Fe_4S_4(SR)_4]^{-}$
Fd=Ferredoxin, HP=High potential protein				

Table 5. Electron transfer series of Fe_4S_4 protein sites and analogues showing core oxidation states and formal iron valence states. Isoelectronic species are arranged vertically. Adapted from V. P. Rao and R. H. Holm.

The oxidation state of the iron atoms has great influence on the structural and reactivity properties of Fe-S and heterometal-Fe-S clusters. As Zhou and Holm report, the $[Fe_4S_4]^+$ core in $[Fe_4S_4(SR)_4]^{3-}$ ($Fe^{2.25+}$) presents variable spin states and a multiplicity of distortions that are not found in more oxidized clusters like the more common compressed tetrahedral geometry of $[Fe_4S_4]^{2+}$ ($Fe^{2.5+}$) cores. Also, it is known that the chalcogenide exchange in $[Fe_4E_4]$ cores from E=S to E=Se occurs more rapidly for the less oxidized systems $[Fe_4S_4(SR)_4]^{3-}/[Fe_4Se_4(SR)_4]^{3-}$ than for their dinegative analogues[46].

2.2.3. Iron-sulfur proteins II. Nitrogenase

One of the challenges of this century is to provide a model of the active site of nitrogenase. Nitrogenase is the enzyme that microorganisms use to fix the atmospheric nitrogen into a usable form such as ammonia[123-128]. It is present in relatively few groups of bacteria, but according to R. R. Eady[128], this enzyme "[…] is responsible for the cycling of some 10^8 tons of N per year". Three types of nitrogenases have been isolated and characterized: Mo-nitrogenase, V-nitrogenase and Fe-nitrogenase. In addition, a new type of nitrogenase has recently been isolated from *Streptomyces thermoautropicus* that contains molybdenum but requires dioxygen and consumes carbon monoxide[128].

Structurally, the Mo-nitrogenase is composed of two proteins[76,128,129]: the Fe protein and the FeMo protein. The Fe protein contains a single [4Fe-4S] cluster bridged between the sub-units and it functions as a specific one-electron donor to the FeMo protein. Additionally, it accomplishes other functions such as initial biosynthesis of FeMo cofactor or insertion of preformed FeMo cofactor into a FeMo cofactor-deficient FeMo protein. The FeMo protein contains two [8Fe-8S] clusters (P clusters), which act as capacitors, storing electrons until

they are required by the active site for the conversion of dinitrogen into ammonia, and two [1Mo7Fe-8S] clusters, which are the site of N_2 to NH_3 conversion. In the next figure, the structure of both P-clusters and the FeMo cofactor of nitrogenase are displayed. In 2004, a more detailed structural research reported the existence of a small atom in the structure of the FeMo cofactor[76,129]. Although its nature has not been fully determined yet, it is believed to be nitrogen.

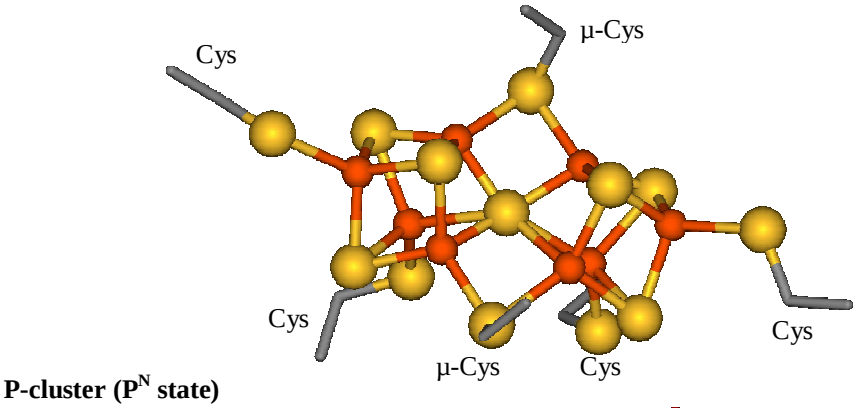

P-cluster (P^N state)
$[Fe_8(\mu_2\text{-}SCys)_2(\mu_3\text{-}S)_6(\mu_6\text{-}S)]$ core

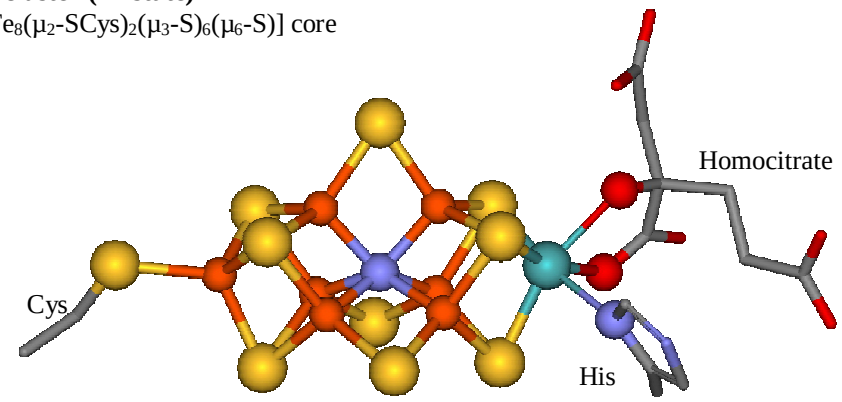

Iron-Molibdenum cofactor (FeMo-co)
$[MoFe_7(\mu_2\text{-}S)_3(\mu_3\text{-}S)_6(\mu_6\text{-}N)]$ core

Fig. 10. Structure of P-cluster and FeMo cofactor of nitrogenase from *Azotobacter vinelandii*. RCSB PDB DOI: 10.2210/pdb2afk/pdb Rendered with Accelrys Discovery Studio Visualizer 1.7.

Under optimal conditions Mo-nitrogenase catalyses the reaction:

$$N_2 + 8e + 8H^+ + 16ATP \longrightarrow 16ADP + 16P_i + 2NH_3 + H_2$$

This reaction takes place at ~ 293K and 0.8 atm of N_2 which contrasts with the high pressure and temperature needed at industrial level (150-300 atm and 300-500K), where ammonia is synthesized by reaction of nitrogen with hydrogen in the Haber Bosch process. This process indirectly supplies about 40% of the world necessities for fertilizers and consumes roughly 1% of the worldwide energy[130]. The study and understanding of the processes that microorganisms use to fix nitrogen could eventually lead to more efficient catalysts.

2.2.4. Iron-sulfur proteins III. Hydrogenases

The current energy crisis has boosted the search for alternative energy sources and systems of energy storage. As a result, some researchers have turned their attention towards hydrogenases. These Fe-S metalloproteins are responsible for the whole cycle of dihydrogen production: formation of H_2, storage and oxidative consumption. Most commonly these metalloproteins are classified according to their phylogenetic origin. This classification is also useful from the structural point of view[131,132] (see the scheme in the next page).

The heterodimetallic cofactor of [Fe-Ni] hydrogenase has been reproduced structurally, but there have been difficulties inserting the bridging hydride within the cluster, which is essential for activity. Only recently, Ogo *et al*[133]. reported the synthesis of an analogue cluster with Ru and Ni that is catalytically active[132].

[Fe-Fe] hydrogenases display a Fe_6S_6 cofactor (the H cluster) which consists of two subclusters bridged by a cysteine: a Fe_4S_4 cubane cluster and a Fe_2S_2 – butterfly-type center. The active site is supported by several iron-sulfur centers. The exact number and the composition of these sites vary depending on the species (one Fe_2S_2 and 3 Fe_4S_4 centers in the case of *Clostridium Pasteurianum*, but only 2 Fe_4S_4 clusters for *Desulfovibrio desulfuricans*[134]). Hydrogenases of this kind are exceptionally efficient, developing 6000-9000 molecules H_2 s^{-1} per site[135]. A functional structural model was reproduced by Gloaguen *et al*. in 2002, the complex $[(PMe_3)(CO)_2\ Fe^{II}(\mu\text{-}H)(SCH_2CH_2CH_2S)Fe^{II}(CO)_2(CN)]$, which can catalyze the electrochemical reduction of protons[132,136].

The second kind of hydrogenases contains a dimetallic Fe-Ni cofactor whose catalytic activity is associated to hydrogen uptake[137]. Like Fe-only hydrogenases, these proteins contain other non-catalytic sites; in this case, two Fe_4S_4 cubane clusters and a Fe_3S_4 cluster.

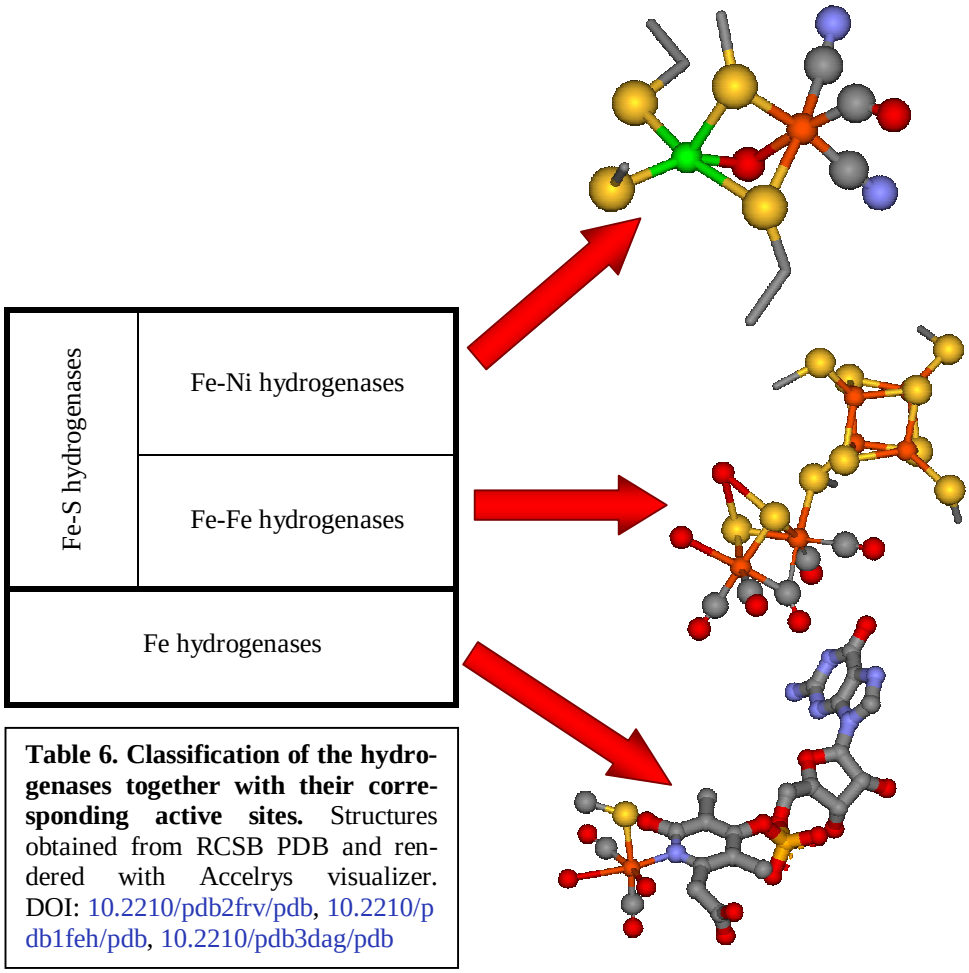

Table 6. Classification of the hydrogenases together with their corresponding active sites. Structures obtained from RCSB PDB and rendered with Accelrys visualizer. DOI: 10.2210/pdb2frv/pdb, 10.2210/pdb1feh/pdb, 10.2210/pdb3dag/pdb

The Fe hydrogenases (also called iron-sulfur_cluster-free hydrogenases) are the least known; they are only produced by some methanogenic archaea and have not been so thoroughly studied. Their structure has been identified recently and the active site consists of a single metal atom bond to an organic pyridinol cofactor[132,138]. For several years after their discovery, they were erroneously labeled as metal-free hydrogenases, but in 2004 it was discovered that they actually contain a Fe-center (although not sulfur), and therefore, the terminology was changed.

2.3. SULFUR

2.3.1. Sulfur in nature

Sulfur is one of the members of the 16th group (VI A) and the only one that can be properly named chalcogen (generator of copper) since:

$$CuS + O_2 \longrightarrow Cu + SO_2$$

While it is one of the most abundant elements in terms of cosmic occurrence, it only accounts for a 0.03% of the composition of the Earth's crust. Despite its scarcity in the crust, sulfur is supposed to make up to a 6% of the Earth's core[139]. In nature, it is commonly found in its elemental form as well as in the combined state as sulfides (galena – PbS, pyrite – FeS_2, cinnabar – HgS, etc), sulfates (gypsum – $CaSO_4.2H_2O$, barite – $BaSO_4$, etc), H_2S and organosulfur compounds in petroleum and coal[140,141]. Elemental sulfur is obtained from natural deposits – often of volcanic origin – either in opencast mines or in underground deposits[141,142] (from where it is retrieved by the Frasch process).

Sulfur is well known for its wide variety of allotropic forms (about 50 of them are known, although only a few have been completely characterized), the most common being orthorhombic (α-S) and monoclinic (β-S). It is insoluble in water, slightly soluble in benzene and well soluble in CS_2. In both α- and β- allotropic forms, sulfur atoms are grouped into S_8 crowns. The conversion between α- and β-S takes place at 94,5 ºC, with α-S being the most dense species. Melting points are 113ºC and 119ºC for α-S and β-S, respectively, although the actual observed m.p. is usually found between those values since often a mixture of both allotropes is present. At temperatures close to the m.p., sulfur is a yellow liquid of very low viscosity. With increasing temperature, the color turns darker and the viscosity increases up to a maximum around 159ºC. At 160ºC, extensive breakage of the S_8 crowns (as well as some other cyclic species formed so far) takes place resulting in the formation of polymeric S chains, which account for a 10000-fold increase of viscosity. Further heating provokes the chains to decrease and the sulfur to regain high mobility. In the proximity of the boiling point (444ºC), sulfur presents again very low viscosity. At this point, sudden cooling leads to the formation of an amorphous form of sulfur characterized by its plasticity[142,143].

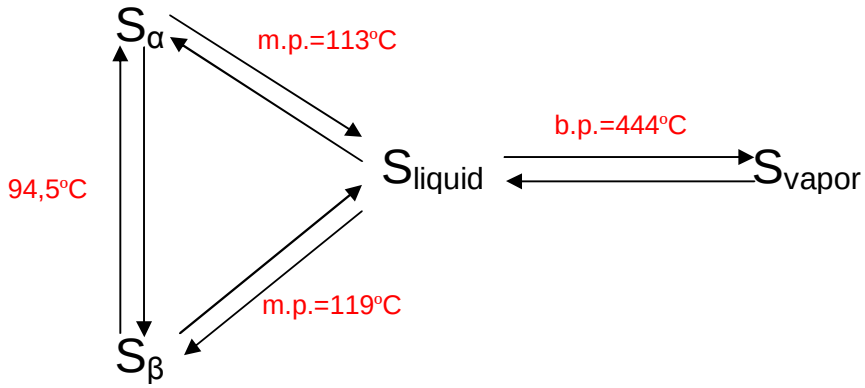

Fig.11. Diagram showing the allotropic forms of sulfur and phase change temperatures.

Sulfur presents an electronic configuration of [Ne] $3s^2$ $3p^4$, and therefore, its oxidation states are -2 (the most common, since it provides a gas noble configuration), +2, +4 and +6. When compared to oxygen, sulfur has fewer tendencies to form $p_\pi p_\pi$ bonds, and shows a stronger preference for catenation. Thus oxygen forms the O_2 molecule with a multiple bond, while sulfur forms the S_8 molecule with single bonds. This also accounts for the observed discrepancies in stability between CS_2 and CO_2 with respect to polymerization. However, it is possible for sulfur to expand its valence shell making use of its d orbitals, forming $d_\pi p_\pi$ bonds. The expanded valence shell also explains the possibility for sulfur compounds to achieve a higher coordination number[144,145] (for instance, SF_6 vs. OF_2).

In biology, sulfur is considered one of the essential bioelements. For instance, the adult human body contains about 2.5g/kg of sulfur. Despite most of it concentrates in hair and nails, it is also found in several compounds, including the amino-acids cysteine and methionine, coenzymes, enzymes, vitamins, ferredoxins and other iron proteins. Elemental sulfur is not poisonous, but delivers toxic H_2S and SO_2 upon contact with tissues.

2.3.2. Thiols and thiolates

Thiols are the sulfured homologues to alcohols where the –OH is substituted by the sulfhydryl (–SH) functional group. Their probably most widely-known characteristic is their intense and unpleasant odor. Thiols of biological origin are amongst the nature's most powerful antioxidants protecting the cells. These compounds are also called mercaptans due to their reactions with mercury ions to yield mercaptides (mercury thiolate salts)[146,147]:

$$2\ RSH + HgCl_2 \longrightarrow Hg(SR)_2 + 2\ HCl$$

The use of thiols is extensive in the fields of surface chemistry and nanotechnology since they have provided an easy route towards the formation of self assembled monolayers (SAMs) on metal surfaces. Traditionally, only noble and coinage metals have been destined to this use, but the potential use of thiols on steel and iron surfaces as an anti-corrosion measure has also drawn some interest[148,149]. This property of thiols has made possible *inter alia* the synthesis of alkanethiol-stabilized gold nanoparticles[150-152] and the development of some mechanisms to amplify the protein-receptor interactions[153]. Also, some authors have postulated a possible DNA-computing device inspired on this technology[154,155].

Thiols have often been used as a source for thiolate ligands. The thiolate group (RS^-) is a fundamental ligand type[156-157]. It is a soft Lewis base which preferably coordinates to later transition metals and lower oxidation states[158,159]. Thiolates are known by its ability to act as a bridging ligand, apart from the more common terminal binding. Thiolate ligands can act as both σ- and π-donors. When π-donation is significant, the M-S bond-length shortens while the M-S-R angle should theoretically be wider; however, the M-S-R angle has proved empirically to be relatively invariable at this respect. At the same time, the M-S-R angle is more unreliable since it can be altered by the packing forces of the crystal, and therefore the changes in M-S distances are preferred as an indicator of the covalence of the bond[160].

The interest that metal thiolate complexes have arisen can be attributed to their heterogeneous features. First, emerging from the fact that sulfur often attains the -2 state of oxidation in its compounds, the chemistry of metal thiolates is clearly related to that of metal sulfides and hydrosulfides[161] (which, in turn, have sometimes been referred as metallathiols). Second, their reactivity, related to S-C bond cleavage reactions and desulfurization, can lead to important applications in the field of desulfurization catalysis or as inorganic functional materials[162]. Also, transition metal thiolates are useful from the point of view of medicine: a group of cyclopentadiene titanium thiolate complexes have demonstrated to possess a certain anti-tumor activity[163] and gold(I) thiolates are often used to fight the joint degrading disease *rheumatoid arthritis*[164].

Finally, the understanding of thiolate-metal ligation can help us to develop and synthesize models for cysteine-metal sites in biological systems (where the metal is also bound to the protein *via* a thiolate sulfur atom).

Metal thiolates are most commonly prepared according to[28,33,147]:

$$MX_n + nRS^- \longrightarrow M(SR)_n + nX^-$$

where RS^- comes from an alkali metal or tertiary amine thiolate.

One of the difficulties traditionally associated to the study of metal thiolates is the ability of these compounds to form aggregates or polymers[165]. This handicap may be overcome not-

withstanding by modifying the electronic properties of the substituents bound to the thiolate. Then, electron-withdrawing groups are preferred since they help to reduce the electronic density of the thiolate[166,167]. The use of aromatic thiolate donors – although they are not present in biology – has extended in modeling studies mainly because they present two important advantages in front of alkyl thiolates. First, aryl thiolates are not so prone to polymerization. Second, as the donor ability of the cysteine ligand is mitigated by H-bond interactions and by the protein dielectric field, the electron-withdrawing aryl thiolates are better models at this respect than their alkyl counterparts[168].

Thiolates are known for being able to undergo redox processes. They are good reducing agents, and can also be oxidized in the presence of oxygen to the corresponding disulfides or to sulphenates or sulphinates. The redox activity remains even after coordination, which qualifies these compounds to be labeled as non-innocent ligands in many cases. This complicates the interpretation of the observed redox properties of the metal complex. Such non-innocent ligands are often found in metalloenzymes, where they play a key role in the catalytic process. Evidently, to avoid problems derived from the redox reactivity of thiolates during the synthesis, Schlenk work under an inert atmosphere is required.

2.3.3. Iron thiolates

Iron thiolates have attracted attention for several years in the field of bioinorganic chemistry due to their relation with rubredoxins or ferredoxins and as precursors for several other iron-sulfur metalloproteins. Also, in conjunction with heme groups, iron arylthiolates have been often used as models for the cysteine residues in biological heme cofactors[169-177]. Homoleptic tetracoordinated thiolates of iron are known for both +2 and +3 oxidation states, forming negatively charged tetrahedral complexes of the type $[Fe(SR)_4]^{2-}$ and $[Fe(SR)_4]^{-}$ correspondingly. As well as in biological $Fe(cys)_4$ centers, these synthetic models do not suffer radical structural variations in going from one oxidation state to the other. The most noticeable feature may be the shorter Fe-S bonds found in Fe(III) complexes.

Ligand type	Oxidation state of the Fe center	Mean Fe-S distance (Å)
Arylthiolates	2	2.339
	3	2.285
Alkylthiolates	2	2.345
	3	2.267

Table 7. Fe-S distance mean values for Fe thiolates according to their oxidation state and the nature of the ligand. Values calculated from data in the CCDC database

One of the most exploited characteristics of iron thiolates is their ability for building Fe-S clusters under mild conditions. Several clusters of biological relevance have been synthesized as well as some others with no known counterparts in nature. As a consequence, iron thiolates and some derived Fe-S clusters have been proposed as precursors for synthetic models of bioinorganic Fe-S active sites such as those of hydrogenases or nitrogenases. Other areas of interest in the field of bioinorganic chemistry are the possibility of building mixed-metal sulfido clusters from mononuclear iron thiolates and the substitution of sulfur atoms in Fe-S synthetic clusters by other elements of the 16th group (most commonly, Se).

From the point of view of technological applications, iron thiolates can be used as unsupported catalysts. Their ability to form iron-sulfur rich clusters could for instance lead to the development of new sulfide nanomaterials related to pyrites (FeS_2). As the latter have been recently postulated as an excellent alternative to silicon from the economical point of view as a material for manufacturing photovoltaic cells[25], it is possible that these theoretical nanomaterials would show similar photovoltaic activity.

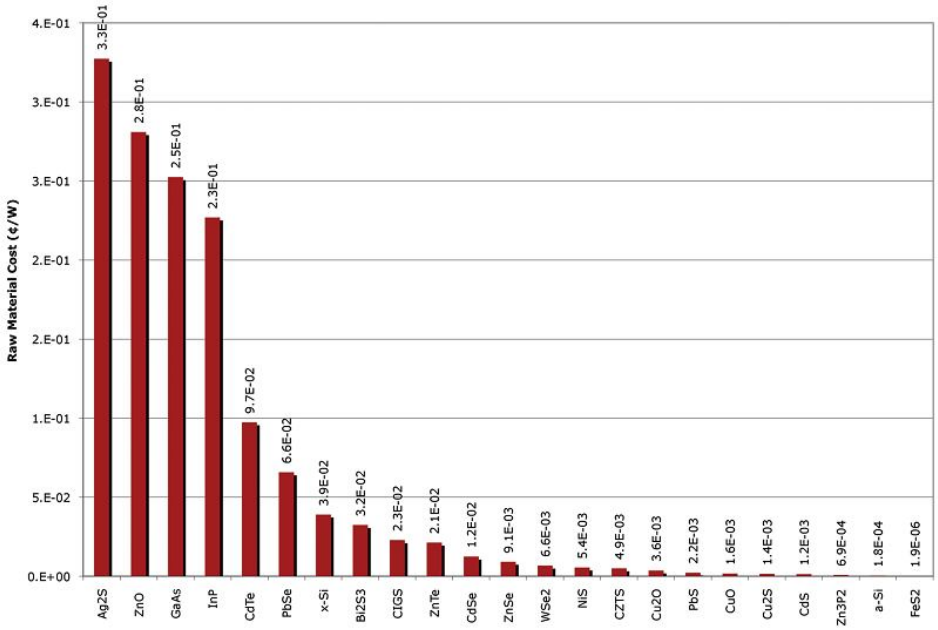

Fig. 12. Minimum raw material cost of extraction (in cents of dollar/W) for 23 inorganic photovoltaic materials. The graphic represents the cost of extracting the minimal amount of substance that will produce 1 W after PV manufacturing. The cost of processing the material for PV grade is not taken into account here. Adapted from Wadia *et al.*

When dealing with mononuclear iron thiolates, many investigations deal with bulky macrocyclic and /or multidentate ligands (*e.g.* porphynes, dithiolates) that in great measure restrict the geometrical disposition of the orbitals of the metal[171,178-181]. Standalone thiolate ligands[182,183] are not so common and the examples found in the literature show a predominance of arylthiolates[184-188] against alkylthiolates[189-191]. As we explained before, the use of thiolates with aromatic substituents presents substantial advantages in front of the simpler alkylthiolates, which could also make them more attractive to researchers.

Metal thiolates are known to present a vast structural diversity, which on the other hand makes their structures difficult to predict. This is also true for iron thiolates. Apart from the most typical octahedral and tetrahedral geometries, iron thiolates often adopt the pentacoordinated trigonal bipyramid[192-194] and square pyramid[170,195,196] configurations. Even the trigonal planar geometry, which is not very often found in iron complexes, has also been reported for the anionic group $[Fe(SC_6H_2\text{-}2,4,6\text{-}{}^tBu_3)_3]^-$ by Holm and coworkers[197]. It is remarkable that tricoordinated compounds of iron are so scarce because their structural stability is not very high – iron complexes generally prefer higher coordination numbers (4, 5 or 6) which allow them to distribute the charge more effectively. The fact that the homoleptic complex $[Fe(SC_6H_2\text{-}2,4,6\text{-}{}^tBu_3)_3]^-$ adopts such an structure can only be explained by the significant steric impediment that the exceptionally bulky $(SC_6H_2\text{-}2,4,6\text{-}{}^tBu_3)^-$ ligand offers.

2.3.4. Silanethiols: Chemistry and reactivity

In 1847, I. Pierre[198] reported the synthesis of a new compound which he identified as Cl_2SiS. Roughly 20 years later, C. Friedel[199] perfected the synthesis and corrected the formula of the compound, which was finally characterized as Cl_3SiSH, the first member of a brand new class of compounds: the silanethiols.

$$SiCl_4 + H_2S \xrightarrow[20\text{-}40\%]{650^oC} Cl_3SiSH + HCl$$

The simplest member of this family, H_3SiSH, theoretically can be obtained from[200]:

$$H_3SiSSiH_3 + H_2S \longrightarrow 2H_3SiSH$$

but it is extremely unstable and has never been characterized since it promptly condenses to yield $(SiH_3)_2S$. Usually bulkier substituents yield more stable silanethiols.

Trialkylosilanethiols can be obtained according to the reaction[200]:

$$R_3SiNHR' + H_2S \xrightarrow[<19\%]{} R_3SiSH + R'NH_2$$

Or with the more efficient pyridine catalyzed reaction[200,201]:

$$R_3SiCl + MSH \xrightarrow[\text{Up to 48\% for M=Li}]{\text{pyridine}} R_3SiSH + MCl$$

A more specific reaction for the synthesis of triethylsilanethiol involves the use of a Pd catalyst[200]:

$$R_3SiH + H_2S \xrightarrow{Pd/Al_2O_3} R_3SiSH + H_2$$

The literature concerning arylsilanethiols is mainly focused on triphenylsilanethiol, which can be obtained with up to 80% efficiency following the equation[200,202,203]:

$$(C_6H_5)_3SiCl + H_2S + R_3N \longrightarrow (C_6H_5)SiSH + R_3N.HCl$$

Making triphenylsilane react with pure sulfur seems a more straightforward method and is equally efficient[200]:

$$(C_6H_5)_3SiH + S \xrightarrow[80\%]{} (C_6H_5)SiSH$$

This method is likewise useful to synthesize other triorganosilanethiols[204], especially those containing aryl substituents.

Another special class within silanethiols, trialkoxysilanethiols – derivatives of the unknown monothioorthosilicic acid – were obtained for the first time in 1961 from the reaction of SiS_2 with secondary alcohols such as alkyl or aryl alcohols[205]. The synthesis was developed by W. Wojnowski and R. Piękoś[206] and it has remained the most common method for obtaining trialkoxysilanethiols since. Likewise, their hypothesis of a mechanism explaining this reaction has been widely accepted. Their postulated route is shown following[206]:

1)

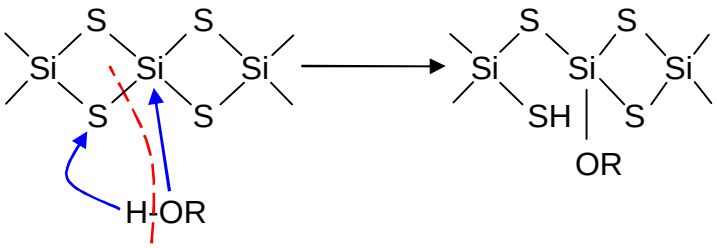

The alcoholysis occurs by breakage of the Si-S bonds of SiS_2. Then, the alcohol molecule splits, binding the more nucleophilic oxygen atom to the silicon and liberating a proton which is captured by the sulfur atom.

2)

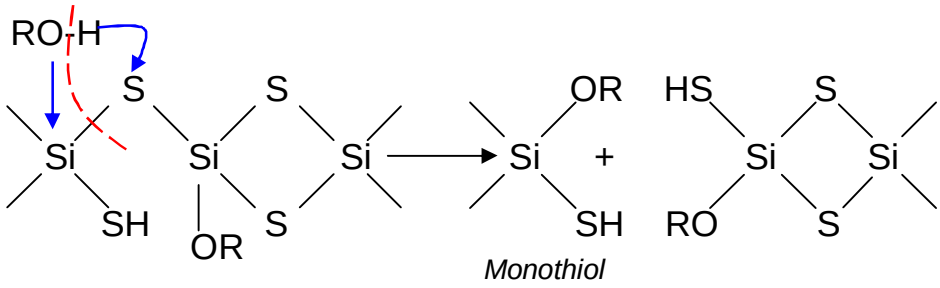

Monothiol

Step **2** is repeated twice more to obtain the corresponding $(RO)_3SiSH$. Of course, it can also occur that two or more thiol groups are bound to the same silicon atom by the same mechanism. The products of the reaction are determined in each case by several factors such as the temperature of the system, reagents ratio and alcohol type (primary, secondary, tertiary).

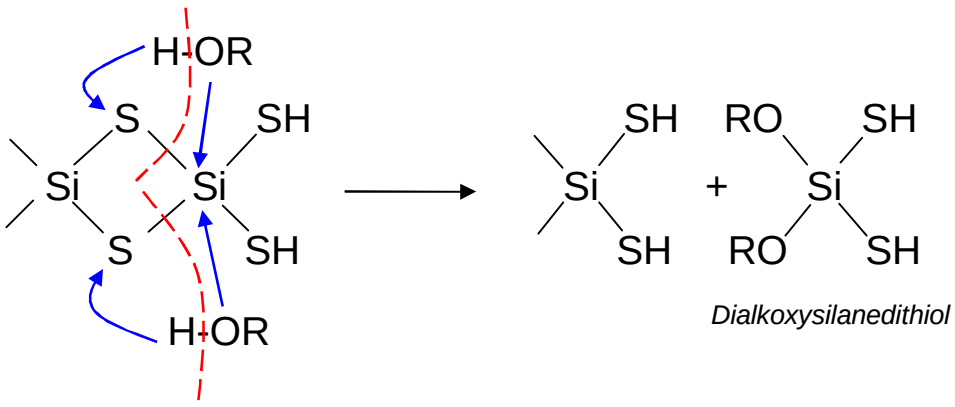

Dialkoxysilanedithiol

Silanedithiols have resulted extremely elusive[207] and their characterization has been complicated since they are very sensitive towards moisture and decompose very fast (see below). Only recently Tokitoh *et al.* reported the first structural characterization of a member of this family[208]. They managed to isolate [Tbt(Mes)Si(SH)$_2$], thanks to the additional protection provided by the sterically hindered 2,4,6-tris[bis(trimethylsilyl)methyl]phenyl and 2,4,6-trimethylphenyl groups.

Depending on external factors such as pH or the temperature, the newly formed thiol groups suffer alcoholysis, freeing H_2S[206]:

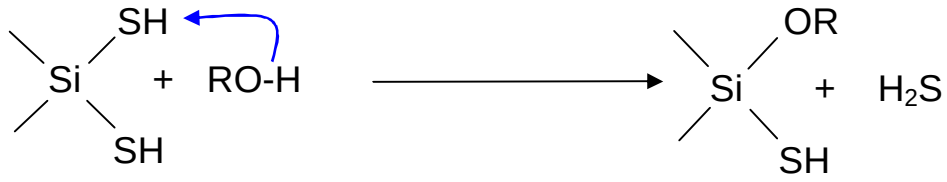

Raman-IR spectroscopy can be used to characterize silanethiols, since the absorption band corresponding to the Si-S-H bond is generally found in the 2530-2580 cm^{-1} range. This determination can be problematic due to the low intensity of that band[200,209].

When compared to their organic equivalents, silanethiols have demonstrated to be stronger acids, in agreement with the series[200,210]:

$(C_6H_5)_3SiSH >> C_6H_5SH > (CH_3)_3SiSH > (C_6H_5)_3CSH > (CH_3)_3CSH$

(^{t}BuO)$_3$SiSH represents the exception to this rule, with an abnormally low acidity constant ($pK_a \simeq 8.0$). This is explained by the great steric impediment provoked by the *tert*-butoxy groups, which restrain the Si-O bonds from attaining their optimal geometric configuration. As a result, the electron density on the thiol group increases and therefore the acidity decreases[32,211].

Bulkier substituents also affect the chromatographic behavior of silanethiolates. Thus, Becker and Wojnowski[212] state that "[…] adsorption of trialkoxysilanethiols on TLC films decreases with increasing number of carbon atoms in the alkyl group and with its branching; adsorption decreases with the decreasing acidity of silanethiols."

Also solvents retain some influence on reactivity of silanethiols, for instance in MeCN solution their reactivities decrease accordingly to the series[201]: i-Bu(i-PrO)$_2$SiSH > i-Bu$_2$(i-PrO)SiSH > (i-PrO)$_3$SiSH > i-Bu$_3$SiSH

Triorganosilanethiols are sensitive towards hydrolysis, decomposing into a silanol and giving away hydrogen sulfide[200]:

$$R_3SiSH + H_2O \longrightarrow R_3SiOH + H_2S$$

The velocity of the decomposition depends in great measure of the pH of the environment. For a neutral environment the hydrolysis takes place in about one hour. The reaction occurs faster in an alkaline ammonia-containing medium. If the pH is acidic, the hydrolysis is also faster but the obtained silanols condense into siloxanes immediately[213].

Their reactions with alcohols and phenols occur similarly to hydrolysis, yielding the corresponding esters[200, 203, 214]:

$$R_3SiSH + R'OH \longrightarrow R_3SiOR' + H_2S, \text{ where } R' = Me, Et, Pr, i\text{-}Pr, s\text{-}Bu, Ph, o\text{-}Kr$$

The use of organic catalysts has proved useful in this case. The protolytic splitting of the SiS bond is significantly accelerated by the addition of a nucleophilic heterocyclic catalyst[215-217] (namely, pyridine, 2-methylimidazole and 4-dimethylaminopyridine). The addition of Et_3N reduces the reaction rate.

The condensation of trialkylosilanethiols takes place more easily than their silanol counterparts, yielding the corresponding disilthianes[200]:

$$2R_3SiSH \longrightarrow R_3SiSSiR_3 + H_2S$$

Bromination of a silanethiol gives the bromosilane[200]:

$$2R_3SiSH + 3Br_2 \longrightarrow 2R_3SiBr + S_2Br_2 + 2HBr$$

Silanethiols react with chlorosilanes in presence of a tertiary amine to give disilthianes[200]:

$$R_3SiSH + ClSiR_3 \longrightarrow R_3SiSSiR_3 + R_3N.HCl$$

If a silanethiol is treated with an acid anhydride, the reaction follows[200]:

$$R_3SiSH + (RCO)_2O \longrightarrow R_3SiOCOR + RCOSH$$

While trialkoxysilanethiolates react with carboxylic acids yielding similar products[218]:

$$(RO)_3SiSH + R'COOH \longrightarrow (RO)_3SiOCOR'$$

Much alike its reaction with alcohols, dimethylsilylene can be inserted into the S-H bond of silanethiols, giving a range of products[219]:

$$({}^{t}BuO)_3SiSH + (Me_2Si)_6 \xrightarrow{h\cdot\nu} ({}^{t}BuO)_3SiSSiMe_2H + ({}^{t}BuO)_3SiS(SiMe_2)_2H + ({}^{t}BuO)_3SiS(SiMe_2)_3H + ({}^{t}BuO)_3SiS(SiMe_2)_4H$$

It is remarkable that the insertion does not occur in the case of organic thiols, due to their lower acidity, forming the corresponding disulfides instead.

For both $({}^{t}BuO)_3SiSH$ and $({}^{i}PrO)_3SiSH$, the relative rate constant for the insertion of Me_2Si: is 1.7, which indicates that bulky alkoxy groups attached to the Si atom do not have much effect on the reactivity of alkoxysilanethiols towards silylene insertion.

Due to their position in the periodic table, one can infer that C and Si share several characteristics. This is true in a broad sense. They behave similarly with other elements, tend to form somehow related compounds, mainly adopt a tetrahedral structure when forming single bonds and both are able to form double and triple bonds (although a significant difference is that the requirements for building such a bond are so hard to fulfill that for several years it was believed that Si could not form them at all – needless to say how mildly C forms these bonds).

Due to these similarities, for several years it was believed that the Si atom of silanethiolates behaved identically as the corresponding C atom in organic thiolates. As a consequence, the shortening of the Si-S distance caused by stronger electron-withdrawing substituents misled some authors to believe that π molecular orbitals were involved[200].

To some extent, the general behavior of silanes added more confusion. For instance, according to Ostdick and McCusker[220], the introduction of an alkoxy-group instead of alkyl group causes a reduction of the electronic density on the Si. Introducing the second and third alkoxy-groups provokes the electron density on the silicon to rise again to higher values than those of tetraalkylosilanes and therefore an increase in π bonding.

Also, Rochow and Newton[221] stated that the electronic substraction from the organic group results in the reinforcement of the p_π-d_π bond between O and Si. The increase of the induction effect +I of the alkyl groups in trialkoxysilanes (Me < Et < n-Pr < i-Bu < n-Bu < i-Pr < s-Bu < t-Bu) leads to an increase of the electron density on the oxygen atom, which increases its donation and reinforces the bond between oxygen and silicon.

Anyhow, this misrepresentation is understandable, given the state of the technology and the limited resources at the time.

It was not until 1992 that Herman and Wojnowski presented an alternative explanation based on quantum mechanics[32]. This model has been recently corroborated by J. Chojnacki[211,222], who ran several computer simulations making use of the Gaussian software package, supporting the fact that no π bonding is established between sulfur and silicon. According to the new theory, the π molecular orbitals are not implicated in the bond distance variations in the case of trialkoxysilanethiolates but the changes are attributed to the anomeric effect (hyperconjugation). Actually, there is an overlapping between the lone pairs from S and the antibonding $\sigma^*_{Si\text{-}O}$ orbitals and as the antibonding orbitals become more populated, the Si-O bonds get weaker.

In figure 13, a variation of the electron density on the sulfur atom induced by protonation of the molecule, causes changes on the Si-S and Si-O distances as well as on the S-Si-O angles[222]. The influence of different substituents on the molecule geometry after deprotonation[211] can be appreciated on the next page in figs. 14 and 15.

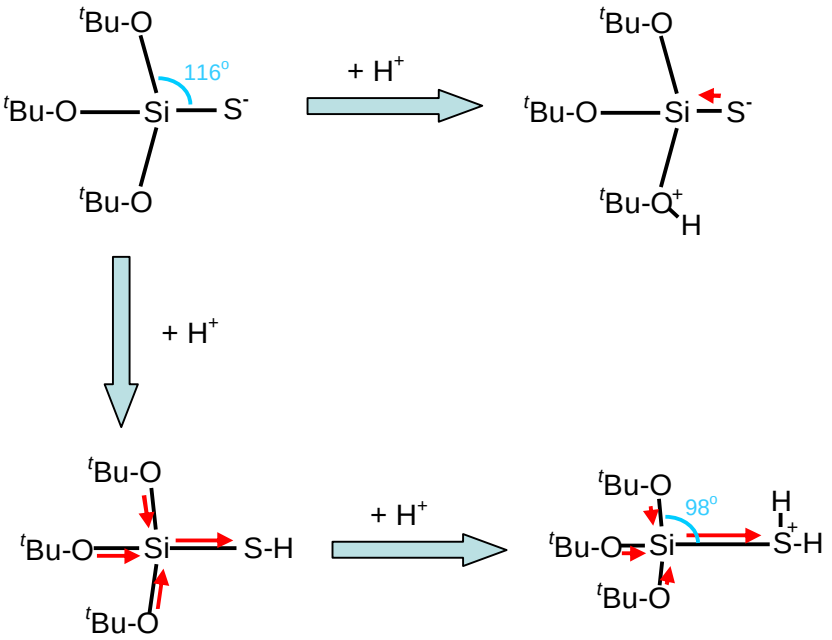

Fig.13. Geometry changes diagram upon protonation in the case of $(^tBuO)_3SiSH$, according to J. Chojnacki.

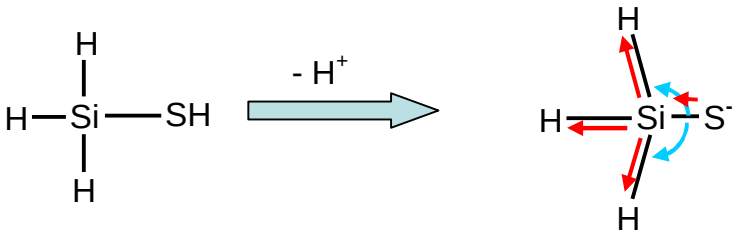

Fig.14. Geometry changes diagram upon deprotonation in the most simple case: H_3SiSH.

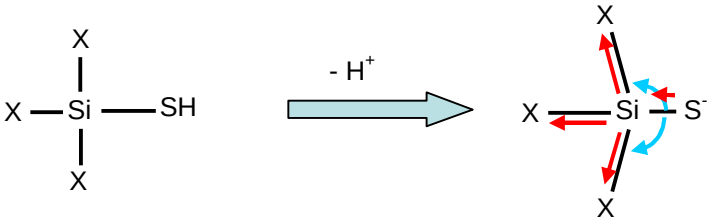

Fig.15. Geometry changes diagram upon deprotonation in a general case. X= F-, Cl-, Br-, CH_3O-, CH_3CH_2-.

According to these findings, the more anionic the character of the $(^tBuO)_3SiS^-$ is, the shorter the Si-S bond[211]. Or reformulating: The higher the positive charge on the S atom, the longer the Si-S bond.

Due to the differences in electronegativity, a dipole is established between the silicon atom and the substituent atoms it is bound to.

X-----Si-----S^-
dipole

For silanethiolates, the energetic stabilization requires the highest possible delocalization of negative charge which is better accomplished by bigger, more polarizable X substituents. If we organize according to stability: Br > Cl > F > O > H > C. However, electronegativity also influences the Si-S bond length. The more electronegative X is, the lesser distance of the Si-S bond will be achieved[211]. Thus, organizing according to Si-S length: F < O < Cl < Br < C < H

Another of the requirements for energetic stability upon deprotonation is the widening of the X-Si-S angle. The higher the difference of electronegativity between the dipole atoms, the bigger the repulsion with the negative charge of the S atom will be, and therefore, the wider the angle X-Si-S. In the case of $(^{t}BuO)_3SiSH$, the bulky *tert*-butoxy groups prevent the molecule from reaching the optimal angles, which explains the abnormally high pK_A of this species[211].

2.3.5. Silanethiolates

Silanethiolates are the silicon substituted analogues of organic thiolates. Transition metal silanethiolate complexes have been studied for more than twenty years[223]. However, it has only been recently that the most common transition metals have started to receive due attention, with prior work mostly centered in group 11 and 12 post transition metals. Kovacs *et al.*[47] point at the analogous chemistry of silanethiolates and hydrosulfides. They rationalized that the insertion of SO_2 into the S-H bond of sulfhydryl complexes to yield the corresponding hydrothiosulfites [M-SS(O)OH] should undergo in an analogue manner as the insertion reactions of SO_2 into the Si-S bond of ruthenium silanethiolates to give O-silyl thiosulfito complexes. While they could not provide any conclusive proof of the formation of such products, they managed to give an alternative explanation based on the reaction of silanethiolates of Ru(II) with isothiocyanates to give 2S,S-dithiocarbamato complexes. Trialkyl- or trialkoxysilanethiolate complexes can be regarded as protected metal sulfides according to some authors[224]. In general, metal silanethiolates offer an alternative view of the S-M bond to those of organic thiolates and sulfides, which could be of interest to solve determined questions in the field of bioinorganic chemistry.
As shown before (see sections 2.3.2 and 2.3.3), intensive research has been done regarding metal thiolates biological importance, such as their function in the active sites of several metalloproteins such as ferredoxins or rubredoxins; modeling these sites, or as antioxidants. Furthermore, thiolates have shown a significant number of technological applications as precursors of metal-sulfur clusters or the development of catalytic models. Metal silanethiolate complexes have arisen interest as an alternative to thiolates in these situations[44] and provide several advantages when compared to them. First, they are more readily cleaved under mild conditions than thiolates. The Si-S bond shows significantly higher lability than the C-S bond, thus providing an energetically more favorable source of metal sulfide clusters than thiolates. What is more, their reactivity can be controlled by the steric and electronic properties of the substituents in the silyl group[36,48].

In any case, the use of silanethiolates is not absent of inconveniences. For instance, they show high sensitivity to temperature and moisture, undergoing hydrolysis easily. One of the few exceptions is tri-*tert*-butoxysilanethiol, which is stable towards water and heat[213].

Silanethiols react readily against alkaline metals to give the corresponding silanethiolates[200,210]:

$$R_3SiSH + M^I \longrightarrow M^ISSiR_3 + ½\ H_2$$

The velocity of this reaction increases with the size of the cations: K > Na > Li

Several silanethiolates (including triarylo- and trialkoxysilanethiolates) have been obtained making use of this method. However, the lithium triphenylsilanethiolate required a different pathway[200]:

$$Ph_3SiSH + PhLi \longrightarrow LiSSiPh_3 + C_6H_6$$

Alkaline trialkoxysilanethiolates are highly hygroscopic, decomposing into the hydroxide and the silanethiol when mixed with water[210]:

$$M^ISSi(OR)_3 + H_2O \longrightarrow (RO)_3SiSH + M^IOH$$

However, the hydrates of these salts are surprisingly stable[225,226]:

$$Ph_3SiSH + Na \longrightarrow NaSSiPh_3.(H_2O)_3$$

With these alkaline salts, triorganothiosilanes and silathianes were obtained[200]:

$$NaSSiPh_3 + RX \longrightarrow Ph_3SiSR + NaX$$

$$NaSSiPh_3 + I_2 \longrightarrow Ph_3SiSSiPh_3$$

With alkaline earth metals, the reaction takes place more slowly[210]:

$$2(RO)_3SiSH + M^{II} \longrightarrow M^{II}\ \{SSi(OR)_3\}_2 + H_2$$

Where M^{II} = Sr, Ba, Ca

Also, the corresponding hydrates have been obtained[227] in a few cases:

$$(^tBuO)_3SiSH + Ba \longrightarrow [Ba\{SSi(O^tBu)_3\}_2].(H_2O)_3$$

The fact that tri-*tert*-butoxysilanethiolates of Hg(II) and Cu(I) can be prepared from oxides, while ZnO does not dissolve in $(^tBuO)_3SiSH$ can be attributed to the tendency for soft bases like thiolates to react more readily with soft acids (Hg^{2+}) than with hard acids (Zn^{2+}).

2.3.6. Silanethiolates of iron(II)

As mentioned before, the study of silanethiolates of the most common transition metals has been neglected for several years and so far, there are very few examples of iron silanethiolates[44-51]. All of them have been synthesized within this decade and despite their number, they already exhibit a variety of heterogeneous structures that rivals that of iron thiolates.

In 2002, Komuro *et al.* reported the first series of silanethiolates of iron(II) ever characterized. Amongst them, the dimeric $[Fe\{N(SiMe_3)_2\}(\mu\text{-}SSiPh_3)]_2$ and $[Fe(SSiPh_3)(\mu\text{-}SSiPh_3)]_2$ already evidenced that the synthesis of biologically relevant Fe-S clusters can be attained by means of inorganic reagents. Likewise, with the synthesis of $(PPh_4)_2[MoS_4\{Fe(SSiPh_3)_2\}_2]$, Komuro[44] demonstrated that silanethiolates can be useful in the development of novel heteronuclear clusters. Additionally, Komuro's group has also managed to isolate and characterize a small group of mononuclear iron(II) silanethiolates: $[Fe(SSiPh_3)_2(4\text{-}^tBupy)_2]$, $[Fe(SSiPh_3)_2(PEt_3)_2]$, $[Fe(SSiPh_3)_2(tmeda)]$ and $[Fe(SSiMe_2Bu^t)_2(tmeda)]$. In 2003, Komuro[228] presented a paper concerning the synthesis of the first silanedithiolates, obtained indirectly by reaction of hexamethylcyclotrisilathiane $(Me_2SiS)_3$ with transition metal acetates and halides. Two reactions of $(Me_2SiS)_3$ with iron acetate yielded the subsequent silanedithiolates: $[Fe(S_2SiMe_2)(PMDETA)]$ and $[Fe(S_2SiMe_2)(Me_3TACN)]$.

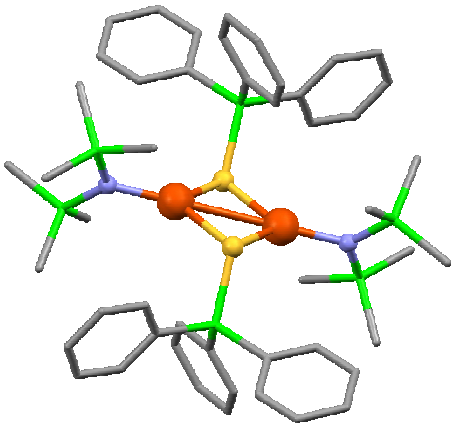

Fig.16. Structure of $[Fe\{N(SiMe_3)_2\}(\mu\text{-}SSiPh_3)]_2$ according to Komuro *et al.*

Regarding silanedithiolates, Tokitoh *et al.* reported recently the synthesis of the first stable silanedithiol which is a remarkable feat, given the extremely instable nature of silanedithiols. This has been accomplished by the utilization of very sterically demanding groups. As a result, more news are expected in the near future from Tokitoh's and Komuro's groups concerning new silanedithiolates.

The problem of aggregation is the main object of study for O. L. Sydora and coworkers[45,49]. Some time ago, they predicted that bulky sterically hindered ligands could lead to the formation of polynuclear clusters. Using iron(II) *tert*-butylsilanethiolates as tetrahedral building blocks of the type $[M(\mu\text{-}X)(\mu\text{-}Y)]_n$ this group was able to synthesize the fascinating structures of two ferrous wheels, $[Fe(\mu\text{-}X)(\mu\text{-}SSi^tBu_3)]_{12}(C_6H_6)_n$ X=Cl, Br, and a "ferrous

ellipse", $[Fe(\mu\text{-}I)(\mu\text{-}SSi^tBu_3)]_{14}(C_6H_6)_n$. Similar gigantic macrocyclic clusters are known for thiolates, but they seldom form iron(II)-only structures and the closest relatives involve iron in its +3 oxidation state.

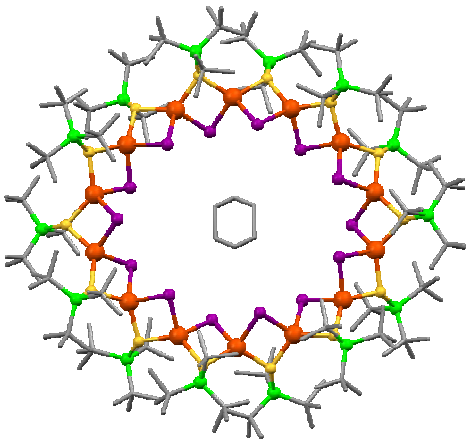

Fig. 17. Structure of the ferrous ellipse $[Fe(\mu\text{-}I)(\mu\text{-}SSi^tBu_3)]_{14}(C_6H_6)_n$ according to O. L. Sydora *et al.*

Another exceptional compound from Sydora's work is the cubane cluster $[\{(^tBu_3SiCC)Fe(\mu\text{-}SSi^tBu_3)\}_4(C_6H_6)_3]$. Although 4Fe-4S clusters are common and their synthesis from organic aryl- and alkylthiolates has been known for several years, this cluster presents several unique features. First, the bridging sulfur atoms come from the silanethiolate instead of being isolated sulfides, reinforcing Kovacs' thesis that silanethiolates can be considered as protected sulfides. Second, the structure of the cube is almost that of a perfect hexahedron which is the only such case for a Fe_4S_4 cluster to be found in the CCDC database. The rest of such clusters in the database present a significant (to say the least) distortion from a perfect cube.

Amongst the rest of Sydora's silanethiolates, we find a few dinuclear complexes: $[\{X_2Fe\}(\mu\text{-}SSi^tBu_3)_2\{FeX(thf)\}]Na$ (where X= Cl, Br), $cis[\{I(thf)Fe\}_2(\mu\text{-}SSi^tBu_3)_2]$ and $[\{(^tBu_3SiS)Fe\}_2(\mu\text{-}SSi^tBu_3)_2]$, which upon additional work produces the tetrahedral $[Fe(SSi^tBu_3)_2(THF)_2]$.

R. H. Holm, whose experience concerning iron-sulfur relationships spans 30 years, presented in 2004 a different approach towards the synthesis of silanethiolate Fe-S clusters[46]. He explored the substitution route starting from a standard $[Fe_4S_4(SR)_4]^{2-}$ cubane cluster. The reaction:

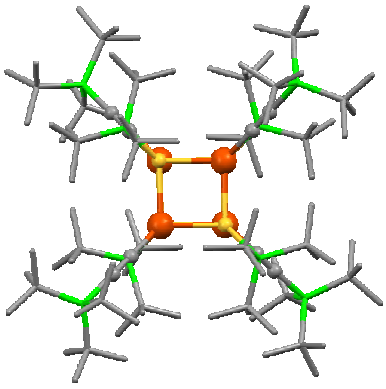

Fig. 18. Structure of the cubane cluster $[(^tBu_3SiCC)Fe(\mu\text{-}SSi^tBu_3)]_4$ according to O. L. Sydora *et al.*

$$[Fe_4S_4(PPr^i{}_3)_4](BPh_4) + (Ph_4P)(SSiPh_3) \xrightarrow{THF/CH_3CN} [Fe_4S_4(PPr^i{}_3)_3(SSiPh_3)]$$

yields a typical cubane cluster with one of its ligands substituted by a silanethiolate moiety. Further work with this cluster, produced the dicubane $[Fe_8S_8(PPr^i{}_3)_4(SSiPh_3)_2]$.
I. Kovacs *et al.*[47], whose interest in silanethiolates stems from the similitude of their reactivity with that of hydrosulfides, have also reported the synthesis of two iron(II) silanethiolates, $[CpFe(CO)_2SSi^iPr_3]$ and $[CpFe(CO)_2SSiPh_3]$. They draw attention to the fact that these iron complexes do "not undergo dimerization via CO loss in solution, which is a typical reaction of complexes of the type $[CpFe(CO)_2SR]$ (R = alkyl, aryl)" and studied the insertion of SO_2 into the Si–S bond.

While studying the chemistry of low-coordinate iron(II) fluoride complexes, Javier Vela and coworkers[50] proposed the use of transition metal fluorides as precursors of other species. Exploiting the silyl affinity of the fluoride ligand to generate new compounds, they managed to synthesize the first three coordinate (trigonal planar geometry) silanethiolate. Thus, the reaction of $[L^{tBu}FeF]$ (L^{tBu} = β-diketiminate) with hexamethyldisilathiane in stoichiometric amounts, yields $[L^{tBu}FeSSiMe_3]$.

Finally, the last addition to the growing family of iron silanethiolates comes from a contribution of Kückmann's group[51], whose general interest towards silylchalcogenolato complexes has led them to the synthesis of $[CpFe(CO)_2SSi^tBu_3]$, which displays a similar structure to Kovacs' silanethiolates.

Note: Annex A summarizes all syntheses of iron silanethiolates published up to date.

3 AIM OF THIS WORK

The study of metal thiolates has provided fructiferous since very important materials from the point of view of both technology and biology have been obtained. Self assembled thiolate monolayers have provided a background for further development of nanotechnology and are still a very active field of investigation. Moreover, several studies demonstrate that the thiolate approach is a good model for certain proteins and enzymes.

Specifically in the field of Fe-S proteins, thiolates have provided a route to the artificial synthesis of metal sites and clusters of capital importance in iron metalloproteins (rubredoxins and ferredoxins) and enzymes such as hydrogenases, aconitases and nitrogenases. However, the use of silanethiolates of iron as models has so far been neglected.

Taking in account the literature, artificial Fe-S clusters are readily synthesized when dealing with iron(II) thiolates, but so far the only examples concerning silanethiolates are a [8Fe-8S] double cubane cluster to which a silanethiolate ligand is bound by substitution and big macromolecular Fe-S wheels, which require of different techniques. At a more advanced level of the investigation, we aim to synthesize such Fe-S clusters making use of the $(^{t}BuO)_3SiS^-$ ligand and to establish its relationship with similar clusters of biological origin.

According to the CCDC database, only a few silanethiolates of iron(II) have been isolated and characterized. Recently, the synthesis of certain triarylosilanethiolates of iron(II) was reported by T. Komuro and co-workers. However, they make use of very specific reagents

which take time – and therefore, money – to synthesize. Instead, we aim to use much simpler, readily available reagents, which are economically affordable. Despite this does not change the scientific value of the work by any means; from the point of view of engineering it is of the uttermost importance to minimize costs so that if the reaction is escalated to the industrial level, the costs are not ridiculously exorbitant.

In this work, we aim to prove the viability of the synthesis of new trialkoxysilanethiolates of iron(II) from common halogenide iron salts ($FeCl_2$ and $FeCl_3$), as well as to determine their structure and general properties and to provide a framework linking them to other metal trialkoxysilanethiolates. With the introduction of $(^tBuO)_3SiSH$ as the reagent, we expect to offer a novel, cheap and purely inorganic approach to the synthesis of these biologically relevant centres. As a result, we aim to expand the general knowledge of silanethiolates of iron(II) and increase the number of compounds belonging to this group.

Most complexes are expected to be heteroleptic, but the possibility of obtaining a homoleptic compound cannot be discarded. Likewise, taking in account previously synthesized transition metal silanethiolates; it may also be possible to obtain a dimeric or tetrameric compound.

4 EXPERIMENTAL

4.1. Materials

Due to the inherent instability of the complexes of iron(II) under aerobic conditions, we were forced to work in an absolutely water and oxygen free atmosphere; therefore, we used standard Schlenk techniques for the manipulation and storage of the reagents and the products.

Because of the sensitivity of the products, all materials had to meet exceptional requirements of purity and cleanliness. Schlenk flasks and tubes were carefully cleaned with methanol and ethyl acetate, and then dried for several hours prior to use. After each use, the flask was further cleaned with an HCl solution in order to remove any residues remaining in the flask. Also, plastic cannulae were preferred instead of more common stainless steel ones – since the metallic cannulae started corroding in the middle term, contaminating the samples.

All the solvents and some reagents in liquid state which were sensitive to the atmosphere had to be conveniently dried and purified. Details for each case are given below:

- Methanol, if necessary, was conveniently dried with magnesium methanolate and distilled prior to use under argon atmosphere.

- Ethanol was purchased from P.P.H. "Standard" (www.standard.com) and used as provided.
- Acetonitrile was purified and dried by addition of phosphorous pentoxide, left still for few days and then distilled.
- Elementary sulfur was available from a commercial supplier in our laboratory and used as provided.
- Tri-*tert*-butoxysilanethiol was prepared for further experiments.

  First, silicon disulfide was synthesized with the method developed in 1962 by R. Piękoś and W. Wojnowski[206]. 820 g of powdered elemental sulfur were used for each batch. They were mixed with 320 g of high purity (95%) ferrosilicon and finally about 2% BaO_2 (~230 g) was added. The whole mixture was put inside a steel container which was set off with the help of a metallic magnesium fuse providing a high enough temperature for the reaction to start. The gray solid silicon disulfide formed afterwards was finely crushed and kept in a desiccator.

  Next, the alcoholysis process of the silicon disulfide took place. 207 g (2.25 mol) of the finely crushed disulfide were poured into a reactor and mixed with stirring in 741ml *tert*-butanol for one day. Following, while the stirring continued, the temperature of the reactor was increased slowly from 50ºC to 75ºC during the first 48 hours and then the temperature was maintained for about three weeks. Afterwards, both heating and stirring were halted and the mixture was left still so that the solid deposited at the bottom.

  Finally, the mixture was separated by decantation and the liquid was distilled. The first fraction (82-83ºC), containing unreacted *tert*-butanol, was dismissed while the second fraction (140-145ºC) collected at reduced pressure of ca 30-40 mm Hg contained tri-*tert*-butoxysilanethiol. It was further purified by addition of a few drops of metallic mercury. The excess of sulfur reacted against the mercury giving a black residue which was removed by filtration. More mercury was added and the mixture was filtered repeatedly until no signs of reaction could be observed.

- Triethylamine was purified by addition of an alkaline hydroxide (KOH or NaOH) and dried by double distillation in presence of the hydroxide.

- 25g of $FeCl_2.4H_2O$ (99.99% pure) were purchased from Sigma-Aldrich Inc. Since we have previously had problems with oxidation of less pure iron(II) chloride, this sample was conveniently stored in a desiccator under vacuum in order to preserve its quality.

- Pyridine, α-picoline, β-picoline, γ-picoline, 3,5-lutidine, piperidine, piperazine (both hexahydrated and anhydrous), morpholine and TMEDA were treated with an

alkaline hydroxide (KOH or NaOH) and distilled in presence of the hydroxide prior to use.

- N-methylimidazole and phenanthroline monohydrate were commercially available and were used as supplied.

- Reactive red selenium was used in a few tests. To avoid the appearance of gray selenium which is not so reactive, red selenium was prepared right before its utilization according to the equation:

$$SeO_3^{2-} + N_2H_4.H_2SO_4 \longrightarrow Se + SO_4^{2-} + N_2 + 3H_2O$$

4.2. Equipment

4.2.1. X-ray diffractometry

The crystal and molecular structure determinations were performed by K. Baranowska using the X-ray facility of the Inorganic Chemistry Department at Gdańsk University of Technology. Experimental intensity data were collected on a KM4 EXCALIBUR (Kuma Diffraction) diffractometer, goniometer equipped with Sapphire 2 CCD detector (Oxford Diffraction) and with an Oxford Cryosystem-Cryostream cooler. Monochromatic MoKα radiation (λ 0.71073Å) and crystal-detector distance of 50 mm were used.

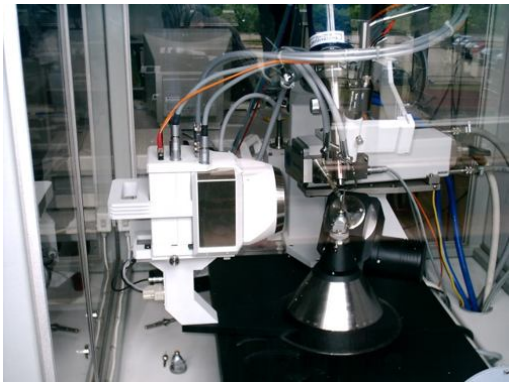

Fig. 19. KM4 EXCALIBUR diffractometer

Data collection: CrysAlis CCD (Oxford Diffraction, 2006); cell refinement: CrysAlis RED (Oxford Diffraction, 2006); data reduction: CrysAlis RED; program(s) used to solve structure: SHELXS97 (Sheldrick, 1997)[287]; program(s) used to refine structure: SHELXL97 (Sheldrick, 1997); molecular graphics: ORTEP-3 (Farrugia, 1997)[288] and Mercury (Macrae *et al.*, 2006)[289]; software used to prepare material for publication: WinGX (Farrugia, 1999)[290].

4.2.2. FTIR spectrometry

The IR spectra registered were obtained from two samples in the solid state. The first one was mixed with 400 mg of KBr and compressed into a pellet, then measured with an FTIR Mattson Genesis II Gold spectrophotometer, controlled externally by a computer using the WinFirst software package and covering the range 4000-400 cm^{-1}. The second sample was in pure state and the measurement was performed with a Momentum microscope attached to the Mattson Genesis Gold spectrometer (IR source). With such a setup, the range covered was only between 4000-700 cm^{-1}.

Fig. 20. Mattson Genesis II Gold spectrometer with Momentum microscope attached.

4.2.3. UV-Vis spectrometry

UV-Vis spectra were recorded in a UNICAM UV300 spectrophotometer, equipped with a wolfram and deuterium lamp and controlled externally with the software package VISION32. The sample was dissolved in CCl_4 and the solution was analyzed in a quartz tray 1cm wide. The spectra obtained covered the range 265-1000nm.

Fig. 21. UNICAM UV300 spectrophotometer and the controlling pc.

4.2.4. Voltammetry

Cyclic voltammetry is the most straightforward method to elucidate the redox activity of a compound. In the case of [4Fe-4S] clusters, this method shows clearly the variation in the charge of the core as well as it can provide a route to obtain other derivative clusters (for instance, of the Fe_3S_4 type). Cyclic voltammetry was performed at the Chemical Technology Department of the Gdansk University of Technology on an AutoLab PGStat 10 (Eco-Chemie, The Netherlands). Carbon cathodes were used for the experiment.

4.2.5. Magnetic susceptibility and electron paramagnetic resonance measurements

The measurements were attempted only for the most stable silanethiolate [4Fe-4S] cluster **[II]** and were kindly performed at the Faculty of Chemistry of the University of Wrocław by J. Jezierska and L. Jerzykiewicz with a Quantum Design SQUID magnetometer and Bruker ESP 300E EPR spectrometer. The preliminary results obtained for two samples of **[II]** could not be reliably interpreted. They were not reproducible most probably due to the chemical changes (*e.g.* decomposition and/or oxidation) of the samples during the storage and operations. Further investigations are necessary.

4.3. Syntheses of iron silanethiolates

To avoid the oxidation of iron(II), all these reactions had to take place in a completely oxygen free environment, under dinitrogen or argon atmosphere, using standard Schlenk techniques. It was of the uttermost importance to keep the reagents in excellent conditions, since the frontier that separates usable from unusable compounds is very thin and can be easily crossed without noticing. The ascertaining of what could have been wrong when a reaction fails is often puzzling, since generally the visual appearance of the reagents is not out of the norm even when they contain enough quantity of O_2 to spoil the reaction. When identified, it is usually enough to distil the troubling reagent once more to recover its lost performance. However, guessing which one is the contaminated reagent (or solvent) is in most cases not trivial.

In case that some O_2 enters the flask during the initial steps of the reaction, the presence of $(^t\text{BuO})_3\text{SiSH}$ will prevent the metal to be oxidized, since it can reduce Fe(III) to Fe(II) while oxidizing itself to $(^t\text{BuO})_3\text{SiSSSi}(\text{O}^t\text{Bu})_3$. In case that there is such reaction, transparent crystalline plates of the disulfide will appear. However, it happened relatively often that the quantity of oxygen that entered the flask was far too much for the silanethiol to counter its effects, causing the total oxidation of the Fe(II) to Fe(III) and, thus rendering the reagents unusable. If the $FeCl_2.4H_2O$ does not meet the desired purity requirements, but is not completely oxidized, it can still be used after adequate filtering.

Note that due to the methodology used, the weight of the reagents could oscillate considerably in subsequent repetitions of the same reaction. Therefore, we offer below the relative quantities in molar ratios; but in any case, it has to be considered that the initial quantity of $FeCl_2$ fell in most cases in the 75-150 mg range.

The procedure to identify our products was mostly the same in all cases. We tried to obtain the product in crystalline state and then, it was submitted to the laboratory of crystallography for X-ray analysis to be performed (see Section 4.2.1.).

4.3.a. Standard procedure

We developed two general methods for the synthesis of silanethiolates of iron(II), depending on the reagents used.

Method 1. Reaction of a trialkoxysilanethiol with an iron(II) salt:

A solution of $FeCl_2$ was made to react with a mixture of $(^tBuO)_3SiSH$ and Et_3N, keeping the proportions at 1:2:2 molar ratio. Variations of these proportions did not provide significantly better results.

Two solutions were prepared as follows:

- Solution 1A. Pure $FeCl_2.4H_2O$ was dissolved in methanol (10 ml MeOH/mmol $FeCl_2$) under inert atmosphere, giving a light yellow solution.

- Solution 1B. $(^tBuO)_3SiSH$ was mixed with Et_3N and 2 ml MeOH/mmol Et_3N were added to dissolve the mixture.

As soon as both solutions were ready, Solution 1B was poured into Solution 1A, which acquired a dark green color.

Reaction 1. At this point, if the flask is left in the fridge for one week, a big amount of small pale transparent crystals of $[Fe\{SSi(O^tBu)_3\}_2(MeOH)_4]$ **[I]** will precipitate on the bottom of the flask. Occasionally, especially if it stands for a long time at low temperature, also thin black needles of $[Fe_4S_4\{SSi(O^tBu)_3\}_4](Et_3NH)_2$ **[II]** may appear. We assume the reaction leading to **[I]** occurs according to:

$$FeCl_2.4H_2O + 2(^tBuO)_3SiSH + 2Et_3N \xrightarrow{methanol} [Fe\{SSi(O^tBu)_3\}_2(MeOH)_4] + 2Et_3NHCl \quad (1)$$

Reaction 2. If the crystallization of the mixture takes place at room temperature, then **[II]** is the only product. Similarly, when crystals of **[I]** were dissolved again at room temperature, a new crystallization in the fridge only yielded needles of the cubane cluster **[II]**. The reaction can be summarized according to the following scheme:

$$4FeCl_2.4H_2O + 8(^tBuO)_3SiSH + 10Et_3N \xrightarrow{methanol} [Fe_4S_4\{SSi(O^tBu)_3\}_4](Et_3NH)_2 + 8Et_3NHCl + (?) \quad (2)$$

However, the exact mechanism has not yet been elucidated. According to the reagent ratio, the product was obtained with an efficiency of about 30% in the best cases.

[I] was too sensitive to be examined without decomposing, but **[II]** resulted stable enough to perform more in-depth analysis. Thus, **[II]** was subject to IR and UV-Vis spectrometry analysis in the laboratory of spectrometry at the Inorganic Chemistry Department of the Gdansk University of Technology. The resulting FTIR spectra are shown in section 5.B.

Method 2. Reaction of a trialkoxysilanethiol with an iron(III) salt:

The procedure was similar to method 1, but an excess of $(^t BuO)_3SiSH$ was added to reduce the Fe(III) to Fe(II). Thus, the proportion $FeCl_3$:$(^t BuO)_3SiSH$:Et_3N was kept at 2:5:4 molar ratio. Again, two solutions are prepared:

- Solution 2A. A 0.4M solution of pure $FeCl_3$ in methanol (2.5 ml MeOH/mmol $FeCl_3$) was prepared. It was filtered under dinitrogen atmosphere to remove impurities.
- Solution 2B. The $(^t BuO)_3SiSH$ was dissolved into a 1M solution of Et_3N in methanol (1 ml MeOH/mmol Et_3N).

Solution 2B was poured into Solution 2A via a cannula. As soon as both liquids entered in contact, the mixture turned dark red.

Reaction 3. Shortly after, several thin plates of $(^t BuO)_3SiSSSi(O^t Bu)_3$ started to appear on the surface of the solvent. They were filtered off and the filtrate was left in the freezer for crystallization. After some weeks, a few needles of **[II]** precipitated on the bottom of the flask. Reaction scheme 3 summarizes the reagents:

$$4FeCl_2 + 10(^t BuO)_3SiSH + 14Et_3N \longrightarrow [Fe_4S_4\{SSi(O^t Bu)_3\}_4](Et_3NH)_2 + 12Et_3NHCl + (^t BuO)_3SiSSi(O^t Bu)_3 + (?) \quad (3)$$

4.3.b. Addition of N-donor heteroligands

We were able to expand the previous methods by addition of different N-donor co-ligands. We used preferably method 1 in order to save reagents – since the reaction is basically the same and part of the silanethiol is consumed only to reduce the metal. Note that according to the following procedures, the co-ligand can be added at different stages of the reaction. In general, the synthesis proceeds anyway independently of the time at which the N-donor

ligand is added, but in some cases no crystals were produced and in others, the crystals obtained were not of the desired quality. Therefore, we reproduce below the description of the work that provided the best results for every synthesis.

Reaction 4. We started from method 1. After the reaction was complete, an excess of pure pyridine was added, which caused the solution to turn bright yellow. The proportion of pyridine respect to iron(II) chloride was 2.5:1 (py:$FeCl_2$). Soon after adding the co-ligand, a lot of small yellow crystals began to precipitate. The flask was left in the fridge for several days until the crystals grew to an appropriate size for performing X-ray analysis, which revealed that they belong to $[Fe\{SSi(O^tBu)_3\}_2(py)_2]$ **[III]**.

$$FeCl_2.4H_2O + 2(^tBuO)_3SiSH + 2Et_3N + 2.5py \longrightarrow [Fe\{SSi(O^tBu)_3\}_2(py)_2] \quad (4)$$

Reaction 5. In this case, we substituted methanol by acetonitrile in method 1. Twice as much acetonitrile was used to dissolve the silanethiol and the triethylamine (*i.e.* solution 1B was 0.5M instead of 1M). At this point, the solution turned red and after a few minutes of vigorous stirring, its color turned to dark green. Finally, some piperidine was added in stoichiometric ratio. After one week, small yellow crystals appeared and were identified as $[Fe\{SSi(O^tBu)_3\}_2(pip)_2]$ **[IV]** by X-ray analysis.

$$FeCl_2.4H_2O + 2(^tBuO)_3SiSH + 2Et_3N + 2pip \longrightarrow [Fe\{SSi(O^tBu)_3\}_2(pip)_2] \quad (5)$$

Reaction 6. Reaction started as stated in method 1. The solution was red in the beginning, but turned dark green after vigorous stirring. Then, an excess of 6 mol of morpholine were added for each mol of $FeCl_2$, according to the following scheme:

$$FeCl_2.4H_2O + 2(^tBuO)_3SiSH + 2Et_3N + 6morph \longrightarrow [Fe\{SSi(O^tBu)_3\}_2(morph)_2] \quad (6)$$

At this point, the flask was left in the freezer for crystallization. After few weeks, yellow crystalline needles could be appreciated within a green precipitate. Some of them were collected for X-ray analysis, which revealed that they correspond to $[Fe\{SSi(O^tBu)_3\}_2(morph)_2]$ **[V]**.

Reaction 7. The synthesis was performed according to method 1, but α-picoline (2:1 molar ratio if compared to $FeCl_2$) was added to Solution 1B before mixing it with Solution 1A. The color of the resultant solution turned lime yellow-green as a fine precipitate started to appear. The flask was left in the fridge at -3ºC overnight. The following day, some amount of the green precipitate had settled on the bottom of the flask and it was left in the freezer at -10ºC. On the third day, some crystals were found on the bottom of the flask and were subsequently submitted to X-ray analysis, revealing that they belonged to the previously unknown complex $[Fe\{SSi(O^tBu)_3\}_2(\alpha\text{-pic})(MeOH)_2]$ **[VI]**.

$$FeCl_2.4H_2O + 2(^tBuO)_3SiSH + 2Et_3N + 2(\alpha\text{-pic}) \longrightarrow [Fe\{SSi(O^tBu)_3\}_2(\alpha\text{-pic})(MeOH)_2] \quad (7)$$

Reaction 8. Again, the co-ligand was added in the previous stages of method 1. In this case, an excess of β-picoline was added to Solution 1A, giving a yellow solution. When mixed with Solution 1B, the color changed into orange-yellowish. The flask was then left in the fridge for some time. Three days later, some small yellow crystals could be appreciated on the bottom of the flask. After three more days, the solution had turned red (a clear indicator of oxidation), but still some yellow crystals remained, which were immediately submitted to X-ray analysis. The obtained structure revealed the crystals belonged to the chelating complex $[Fe\{SSi(O^tBu)_3\}_2(\beta\text{-pic})]$ **[VII]**. A scheme for this reaction is shown next:

$$FeCl_2.4H_2O + 2(^tBuO)_3SiSH + 2Et_3N + 2(\beta\text{-pic}) \longrightarrow [Fe\{SSi(O^tBu)_3\}_2(\beta\text{-pic})] \quad (8)$$

Reaction 9. As in the previous synthesis, the heteroligand was added to Solution 1A of method 1. Thus, a 3:1 molar excess of γ-picoline was added to it, before mixing with Solution 1B. It was observed that as soon as half of the content was transferred to the flask containing Solution 1B, a very fine red precipitate started to appear. The flask was then left still in the freezer for six days. After this time, relatively big and well formed yellow crystals appeared on the bottom of the flask. Some of them were collected and submitted for X-ray analysis, which revealed that they belonged to a previously unknown compound: $[Fe\{SSi(O^tBu)_3\}_2(\gamma\text{-pic})]$ **[VIII]**.

$$FeCl_2.4H_2O + 2(^tBuO)_3SiSH + 2Et_3N + 3(\gamma\text{-pic}) \longrightarrow [Fe\{SSi(O^tBu)_3\}_2(\gamma\text{-pic})] \quad (9)$$

Reaction 10. Immediately after performing method 1 as described in section 4.2.a, an equivalent of 3,5-lutidine was added for each mol of $FeCl_2$, according to the following equation:

$$FeCl_2.4H_2O + 2(^tBuO)_3SiSH + 2Et_3N + (3,5\text{-lut}) \longrightarrow [Fe\{SSi(O^tBu)_3\}_2(3,5\text{-lut})] \quad (10)$$

After some weeks, small yellow plates with a tendency to stick to each other appeared on the bottom of the flask and were submitted to X-ray analysis. The results showed that the previously unknown complex $[Fe\{SSi(O^tBu)_3\}_2(3,5\text{-lut})]$ **[IX]** had been successfully synthesized.

Reaction 11. For this reaction, we slightly modified method 1 by adding tmeda in a proportion 2:1 (compared to $FeCl_2$) to Solution 1B. Shortly after the modified Solution 1B is poured into the Solution 1A, small transparent crystals started to precipitate. They were left in the freezer for 3-4 hours and then submitted to X-ray analysis. The results revealed its structure belongs to the tetrahedral chelate $[Fe\{SSi(O^tBu)_3\}_2(tmeda)]$ **[X]**. The stoichiometry of the reaction is shown next:

$(^{t}BuO)_3SiSH + FeCl_2.4H_2O + Et_3N + 2tmeda \longrightarrow [Fe\{SSi(O^{t}Bu)_3\}_2(tmeda)]$ (11)

Reaction 12. This reaction was performed under dinitrogen atmosphere using ordinary Schlenk techniques. 200 mg $FeCl_2.4H_2O$ (~1 mmol) were partially dissolved in 20 ml of acetonitrile and then filtered. Following, 1.2 ml N-methylimidazole (~6 mmol) were added which caused the color of the solution to change from pale yellow to orange. Shortly after, small transparent crystals started to precipitate. The flask was left still three days at room temperature for further precipitation and then a few crystals were collected for analysis. X ray revealed that their structure corresponded to $[Fe(N\text{-meimid})_6]Cl_2.2H_2O$ **[XI]**. Thus, the corresponding stoichiometry being:

$$FeCl_2.4H_2O + 6N\text{-meimid} \xrightarrow{\textit{acetonitrile}} [Fe(N\text{-meimid})_6]Cl_2.2H_2O \quad (12)$$

Reaction 13. 100 mg of $FeCl_2.4H_2O$ (~0.5 mmol) were dissolved in 4 ml of methanol. Traces of impurities were removed by filtration under a nitrogen atmosphere using standard Schlenk techniques. Next, 120 mg of hexahydrated phenanthroline (~0.6 mmol) were added, which caused the color of the solution to turn red and a dark-red crystalline solid to precipitate. The mixture was left undisturbed for some days at room temperature for crystallization, affording large dark-red crystals (ca 4 mm) of $[Fe(phen)_3]Cl_2.6MeOH$ **[XII]** according to:

$$FeCl_2.4H_2O + phen \xrightarrow{\textit{methanol}} [Fe(phen)_3]Cl_2.6MeOH \quad (13)$$

A few words on the instability of the silanethiolates of iron.

An account on the synthesis of the recently synthesized tri-*tert*-butoxysilanethiolates of iron would not be complete without putting special emphasis on the complications associated to the instability of these complexes. Work under inert atmosphere was necessary in all cases, as has been discussed before, but after some negative experiences we learned a few details that, although they might seem insignificant to the accidental observer, had to be taken into account because their influence played a key role in the outcome of the reaction.
First, all the reagents had to be in excellent conditions. This means that the solvents and most reagents in liquid state had to be freshly distilled prior to use. The only exception to this rule was tri-*tert*-butoxysilanethiol, which could be stored after distillation in a closed recipient for some months with no significant effects on its performance.

$FeCl_2.4H_2O$ of high purity (99.99% pure) was purchased from Sigma-Aldrich Inc. was stored under vacuum in a desiccator to avoid oxidation. Cheaper, but less pure iron(II) chloride salt is prone to oxidation, which provokes a considerable drop in reaction perform-

ance after a short time – even when it is stored in a closed recipient. Sometimes, this can be overcome by filtration of the insoluble impurities, but if these surpass a certain amount, the reaction may be restrained.

Special care has to be taken with the instruments and tools employed during the reaction. Schlenk flasks have to be carefully cleaned with HCl after each use and rinsed with distilled water in order to eliminate all possible rests that may remain on the walls. If a minimum of cleanliness is not met, the reaction will fail.

Also, plastic cannulae are preferred over metallic ones. After some use, we discovered that inoxidable steel cannulae tend to corrode fast (this is probably motivated by the high acidity of $FeCl_2$) and contaminate the sample. In order to avoid this, we substituted them with thin PVC tubes.

5 RESULTS AND DISCUSSION

5.A. Description of the synthetic road leading to the discovery of new silanethiolates of iron

We have conducted several experiments in our laboratory concerning the synthesis of silanethiolates of iron(II). As a result, we have successfully isolated and identified ten new members of this class of compounds. Namely, the following trialkoxysilanethiolates have been characterized:

$[Fe\{SSi(O^tBu)_3\}_2(MeOH)_4]$ **[I]**,
$[Fe_4S_4\{SSi(O^tBu)_3\}_4](Et_3NH)_2$ **[II]**,
$[Fe\{SSi(O^tBu)_3\}_2(py)_2]$ **[III]**,
$[Fe\{SSi(O^tBu)_3\}_2(pip)_2]$ **[IV]**,
$[Fe\{SSi(O^tBu)_3\}_2(morph)_2]$ **[V]**,
$[Fe\{SSi(O^tBu)_3\}_2(\alpha\text{-pic})(MeOH)_2]$ **[VI]**,
$[Fe\{SSi(O^tBu)_3\}_2(\beta\text{-pic})]$ **[VII]**,
$[Fe\{SSi(O^tBu)_3\}_2(\gamma\text{-pic})]$ **[VIII]**,
$[Fe\{SSi(O^tBu)_3\}_2(3,5\text{-lut})]$ **[IX]**, and
$[Fe\{SSi(O^tBu)_3\}_2(tmeda)]$ **[X]**.

Additionally, in the course of the investigation two unrelated compounds were discovered:

$[Fe(N\text{-meimid})_6]Cl_2.2H_2O$ **[XI]**, and
$[Fe(phen)_3]Cl_2.6MeOH$ **[XII]**.

Some reactions concerning the direct synthesis of silanethiolates of iron(II) have already been reported by T. Komuro, O. L. Sydora and others[44-51]. However, in every case they performed a somehow arduous preliminary work[44-47] in order to obtain the substrate. In contrast, we intend to make the synthesis from more readily available materials which should require little to none preliminary work and are more economical. Therefore, we prepared some preliminary tests with $FeCl_2.4H_2O$ and $(^tBuO)_3SiSH$ as the reagents, and Et_3N as the proton acceptor.

5.A.1. Standard reaction of tri-*tert*-butoxysilanethiol with an iron(II) salt.

In our preliminary tests, we tried four different solvents: water, toluene, methanol and acetonitrile. The rationale behind the choice of the solvents is directly related to the previous synthesis of transition metal trialkoxysilanethiolates as described in the literature. According to the literature, benzene and water are two of the most common solvents and cover a wide range of transition metals, thus we thought they would be good candidates for our synthesis, although due to safety concerns, we decided to substitute benzene with toluene to minimize risks. An additional reason for choosing water is obviously its ubiquity on Earth. Also, Kasterka, Chojnacki *et al.*[229,230] postulated the use of tri-*tert*-butoxysilanethiol for preconcentrating metal cations in a water stream, which could be of interest from an environmental point of view. Acetonitrile and methanol, on the other hand, despite not being so widely used have been reported[41,231-233] to give excellent results in the synthesis of tri-*tert*-butoxysilanethiolates of manganese(II) and were considered worth trying. In our case, all tests showed signs of a reaction going on, but only from methanol and acetonitrile could crystals be obtained as will be discussed below.

It was soon discovered that toluene was not a good option as a solvent in our case. Certainly, some reaction occurred, yielding a green-bluish powder which decomposed slowly at room temperature under aerobic conditions. However, this precipitate could not be obtained in crystalline form. It was insoluble in other solvents (ethanol, acetonitrile, THF) and it could not be re-dissolved in toluene.

If the same tests were performed in water, there was a reaction indeed as a grayish precipitate appeared after a few minutes. This solid could be dissolved in hexane, giving a dark green solution; nevertheless, it was not possible to accomplish a successful crystallization.

Following, we thought that we should focus in those reactions involving the metals more akin to iron and, as their proximity in the periodic table indicates, we judged that manga-

nese would be a good candidate. Therefore, we planned to mimic two reactions that have proven very useful in the synthesis of tri-*tert*-butoxysilanethiolates of manganese(II):

$$MnCl_2 + 1.5(^tBuO)_3SiSH + 2Et_3N \xrightarrow{\textit{acetonitrile}} [Mn\{SSi(OBu^t)_3\}_2(NCMe)]$$

$$MnCl_2 + 1.5(^tBuO)_3SiSH + 2Et_3N \xrightarrow{\textit{methanol}} [Mn\{SSi(OBu^t)_3\}_2(MeOH)_4]$$

We performed a similar reaction starting from iron(II) chloride, tri-*tert*-butoxysilanethiol and triethylamine in a 1:2:2 molar ratio. The solution rapidly turned dark green with stirring and after a few days left still in the fridge at -10ºC small transparent triclinic crystals of $[Fe\{SSi(OBu^t)_3\}_2(MeOH)_4]$ **[I]** and black thin needles of $[Fe_4S_4\{SSi(OBu^t)_3\}_4](Et_3NH)_2$ **[II]** precipitated (see pictures below). We observed that the formation of **[II]** depended on time and temperature. If the crystallization took place at room temperature, only crystals of **[II]** could be obtained. Likewise, if **[I]** was re-dissolved in methanol and re-crystallization was tried, **[II]** was the only product. As has been pointed out before somewhere else[28], such a situation strongly suggests that **[II]** is the thermodynamic product of this reaction.

When we repeated the same experiment in acetonitrile, a similar reaction seemed to take place – judging by the variation of color of the solution to dark green – and after some time in the freezer also two kinds of crystals precipitated: thin needles of **[II]** and small transparent crystals which soon decomposed under aerobic conditions turning red in the process. It is possible that these crystals belong to the iron(II) analogue of $[Mn\{SSi(OBu^t)_3\}_2(NCMe)]$, but we have no decisive proof of that since we did not succeed in producing crystals of good enough quality. The tendency for twinning of these crystals and their small size rendered them completely useless for X-ray analysis.

5.A.2. Standard reaction of tri-*tert*-butoxysilanethiol with an iron(III) salt.

Next, we decided to take a slightly different approach to the same set of reactions, taking advantage of the reducing properties of $(^tBuO)_3SiSH$. We thought that it would be possible to introduce the use of $FeCl_3$ as the reagent if an excess of $(^tBuO)_3SiSH$ was utilized to reduce all the Fe(III) to Fe(II). Thus, iron(III) chloride was made to react with a mixture of tri-*tert*-butoxysilanethiol and triethylamine keeping the molar ratio at 2:5:4. In this case, the solution first turned deep red and after some minutes stirring, it adopted a dark green color. Then, it was left in the fridge at -10ºC. After some days, black thin crystals of **[II]** appeared. This confirms that the reduction of iron is accomplished – at least to some extent –, which is in agreement with the bibliography[28]. The products are of similar quality as those obtained using iron(II) as the reagent. As mentioned before, one of the aims of this work is to achieve an economically viable method for developing silanethiolates. Since this method

requires a bigger amount of silanethiol in order to reduce the metal, the use of iron(II) salts is preferred.

5.A.3. Reaction of tri-*tert*-butoxysilanethiol with an iron(II) or an iron(III) salt in presence of elemental S.

The fact that the reactions performed previously were very similar to Christou and Garner's method[234] for obtaining $[Fe_4S_4]^{2+}$ clusters did not go unnoticed:

$$4FeCl_2 + 10RS^- + 4S \xrightarrow{methanol} [Fe_4S_4(SR)_4]^{2-} + 3RSSR + 8Cl^-$$

$$4FeCl_3 + 14RS^- + 4S \xrightarrow{methanol} [Fe_4S_4(SR)_4]^{2-} + 5RSSR + 12Cl^-$$

Therefore, we programmed two more reactions with addition of sulfur to check if we could maximize the production of **[II]**:

$$4FeCl_2 + 8(^tBuO)_3SiSH + 8Et_3N + 4S \xrightarrow{methanol} [Fe_4S_4\{SSi(O^tBu)_3\}_4](Et_3NH)_2$$

$$4FeCl_3 + 10(^tBuO)_3SiSH + 10Et_3N + 4S \xrightarrow{methanol} [Fe_4S_4\{SSi(O^tBu)_3\}_4](Et_3NH)_2$$

In both cases a lot of a black powder precipitated after some days at room temperature. However, the powder started to decompose very fast when the flasks were open, leaving an orange residue after some minutes. We repeated the same reaction several times and in some cases we managed to isolate a small amount of crystals of **[II]**, but in any case, most of the product precipitated as a black powder.

5.A.4. Study of a potential chalcogen substitution at the core of the $[Fe_4S_4\{SSi(O^tBu_3)\}_4]^{2-}$ cluster.

There is evidence that selenium can substitute the sulfur atoms in certain [4Fe-4S] clusters under mild conditions[114,117,235]. Therefore, we tried to perform such a substitution with **[II]**. Some red selenium was prepared and inserted into a flask where we had previously performed the standard reaction according to **method 1** (see section 4). After some days at room temperature, small black needles of **[II]** were isolated as the only product. The same results were obtained if the selenium was added in the first stages of the reaction, prior to the addition of silanethiol, or if preformed crystals of **[II]** were dissolved in methanol in presence of red Se.

5.A.5. Reaction of tri-*tert*-butoxysilanethiol with an iron(II) salt and N-donor coligands.

At the same time, we had continued experimenting with **reaction (1)** trying to develop new mononuclear compounds. Given that Fe^{2+} is a borderline Lewis acid, we supposed that it would be possible to obtain new structures with the use of N-donor ligands. This kind of ligands has been often used with other transition metals (*e.g.* Zn, Mn, Co, Cd), leading to the synthesis of different heteroleptic silanethiolates[34,40,236,232,237]. Influenced by these previous experiences and led by our own accomplishments, we ended up establishing several parallel routes towards new coordination complexes. This means that it was never a linear project, but rather it was branched, opening new routes as discoveries were being made. However, project branching can easily degenerate into chaos if the aim is not clear or wrong decisions are taken. To avoid this, we provided a tight control of our project by following a sensible rationale based on close relationships amongst ligands. Regrettably, not all the reactions with these ligands performed likewise and some of them did not produce any results as will be discussed below. However, our final goal, what we pretended to achieve, was in every moment clear.

The rationale behind the selection of the different heterocyclic coligands, based on their relationships and analogies, can be seen summarized in the following scheme:

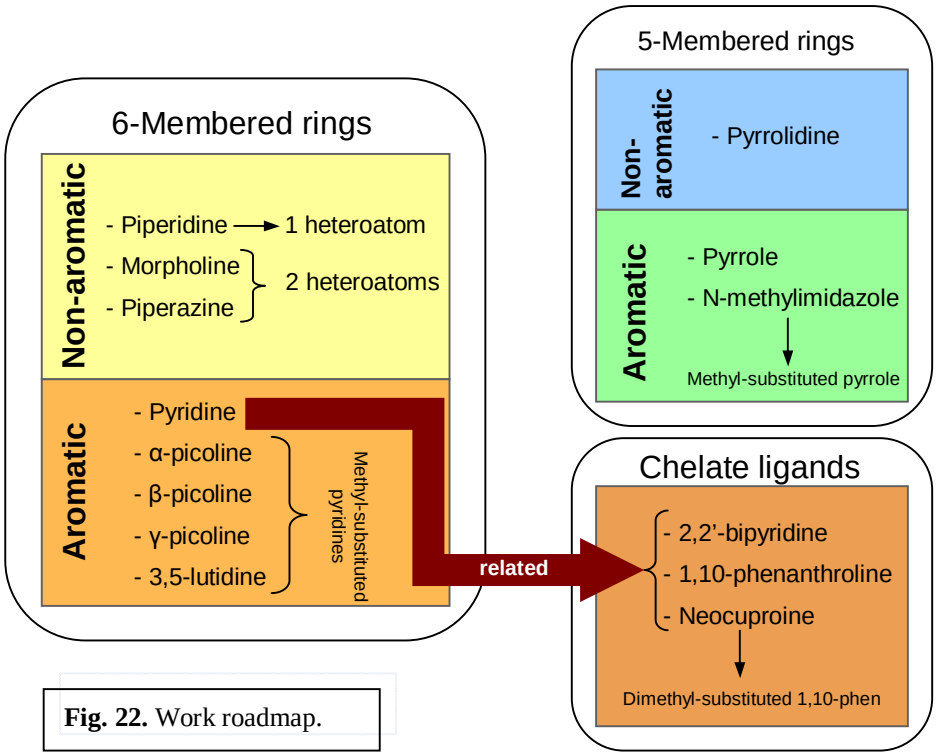

Fig. 22. Work roadmap.

Additionally, reactions with the chelating agents dmeda and tmeda were also performed. The main reason behind the choice of these two ligands was the fact that two silanethiolates of iron(II) with tmeda have already been isolated by another research group[44,48], namely $[Fe(SSiMe_2{}^tBu)_2(tmeda)]$ and $[Fe(SSiPh_3)_2(tmeda)]$ – although only the latter has been characterized structurally – and therefore the relationship trialkyl-triaryl-trialkoxy substituted silanethiolates could be established.

When dealing with this set of reactions, acetonitrile worked reasonably well as a solvent, but crystallization was complicated and only crystals of **[IV]** obtained from acetonitrile solution attained good quality. In the rest of cases, methanol gave better results, indistinctively of what coligand was involved in the reaction. Thus, after these experiments we chose to use methanol exclusively and reserve acetonitrile just for the cases were crystallization could not be accomplished from methanol. However, it turned out that in those cases where crystals could not be obtained from methanol, acetonitrile was of little use.

5.A.5.1. N-donor 6-membered rings as coligands

The reactions of tri-*tert*-butoxysilanethiol with 6-membered rings proved fructiferous. In most cases, the synthesis of the expected heteroleptic complexes was achieved. All of them were isolated as disilanethiolates, and they stand out for their structural heterogeneity. It was empirically demonstrated that the order of the reagents does not affect the synthesis of the products, although generally the N-donor ligand was introduced in a final step.

If pyridine or piperidine are added to **reaction (1)**, the corresponding reactions afford the tetrahedral complexes $[Fe\{SSi(O^tBu)_3\}_2(py)_2]$ **[III]** and $[Fe\{SSi(O^tBu)_3\}_2(pip)_2]$ **[IV]**, respectively. **[III]** was isolated as small yellowish triclinic crystals with high tendency to twinning, which made difficult its structural characterization. The yellow monoclinic crystals of **[IV]** were in a purer state and were soon characterized structurally.

These results encouraged us to keep on this investigation line. Thus, we chose two other N-donor heterocyclic bases which are closely related to piperidine: morpholine and piperazine. In both cases, the reaction seemed to occur in a similar way. After the standard procedure – **reaction (1)** – was concluded, addition of the coligand provoked a change in the color of the solution. The flask was then left at low temperature for some days until small yellow crystals appeared. However, despite apparently there were no differences between both flasks; only with morpholine did we achieve to isolate crystals of **[V]** of the desired quality. The crystals that precipitated from the solution containing piperazine showed a high tendency to twinning and as a result, they were deemed not apt for X-ray analysis. It is possible that the structure of piperazine favourishes polymerization, which would explain the difficulties met in crystallization.

At this point, we decided to test the influence that the addition of bulkier ligands would have into the synthesis of trialkoxysilanethiolate complexes of iron(II). After unsuccessfully trying to synthesize a heteroleptic complex with bulky heteroatomic polycycles (see section 5.5.2), we decided to use 3,5-lutidine (3,5-dimethylpyridine), a smaller ligand whose two methyl substituents make it more sterically hindered than the heterocyclic single rings we had been trying until this moment. Product of this reaction, some yellow monoclinic crystals were isolated and analyzed, revealing the interesting pentacoordinated complex **[IX]**.

The next few tests were performed with picolines (methylpyridines). The reaction occurred mildly in all of them and crystals were obtained after one day or two at low temperature (-10ºC). β-picoline **[VII]** and γ-picoline **[VIII]** complexes were isolated first and the structure showed a very similar geometry to that of **[IX]**.

α-Picoline, on the other hand, provided somehow surprising results. We assumed that the resulting compound would be another chelating complex similar to the previous ones (**[VII]**, **[VIII]** and **[IX]**). However, **[VI]** resulted in a different kind of pentacoordinated complex which involved one molecule of α-picoline and two of methanol as coligands.

5.A.5.2. N-donor polycyclic coligands.

Four polycyclic heteroatomic bases were selected as potential coligands: 2,2'-bipyridine, 1,10-phenanthroline, neocuproine and 4,9-dichloroacridine. All of them being close relatives of pyridine (*i.e.* containing at least one pyridyl ring), we thought at first that they should undergo a similarly mild reaction unless their bigger size imposed more strict steric constrictions. Reactions with 1,10-phenanthroline and 2,2'-bipyridine have been reported to produce other transition metal silanethiolates[36,231,238,239] such as $[Mn\{SSi(O^tBu)_3\}_2(phen)(MeOH)]$, $[Cu\{SSi(O^tBu)_3\}(phen)]$, $[Mn\{SSi(O^tBu)_3\}_2(bipy)]$, $[Zn\{SSi(O^tBu)_3\}_2(bipy)]$ and $[Cd\{SSi(O^tBu)_3\}_2(bipy)]$ (refcodes: RENBUI, PAFZUR, RENBOC, REWJAE and VERXIA, respectively).

However, it was impossible for us to obtain heteroleptic compounds of this kind. Neocuproine and 4,9-dichloroacridine did not show any sign of reaction. Bipyridine gave an orange precipitate which could not be isolated in crystalline form but most probably it was a bipyridine-only complex since the reaction seemed to occur equally without addition of silanethiol. Phenanthroline reacted to give the extremely stable and previously unknown $[Fe(phen)_3]Cl_2.6MeOH$ **[XII]**. Of course, the silanethiolates were not involved in this synthesis, so we removed them from the equation to acquire big red crystals of **[XII]** (see picture below). Similar complexes were already known, but this was the first time that a methanol solvate had been obtained. Crystals of **[XII]** are very stable and can be safely manipulated and stored without the need of using Schlenk techniques. The crystals were

completely characterized by X-ray analysis and the results were published in Acta Crystallographica Section E[240].

After these results, the big polycyclic ligands were soon dismissed in favor of the smaller (more labile and less sterically hindered) ones.

5.A.5.3. N-donor 5-membered rings as coligands

The coligand ability of three N-donor 5-membered rings, namely pyrrole, pyrrolidine and N-methylimidazole (resembling the 6-membered pyridine, piperidine and α-picoline, respectively) was tested with our iron(II) silanethiolates.

Pyrrole and pyrrolidine both seemed to give signs of reaction, although ultimately no crystals could be isolated. The addition of N-methylimidazole in the last step of reaction (1) led to the synthesis of the homoleptic $[Fe(C_4H_6N_2)_6]Cl_2.2H_2O$ **[XI]**, the structure of which was previously unknown. Thus, a short structural description of this compound was published in Acta Crystallographica Section E[241].

5.A.5.4. Ethylenediamines as coligands

Finally, two more coligands were tested: dmeda and tmeda. These are chelating ligands sharing the N-C-C-N backbone. In general, chelating ligands of the Y-C-C-Y kind account for very stable complexes and what is more, Komuro *et al.*[44,48] have reported the synthesis of two similar iron(II) silanethiolates. The first one, $[Fe(SSiPh_3)_2(tmeda)]$, has demonstrated to be more stable than our monometallic alkoxysilanethiolates, while the other, $[Fe(SSiMe_2{}^tBu)_2(tmeda)]$, did not afford crystals of enough quality for X-ray structural analysis to be performed and has only been characterized by FTIR.

In our case, the use of dmeda did not provide any significant results, but the reaction with tmeda soon afforded small yellow crystals of **[X]**. In comparison with the rest of the monometallic trialkoxysilanethiolates of iron(II), these crystals oxidized more slowly when in presence of atmospheric O_2, although it did not take longer than half a minute for the decomposition to be complete. Also they demonstrated to be unstable in solution under inert atmosphere since they decayed after a few days. This behavior contrasts with that of $[Fe(SSiPh_3)_2(tmeda)]$, which seems to be relatively stable in the atmosphere under normal conditions.

5.A.6. Synthesis of homoleptic complexes of iron(II) with N-donor ligands

Finally, although they are not directly related with silanethiolates, we decided to polish the synthesis of **[XI]** and **[XII]** to obtain purer crystals with a low enough R factor to be apt for publication. In both cases we suppressed the addition of silanethiol and Et_3N, since the reaction seemed to occur independently of these reagents. The reaction with N-methylimidazole follows the equation:

$$FeCl_2.4H_2O + 6(\text{N-meimid}) \xrightarrow{\textit{methanol}} [Fe(\text{N-meimid})_6]Cl_2.2H_2O + 2H_2O$$

And the reaction with phenanthroline:

$$FeCl_2.4H_2O + 3(\text{phen}) + 6MeOH \xrightarrow{\textit{methanol}} Fe(\text{phen})_3Cl_2.6MeOH$$

These direct reactions yielded bigger crystals of higher purity than when the silanethiol was present, possibly indicating a potential interference of the silanethiol and/or triethylamine in crystallization. The structural data of these complexes were submitted and published in Acta Crystallographica Sect.E[240,241].

5.B. Discussion and analysis of the new silanethiolates of iron(II) and two additional iron(II) complexes

5.B.1. Mononuclear iron(II) disilanethiolates

Our investigation has revealed a wide range of structures for mononuclear silanethiolates of iron(II) with coordination numbers ranging from 4 to 6. It is worth mentioning that silanethiolates of iron(II) with coordination number 5 are reported for the first time. Correspondingly, examples of typical tetrahedral arrangements, not-so-common square pyramidal and octahedral structures have all been identified and characterized. All these mononuclear iron(II) complexes are disilanethiolates which present extreme sensitivity to heat and light and decompose in few seconds under the atmosphere.

We proved that the order of introduction of reagents into the flask is not important in most cases. Thus, while we generally achieved the best results introducing the silanethiol and Et_3N together followed by introduction of the coligand in the final step, in some occasions the quality of the crystals was better if the coligand was introduced first – right before the silanethiol and the amine.

On the classification of silanethiolates of iron

When dealing with silanethiolates, it is reasonable to try to compare them to thiolates, their organic homologues. Regrettably, we have found that in our case the comparison is certainly difficult. Despite iron(II) thiolates and other thiol derivatives have been thoroughly studied and the bibliography about the subject seems to be extensive, not many examples of complexes containing both thiolate and N-donor heterocyclic ligands can be found in the CCDC database. Most examples of N- and S-donor coordination consist of bulky multidentate ligands, or a heme group ligated by a thiolate. What is more, in most cases where a standalone N-donor ligand appears, generally it is a small nitrosyl NO moiety and the compounds containing a heterocycle as the coligand are surprisingly few. This perceptibly complicates the comparison of our complexes with thiolates of iron(II). A possible explanation for this lack of examples can be that complexation with the N-donor ligands is so stable that the thiolate cannot displace them (and is displaced by them when it is already complexed) as it seems to be the case for the tri-*tert*-butoxysilanethiolate and the 1,10-phenanthroline ligands.

Thus, it seems more appropriate to compare our iron trialkoxysilanethiolates with other transition metal silanethiolates. Some complexes of iron(II) already exist, and other metal silanethiolates share a few characteristics.

One of the simplest ways to classify these compounds is according to the S-M bond length, which is also a relative measure of the covalency of the bond. We considered more appropriate first to make a distinction according to the coordination number – since generally the more bonds, the lesser the electronic withdrawing by the metal for each of them and therefore, the longer the S-M distance.

Therefore, if we represent graphically the mean S-M bond length for different metals, we obtain the following plot for tetracoordinated complexes:

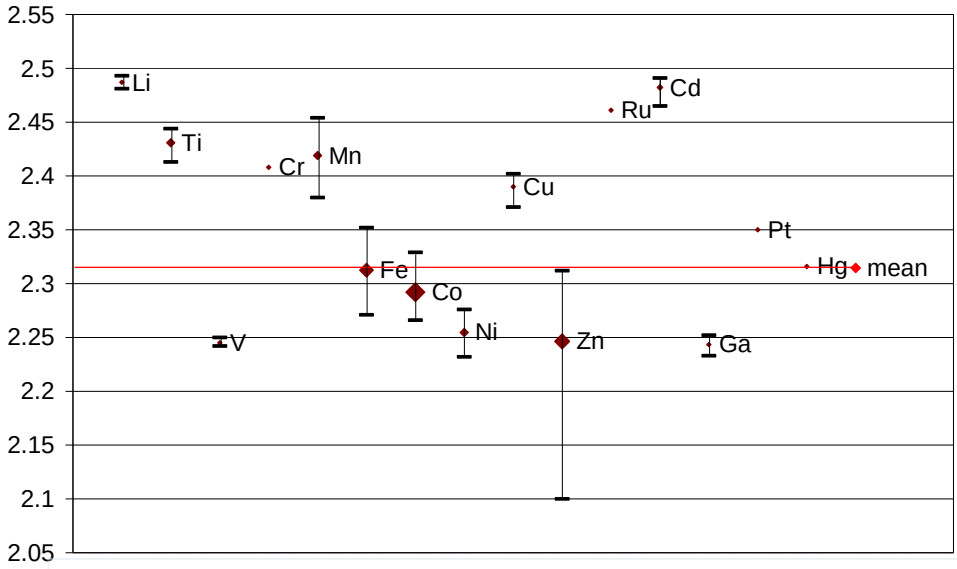

Fig. 23. Mean M-S values for tetracoordinated silanethiolates. The range of values for a given metal is indicated whenever possible by the black bars. The relative size of the dots is an indicator of the number of data involved, *i.e.* the bigger the dot, the more weight the metal has on the global mean value.

As can be seen, the global mean value for the M-S bond in tetrahedral silanethiolate complexes is 2.31Å, with the value for the different metals oscillating between 2.24 and 2.49Å. A few metals show relatively high values, but they are also not very numerous and therefore they do not have much weight on the absolute mean value. Coincidentally, the mean value for iron is very close to the absolute mean value for all existent silanethiolates.

Similar graphs for penta- and hexacoordinated complexes do not provide so much information, given the small number of complexes with such coordination numbers.

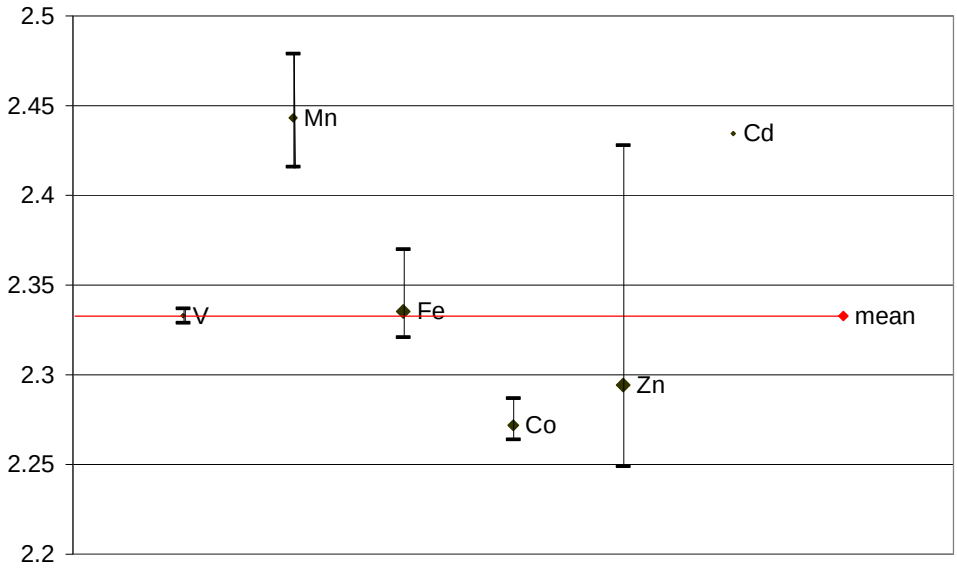

Fig. 24. Mean M-S values for pentacoordinated silanethiolates. The range of values for a given metal is indicated whenever possible by the black bars. The relative size of the dots is an indicator of the number of data involved, *i.e.* the bigger the dot, the more weight the metal has on the global mean value.

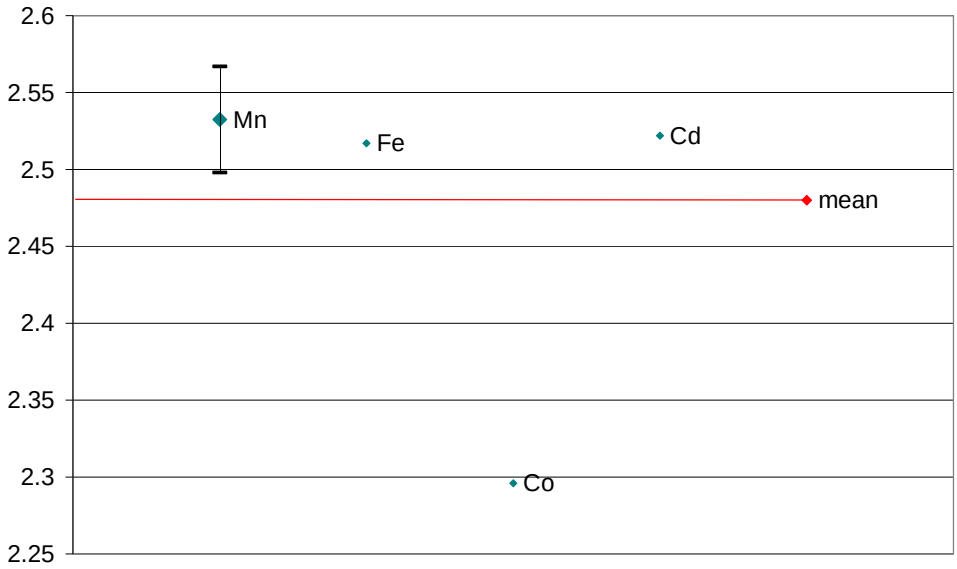

Fig. 25. Mean M-S values for hexacoordinated silanethiolates. The range of values for manganese is indicated by a black bar. The relative size of the dots is an indicator of the number of data involved, *i.e.* the bigger the dot, the more weight the metal has on the global mean value.

In the case of pentacoordinated complexes, we can appreciate how the mean Fe-S distance adopts again a close value to the absolute mean M-S bond length. Once more, the values of Cd and Mn stand well over the mean and Co and Zn are slightly below it.

In the case of octahedral complexes, except cobalt, all other metals present similar M-S distances (~ 2.5Å), however there are not enough values to withdraw any definitive conclusion from this set of data. Nevertheless, it is possible to observe how the mean M-S values for a given metal suffer a slight increase with higher coordination numbers as expected.

On the geometry of coordination polyhedra

In order to classify coordination polyhedra, one comes about several different methods to determine the degree of distortion. Regrettably, no method is perfect and they are often met with criticism.

One of the oldest and so far also one of the most common methods to measure distortion was proposed by Robinson *et al.* in 1971[242]. This method provides a comparison of the length of the bonds and the angles in a given coordination polyhedron to the corresponding values in an ideal polyhedron of equal volume. Then, if the mean quadratic elongation (λ) is represented as a function of the bond angle variance (σ^2), a linear correspondence can be appreciated. Although it is a very practical method since it makes use of geometrical parameters that should be readily available given the structure of the complex; Fleet warns that it can become inconsistent as the size of the polyhedra tends to zero[243], especially when applied to octahedral geometries and, in general, discourages of using Gibbs' method lightly. In other studies, the measurement of the distortion is based on related parameters such as (Σ)[244,245] which also provide simple measurements of the deviation of a given structure from a perfect octahedron.

In 1998, Makovicky and Balić-Žunić presented their "New Measure of Distortion for Coordination Polyhedra"[246]. Their method was based on the ratio between the volumes of the real polyhedron and the ideal polyhedron that occupies the same circumsphere. Despite it seems reasonable, Brown[247] points out that this and similar methods are sensitive to the choice of the method of fitting.

More recently, Lalik suggested the use of the Shannon's information theory as a measure of the distortion[248] of a coordination polyhedron. He postulated that since the same values of elongation affect in a different degree depending on bond length, the bond order should be used for calculating the distortion instead. Brown found this method reasonable albeit slightly scattered and proposed an alternative based on the distortion theorem of the bond-valence model[247]. However, Brown's method is difficult to apply when no ideal polyhedra can be found from the complexation with a determined ligand.

Despite its limitations, in this work we will make use of the Robinson-Gibbs-Ribbe method. We find that the quadratic elongation and the bond angle variance are easy to calculate and provide good information about the distortion of a given polyhedron. Also, it is probably the most straightforward method amongst those reviewed since it does not require of additional empiric or semi-empiric parameters and given the geometry of the molecule, the calculations are relatively simple. It is necessary to remark, though, that the procedure is purely geometric and does not take in account the error assigned to each measurement since it makes use of the single space points provided by the .cif files. As a result, this method is only worth as an approximation. In order to obtain a coherent method for measuring the distortion, a procedure that has in account the error has to be developed.

Probably, the most difficult step when using this method is the determination of the volume of the polyhedra; but since every polyhedron can be decomposed into simpler ones, the calculation simplifies greatly if we decompose them into the sum of *n* distorted tetrahedra. Thus an octahedron can be built from four distorted tetrahedra and a trigonal bipyramid is composed of two tetrahedra.

The volume of a distorted tetrahedron can be determined from its edges making use of the Cayley-Menger determinant[249,250]:

$$288V^2 = \begin{vmatrix} 0 & 1 & 1 & 1 & 1 \\ 1 & 0 & d_{12}^2 & d_{13}^2 & d_{14}^2 \\ 1 & d_{21}^2 & 0 & d_{23}^2 & d_{24}^2 \\ 1 & d_{31}^2 & d_{32}^2 & 0 & d_{34}^2 \\ 1 & d_{41}^2 & d_{42}^2 & d_{43}^2 & 0 \end{vmatrix}$$

Where d_{ij} represents the length between edges i and j o the tetrahedron. This determinant is easily calculated with the help of the **Scilab** mathematics software package[251]. From this, the calculation of the volume of any given polyhedron is trivial.

For an octahedron:

$V_{Oh} = V_{Th1} + V_{Th2} + V_{Th3} + V_{Th4}$

For a trigonal bipyramid:

$V_{BT} = V_{Th1} + V_{Th2}$

Where, V_{Thi} denotes the volume of the distorted tetrahedra that shape the bigger polyhedron.

The determination of the ideal bond length is reduced to the problem of determining the center to vertex distance in the corresponding ideal polyhedron; that is, its circumradius. This value can be calculated easily, with a few particularities depending on the polyhedron, as shown below:

a) For a regular tetrahedral structure[250], we know that the relationship between the edge, *a*, and the volume is given by the equation:

$$V = \frac{1}{12}\sqrt{2}\ a^3$$

From where the length of the edge can be obtained. Then, the distance from the vertex to the circumcenter is:

$$R = \frac{1}{4}\sqrt{6}\ a,$$

which can be easily demostrated by simple trigonometric relationships.

The angles between the circumradii in a regular tetrahedron are 109.47º in every case.

b) For a regular octahedral structure[252], the volume is two times the volume of a square pyramid:

$$V = \frac{1}{3}\sqrt{2}\ a^3$$

From where we can determine the value of *a*. The corresponding circumradius for this polyhedron is given by the equation:

$$R = \sqrt{a^2 - \frac{1}{2}a^2} = \frac{1}{2}\sqrt{2}a \approx 0.7071a$$

Which can be easily demonstrated by means of trigonometric relationships.

Every circumradius in a regular octahedron forms a right angle (90º) with the four closest circumradii and a straight angle with the circumradius opposed to it (180º).

c) For a trigonal bipyramidal structure[253,254] it is arguable that a regular trigonal bipyramid (that is, all the edges have the same length, *a*) is the most appropriate to represent the ge-

ometry of a coordination polyhedron, since all its vertex cannot be circumscribed in a sphere at the same time. Instead, we may want to consider an irregular trigonal bipyramid which has all of its vertex on the surface of the circumsphere as a more accurate model for a complex with five ligands that are equally bond to the metal.

Both models will be contemplated in our calculations.

c.1) For a regular trigonal bipyramid, the volume is two times the volume of a regular tetrahedron:

$$V = \frac{1}{6}\sqrt{2}a^3$$

And the circumradius is given by the semiheight of the bipyramid, which is the height of a tetrahedron:

$$R = h = \frac{1}{3}\sqrt{6}a$$

However, the distance from the circumcenter to any equatorial vertex is shorter:

$$r = \frac{1}{3}\sqrt{3}a$$

c.2) For an irregular trigonal bipyramid, whose vertices are included in a single circumsphere, we have that its volume is determined by the equation:

$$V = \frac{2}{3}A \cdot h,$$

Where *A* is the area of the equatorial triangular base and *h* is the semiheight of the dipyramid (*i.e.* the diameter of the circumsphere). Upon calculation we can write the volume as a function of the circumradius *R*:

$$V = \frac{1}{2}\sqrt{3}R^3$$

from where the value of *R* can be obtained.

In the last two models, the angles do not vary. Given that A= apix, C=circumcenter and E= equatorial vertex, A-C-E is a right angle (90º) and E-C-E is an obtuse angle equal to 2/3 π rad (=120º).
The previous mathematic development was necessary to understand how to apply the Robinson-Gibbs-Ribbe method. It is based on two parameters, the quadratic elongation and the variance of the angles (< **λ** > and $\boldsymbol{\sigma}^2$, respectively) defined as follows:

I) Mean quadratic elongation (< **λ** >)

The quadratic elongation can be written as:

$$\lambda = \left(\frac{l_i}{l_0} \right)^2$$

where l_i is the length of the bond in the coordination polyhedron and l_0 is the equivalent length in an ideal polyhedron of the same volume.

Thus, to calculate the mean:

For a tetrahedron: $\langle \lambda \rangle = \dfrac{\sum_{i=1}^{4} \left(\frac{l_i}{l_0} \right)^2}{4}$

For an octahedron: $\langle \lambda \rangle = \dfrac{\sum_{i=1}^{6} \left(\frac{l_i}{l_0} \right)^2}{6}$

For a trigonal bipyramid: $\langle \lambda \rangle = \dfrac{\sum_{i=1}^{5} \left(\frac{l_i}{l_0} \right)^2}{5}$

Observe that if we choose a regular trigonal bipyramid model, l_0 is dependent on the position of the ligand, giving longer values for the apical bonds.

II) Angle variance

The angle variance is measured according to the equation:

$$\sigma^2 = \frac{\sum_{i=1}^{N}(\theta_i - \theta_0)^2}{(N-1)}$$

where θ_i are the angles in the coordination polyhedron, θ_0 are the corresponding angles in an ideal polyhedron and N is the number of angles in the complex. Notice that the bias correction factor of the variance[255] is *N-1* in agreement with the original publication by Robinson *et al*[242].

5.B.1.1. The octahedral [Fe{SSi(O^{t}Bu)$_3$}$_2$(MeOH)$_4$]

The unstable [Fe{SSi(O^{t}Bu)$_3$}$_2$(MeOH)$_4$] **[I]** is easily synthesized in methanol following the stoichiometric reaction:

$$2\ (^t\text{BuO})_3\text{SiSH} + \text{FeCl}_2.4\text{H}_2\text{O} + 2\text{Et}_3\text{N} \longrightarrow [\text{Fe}\{\text{SSi}(\text{O}^t\text{Bu})_3\}_2(\text{CH}_3\text{OH})_4] \quad (1)$$

[I] precipitates as transparent triclinic crystals, crystallizing in the P-1 space group. **[I]** is a singular complex in several ways and a series of searches in the CCDC database reveal several interesting features. For instance, **[I]** is the first octahedral silanethiolate of iron(II) ever characterized as well as it is the first and only example of a thiolate-related iron complex which contains single alcohol molecules as coligands. It is worth noting that iron complexes containing alcohol moieties as ligands are in general very rare and that octahedral dithiolates of iron(II) are likewise not very frequent. Lastly, another unique feature is the presence of four H-bonds linking each of the methanol molecules to the closest oxygen of the *tert*-butoxy groups. The higher polarizability of the oxygen atom (compared to the carbon atom that would occupy the same position in alkyl- and arylsilanethiolates) makes possible for alkoxysilanethiolates to form H-bonds .

Very few complexes of iron(II) show octahedral coordination with alcohol ligands. Of these, only three[256-258]: [Fe(BmtCO$_2$)$_2$(MeOH)$_4$]·2MeOH, [Fe(benz)$_2$(MeOH)$_4$] and [Fe(MeOH)$_4$(TCNQ)$_2$]TCNQ·2MeCN (refcodes: QATBUI, YOHZUQ and ZIFJON, respectively) contain methanol as the coligand (see pictures below). These complexes present several resemblances with **[I]** from the structural point of view. For instance, all of them adopt a slightly distorted octahedral configuration with the methanol moieties occupying the equatorial positions. However, the angles between opposed ligands are 180º in every

case, and the distortion is given by the relative position of the methanol moieties with respect to each other (angles ≠90º) and to the ideal equatorial plane.

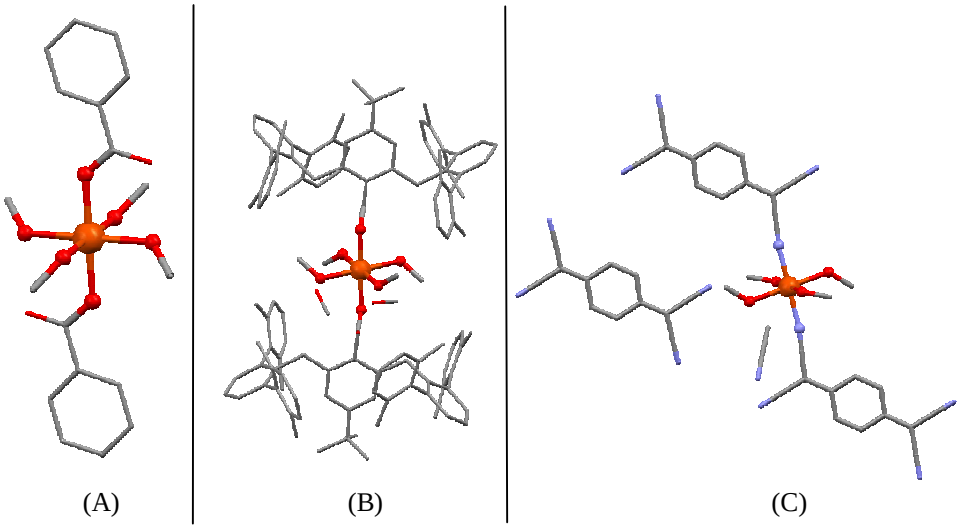

Fig. 26. Structures of $[Fe(benz)_2(MeOH)_4]$ **(A),** $[Fe(BmtCO_2)_2(MeOH)_4].2MeOH$ **(B)** and $[Fe(MeOH)_4(TCNQ)_2]TCNQ.2MeCN$ **(C)**

As a difference, all these complexes present 4 methanol moieties in the equatorial plane in a classical chair configuration with two of the methanol molecules twisted over the equatorial plane and the other two twisted down the plane while in **[I]** only two of the methanol coligands determinate clearly the chair configuration, as the other two molecules remain approximately in the equatorial plane.

Although the aforementioned particularities make difficult to find compounds to be directly compared with **[I]**, a certain parallelism can be established with the $[Co\{SSi(O^tBu)_3\}_2(NH_3)_4]^+$ cation[33], (refcode: WOWQAA) where the equatorial positions are occupied by ammonia moieties instead of methanol. Both complexes present a similar octahedral structure, with four small polar moieties occupying the positions at the equatorial plane. A more straightforward relationship stems from the isomorphism[41] with the previously described $[Mn\{SSi(O^tBu)_3\}_2(MeOH)_4]$ (refcode: CEHZIZ), which can be appreciated in detail in the table below:

Table 8. Crystal data	**$[Fe\{SSi(O^tBu)_3\}_2(MeOH)_4]$ [I]**	**$[Mn\{SSi(O^tBu)_3\}_2(MeOH)_4]$ [CEHZIZ]**
Space group	Triclinic, P-1	Triclinic, P-1
Cell length a (Å)	8.757(11)	8.739(5)
Cell length b (Å)	9.277(2)	9.274(9)
Cell length c (Å)	14.812(15)	14.848(10)
Cell angle α	94.689º(16)	95.14º(8)
Cell angle β	100.554º(10)	100.35º(5)
Cell angle γ	116.327º(14)	116.37º(5)
Cell volume ($Å^3$)	1042.0	1040.81
Cell formula units Z	1	1
Measurement temperature (K)	120	100
R factor	6.69%	3.42%

Table 9. Selected distances(Å) and angles(°)	$[Fe\{SSi(O^tBu)_3\}_2(MeOH)_4]$	$[Mn\{SSi(O^tBu)_3\}_2(MeOH)_4]$
M-O(4)	2.153(4)	2.238(1)
M-O(5)	2.178(3)	2.226(7)
M-S(1)	2.517(1)	2.567(4)
S(1)-Si(1)	2.056(2)	2.051(4)
Si(1)-O(1)	1.652(4)	1.652(1)
Si(1)-O(2)	1.631(3)	1.661(8)
Si(1)-O(3)	1.659(3)	1.631(9)
S(1)-M-O(4)	90.53(9)	91.45(3)
S(1)-M-O(5)	90.51(9)	90.28(2)
S(1)-M-S'(1)	180.00(4)	180.00(1)
Si(1)-S(1)-M	105.43(6)	105.29(1)
O(4)-M-O(5)	90.8(1)	91.41(3)
S(1)-M-O(4)-C(14)*	-83.2(4)	-84.3(1)
S(1)-M-O(5)-C(13)*	-172.0(4)	-168.3(1)
$\langle\lambda\rangle$	1.0107	
σ^2	0.429	

* For the Mn isomorph, the carbon atoms attached to O4 and O5 are labeled C1 and C2, respectively.

As can be seen from the data in the table above, there are no drastic geometric differences between both molecules. The most relevant discrepancies concern the ligand-metal bonds, which can be easily explained by the slightly different electronic configuration of Fe^{2+} and Mn^{2+}.

Considering the values of $< \lambda >$ and σ^2 for the coordination polyhedron of **[I]**, we observe that the distortion is mainly driven by the different lengths of the bonds, while the angles remain close to the ideal values.

It was somehow complicated to obtain a low error structure determination of **[I]**, due to the tendency of these crystals to twinning. Finally, the structure was solved with the help of

some special mathematical treatment. The structure itself can be visualized in the following figure:

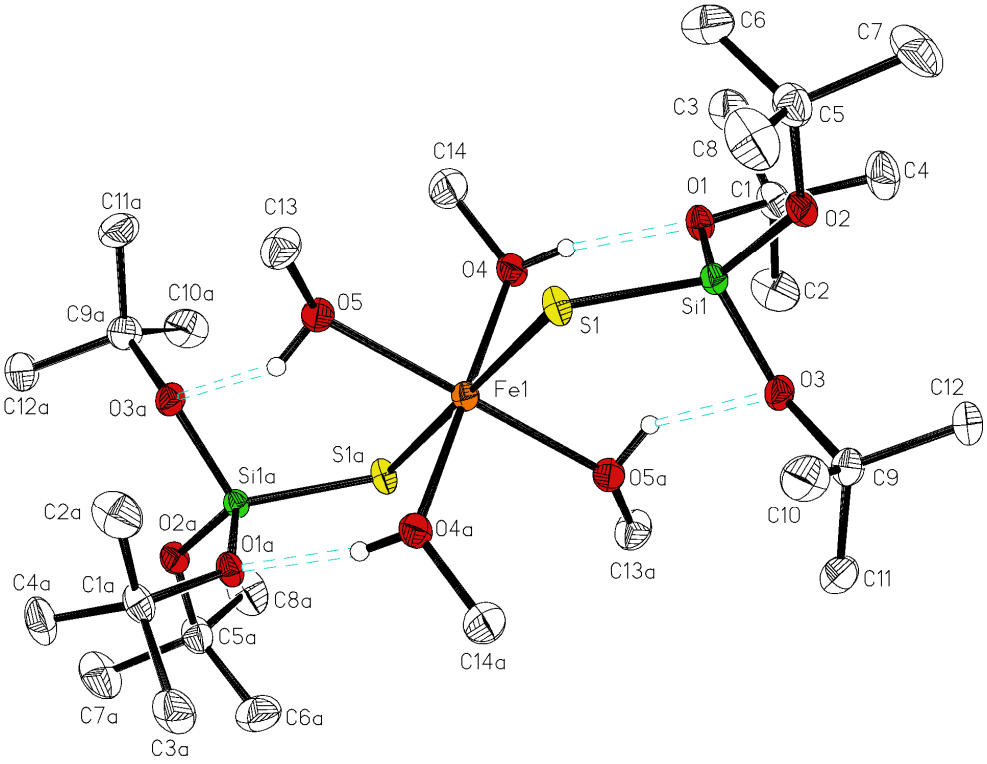

Fig 27. Structure of [I]. Only H atoms implied in H-bonding are shown for clarity. Thermal ellipsoids 50%.

5.B.1.2. Tetracoordinated complexes

Heterogeneous N-donor bases have been successfully used as co-ligands. However, not all the N-donor molecules are apt to form a heteroleptic complex together with silanethiolates. In some cases, the homoleptic complex formed with the N-donor bases was too stable for the silanethiolates to achieve coordination.

Our investigations have led us to the discovery of three structurally similar iron(II) complexes with tetrahedral coordination (CN=4): $[Fe\{SSi(O^tBu)_3\}_2(py)_2]$ **[III]**, $[Fe\{SSi(O^tBu)_3\}_2(pip)_2]$ **[IV]** and $[Fe\{SSi(O^tBu)_3\}_2(morph)_2]$ **[V]**. The main difference amongst them is the number of H-bonds established between the N-donor moiety and the closest oxygen atoms of the *tert*-butyl groups. Pyridine lacks the H atom at nitrogen and

thus, **[III]** is unable to establish H-bonds as the other complexes do. **[IV]** and **[V]** both form H-bonds, one in the case of the morpholine complex and two in the case of the piperidine one (see figs. 28 and 29 below). The *tert*-butoxy groups of one of the silanethiolates of **[V]** are more twisted away from the co-ligands than they are in **[IV]**.

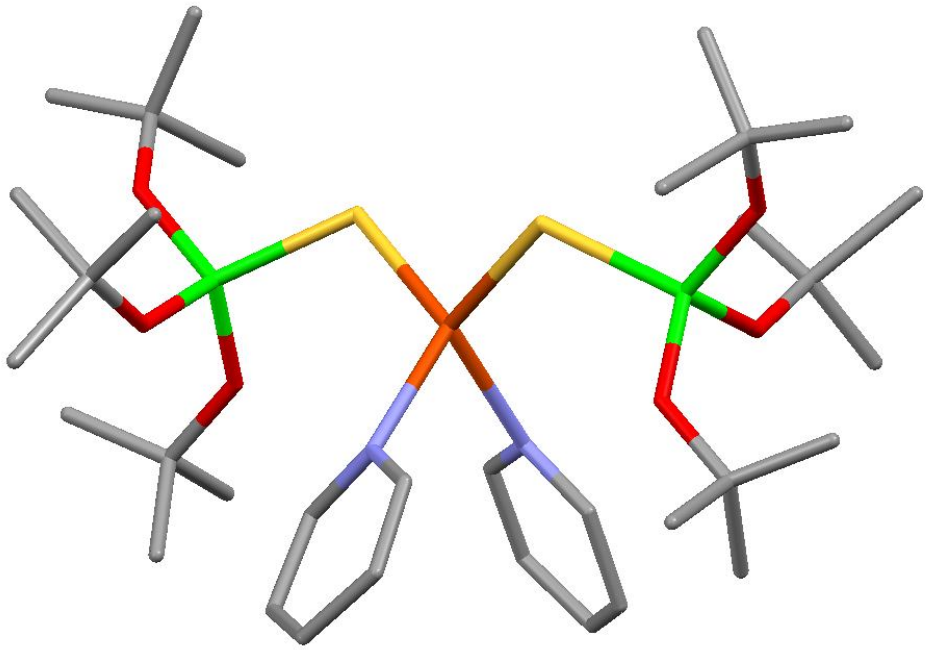

Fig. 28. A first approximation to the structure of [III]. Notice the planar heterocyclic rings. H-atoms omitted for clarity.

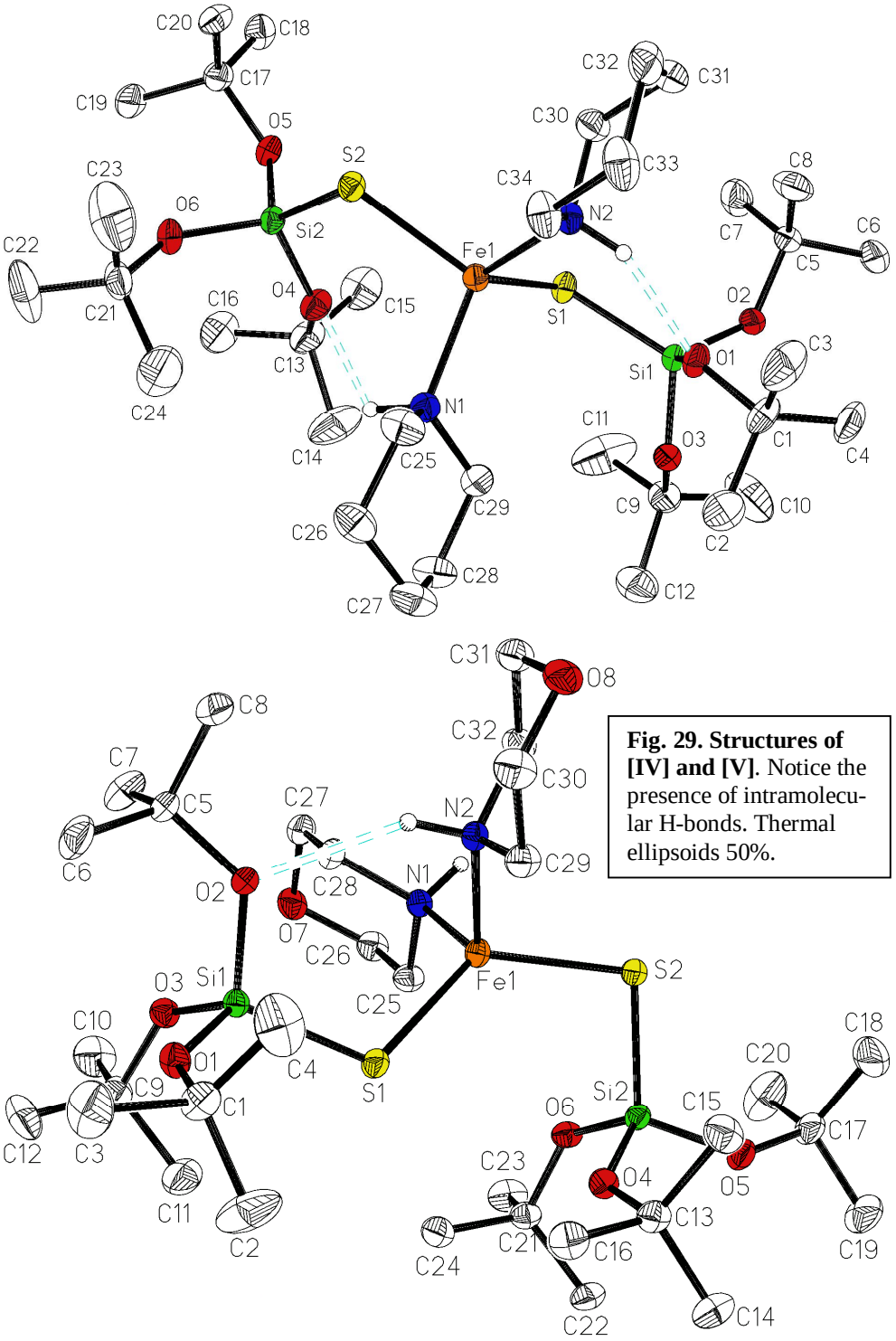

Fig. 29. Structures of [IV] and [V]. Notice the presence of intramolecular H-bonds. Thermal ellipsoids 50%.

In the next table, selected angles and distances from **[IV]** and **[V]** can be appreciated and compared to $[Fe(SSiPh_3)_2(4\text{-}^tBupy)_2]$ and $[Fe(SSi^tBu_3)_2(THF)_2]$ (refcodes: LUGNUW and YECRII, respectively), which are the closest relatives of these iron(II) compounds found on the CCDC database[44,49].

Compound	H-bonds	Fe-S1 (Å)	Fe-S2 (Å)	N1···O (Å)	N2···O (Å)	X-Fe-X
$[Fe\{SSi(O^tBu)_3\}_2(morph)_2]$ [V]	1	2.309	2.346	3.155*	4.102	107.81º
$[Fe\{SSi(O^tBu)_3\}_2(pip)_2]$ [IV]	2	2.335	2.352	3.247*	3.067*	116.08º
$[Fe(SSiPh_3)_2(4\text{-}^tBupy)_2]$ [LUGNUW]	0	2.303	2.304	-	-	91.26º
$[Fe(SSi^tBu_3)_2(THF)_2]$ [YECRII]	0	2.289	2.271	-	-	86.82º

Table 10. Observe that the N-Fe-N angle of $[Fe(SSiPh_3)_2(4\text{-}^tBupy)_2]$ and the O-Fe-O angle of $[Fe(SSi^tBu_3)_2(THF)_2]$, which do not contain H-bonds are closer to 90º.
* indicates H-bond. X = N, O

From the results in table 10, it seems reasonable that a direct relationship can be established between the number of hydrogen bonds – linking the hydrogen atom attached to the nitrogen of the heterocyclic base and the nearest oxygen atomn – and the N-Fe-N angle in tetrahedral iron(II) silanethiolates, leading to the conclusion that the H-bonds distort the structure by widening the N-Fe-N angle. Furthermore, the distance from the nitrogen atom to the closest oxygen is considerably reduced if the oxygen atom is bound via an H-bond.

The ligands in **[III]**, **[IV]** and **[V]** coordinate tetrahedrically to iron similarly as $[Fe(SSiPh_3)_2(4\text{-}^tBupy)_2]$ and $[Fe(SSi^tBu_3)_2(THF)_2]$ do[44,49] ; however, in case of the morpholine **[V]** and the piperidine **[IV]** adducts, the presence of H-bonds between the heterocyclic bases and the oxygen atoms of the silanethiolate moieties adds deformation to these structures. The N-Fe-N angles in the complexes with no H-bonds ($[Fe(SSiPh_3)_2(4\text{-}^tBupy)_2]$ and $[Fe(SSi^tBu_3)_2(THF)_2]$) are close to a right angle ranging from 86.82º to 91.26º. In contrast, the strain imposed by the two H-bonds of **[V]** cause the N-Fe-N angles to be significantly wider (116.08º) than the complexes without H-bonds. Complex **[IV]**, which presents only one H-bond, shows less deviation from this trend (107.81º). Also, the silanethiolate

moieties in **[IV]** are not so twisted away from each other and rather remain in the same plane.

As in the case of **[I]**, it is difficult to establish relationships with other transition metal silanethiolates. For instance, **[IV]** is the only example of a tetracoordinated silanethiolate containing piperidine. Nevertheless, some relationships could be traced between **[III]** and other heteroleptic pyridyl silanethiolates such as $[Co\{SSi(O^tBu)_3\}_2(py)_2]$ (refcode: IDADEW) and $[Zn\{SSi(O^tBu)_3\}_2(py)_2]$ (refcode: AREJOW)[34,40] if the preliminary results are confirmed by newer, more accurate structures. On the other hand, **[V]** is the only tetracoordinated silanethiolate of iron(II) for which an isomorph has been found: $[Co\{SSi(O^tBu)_3\}_2(morph)_2]$ (refcode: IDAFEY)[34].

Table 11	**$[Fe\{SSi(O^tBu)_3\}_2(pip)_2]$ [IV]**	**$[Fe\{SSi(O^tBu)_3\}_2(morph)_2]$ [V]**	**$[Co\{SSi(O^tBu)_3\}_2(morph)_2]$ [IDAFEY]**
Space group	Monoclinic, C2/c	Triclinic, P-1	Triclinic, P-1
Cell length a (Å)	36.668(5)	9.819(4)	10.011(2)
Cell length b (Å)	10.024(14)	13.920(5)	14.002(3)
Cell length c (Å)	28.173(3)	16.235(8)	16.351(3)
Cell angle α	90º	88.178º(3)	88.31º(3)
Cell angle β	119.197º(13)	80.903º(4)	80.80º(3)
Cell angle γ	90º	81.497º(3)	81.17º(3)
Cell volume ($Å^3$)	9039.97	2166.93	2235.66
Cell formula units Z	8	2	2
Measur. temp. (K)	120	120	Room temperature
R factor	5.85%	3.75%	7.76%

T.12.Selected distances(Å) and angles(º)	$[Fe\{SSiR_3\}_2(pip)_2]$ [IV]	$[Fe\{SSiR_3\}_2(morph)_2]$ [V]	$[Co\{SSiR_3\}_2(morph)_2]$ [IDAFEY]
M-N(1)	2.133(3)	2.128(2)	2.075(4)
M-N(2)	2.137(3)	2.129(1)	2.065(4)
M-S(1)	2.335(9)	2.309(4)	2.278(2)
M-S(2)	2.352(1)	2.346(4)	2.306(1)
S(1)-Si(1)	2.087(1)	2.083(6)	2.062(2)
Si(1)-O(1)	1.647(2)	1.628(1)	1.615(4)
Si(1)-O(2)	1.633(3)	1.653(1)	1.638(3)
Si(1)-O(3)	1.637(2)	1.631(1)	1.598(5)
S(2)-Si(2)	2.084(1)	2.106(6)	2.082(2)
Si(2)-O(4)	1.640(2)	1.628(1)	1.579(4)
Si(2)-O(5)	1.635(2)	1.634(1)	1.522(9)
Si(2)-O(6)	1.631(3)	1.633(1)	1.559(7)
N(1)-M-N(2)	116.1(1)	107.81(5)	108.4(2)
N(1)-M-S(1)	109.70(9)	111.32(4)	102.7(1)
N(2)-M-S(2)	97.04(9)	106.47(4)	104.2(1)
S(1)-M-S(2)	133.24(4)	128.60(2)	124.04(5)
Si(1)-S(1)-M	109.45(5)	112.40(2)	112.70(7)
Si(2)-S(2)-M	101.45(4)	100.24(2)	107.61(6)
Si(1)-S(1)-M-N(1)	-66.6(1)	-58.29(5)	-51.5(1)
Si(1)-S(1)-M-N(2)	55.7(1)	55.26(4)	64.9(1)
Si(2)-S(2)-M-N(1)	-72.0(1)	-103.46(4)	-148.7(1)
Si(2)-S(2)-M-N(2)	169.58(9)	143.77(4)	97.9(1)
$\langle\lambda\rangle$	1.06011406	1.034839	
σ^2	185.38522	107.47852	

R=^{t}BuO

A tetrahedral complex is also formed when the chelating tmeda is added to reaction (1). Bidentate ligands with YCCY skeletons are very flexible and are often utilized to develop 5-membered chelate rings due to their stability. Such assemblies have little ring strain and form readily.

One of the first silanethiolates of iron(II) ever discovered was the related $[Fe(SSiPh_3)_2(tmeda)].CH_2Cl_2$ (refcode: LUGPEI)[44], which until now has remained as the only fully characterized example of a silanethiolate with tmeda as the co-ligand. The only other example of such a compound corresponds to the alkylsilanethiolate $[Fe(SSiMe_2{}^tBu)_2(tmeda)]$, which has only been characterized by its FTIR spectra[48].

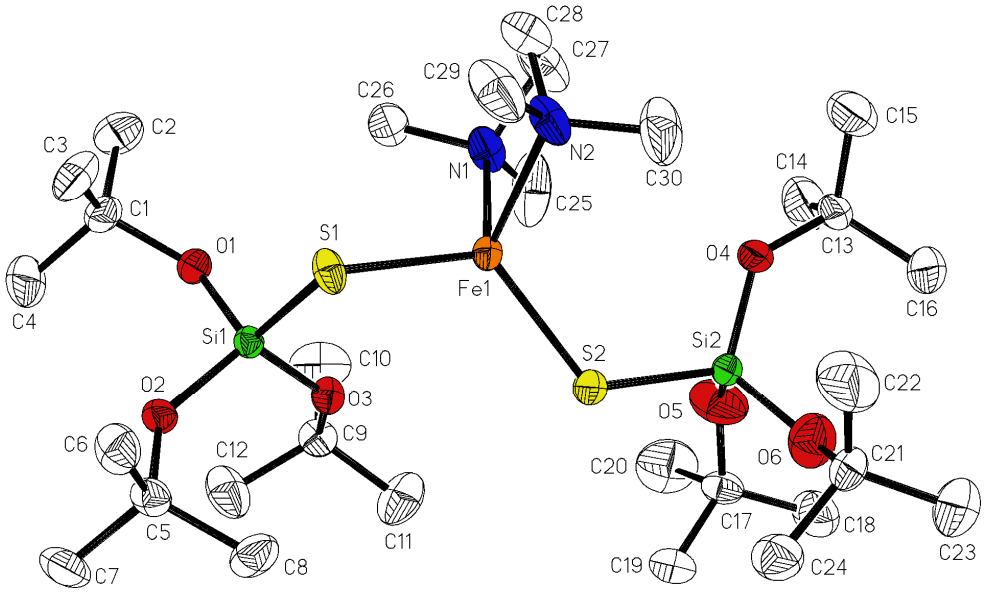

Fig. 30. Structure of [X]. In this case, tmeda is the chelating ligand. H atoms have been omitted for clarity. Thermal ellipsoids 50%.

$[Fe\{SSi(O^tBu)_3\}\}_2(tmeda)]$ **[X]** and $[Fe(SSiPh_3)_2(tmeda)].CH_2Cl_2$ both present a distorted tetrahedral structure.

Table 13. Selected distances(Å) and angles(º)	$[Fe\{SSi(O^tBu)_3\}_2(tmeda)]$ [X]	$[Fe(SSiPh_3)_2(tmeda)].CH_2Cl_2$ [LUGPEI]
Fe-N(1)	2.173(5)	2.191(5)
Fe-N(2)	2.204(4)	2.218(4)
Fe-S(1)	2.313(1)	2.326(2)
Fe-S(2)	2.283(2)	2.321(2)
S(1)-Si(1)	2.088(2)	2.103(2)
Si(1)-O(1)	1.627(3)	-
Si(1)-O(2)	1.620(3)	-
Si(1)-O(3)	1.626(3)	-
S(2)-Si(2)	2.077(2)	2.103(2)
Si(2)-O(4)	1.615(4)	-
Si(2)-O(5)	1.638(5)	-
Si(2)-O(6)	1.615(4)	-
N(1)-Fe-S(1)	113.7(1)	100.0(1)
N(2)-Fe-S(2)	116.6(1)	105.7(1)
N(1)-Fe-N(2)	82.0(2)	82.9(2)
S(1)-Fe-S(2)	120.58(6)	136.08(5)
Si(1)-S(1)-Fe	103.53(6)	111.53(6)
Si(2)-S(2)-Fe	121.64(8)	109.30(6)
S(1)-Fe-N(1)-C(27)	108.9(4)	-89.3(3)
S(1)-Fe-N(2)-C(28)	-98.4(3)	107.0(3)
S(2)-Fe-N(1)-C(27)*	-103.8(4)	124.0(3)
S(2)-Fe-N(2)-C(28)*	130.3(3)	-99.1(3)
$\langle\lambda\rangle$	1.06932581	
σ^2	219.40012	

* In LUGPEI, the carbons in the N-C-C-N backbone are labeled C1 and C2 accordingly to the nitrogen atom they are attached to (*i.e.* N1 and N2, respectively).

As expected due to the longer Si-O distances in **[X]** compared to the Si-C distances in $[Fe(SSiPh_3)_2(tmeda)].CH_2Cl_2$ (see section 2.3.4.), the Si-S distances in **[X]** are slightly shorter.

If we compare the crystal data in both complexes:

Table 14	**$[Fe\{SSi(O^tBu)_3\}_2(tmeda)]$ [X]**	**$[Fe(SSiPh_3)_2(tmeda)].CH_2Cl_2$ [LUGPEI]**
Space group	Monoclinic, $P2_1/n$	Triclinic, P-1
Cell length a (Å)	18.3612(8)	14.243(9)
Cell length b (Å)	9.2138(4)	16.064(9)
Cell length c (Å)	24.6405(10)	10.451(4)
Cell angle α	90º	92.06º(4)
Cell angle β	94.549º(4)	100.20º(3)
Cell angle γ	90º	66.42º(5)
Cell volume ($Å^3$)	4155.46	2155.2
Cell formula units Z	4	2
Measurement temperature (K)	120	193.2
R factor	7.44%	7.10 %

we can appreciate how they differ in their crystallization mode, with **[X]** displaying a higher degree of symmetry. **[X]** belongs to the $P2_1/n$ space group (monoclinic), while $[Fe(SSiPh_3)_2(tmeda)].CH_2Cl_2$ is triclinic, crystallizing in the P-1 space group.

The representation of the angle variance vs. the mean quadratic elongation for tetrahedral silanethiolates of iron(II) gives the following graph:

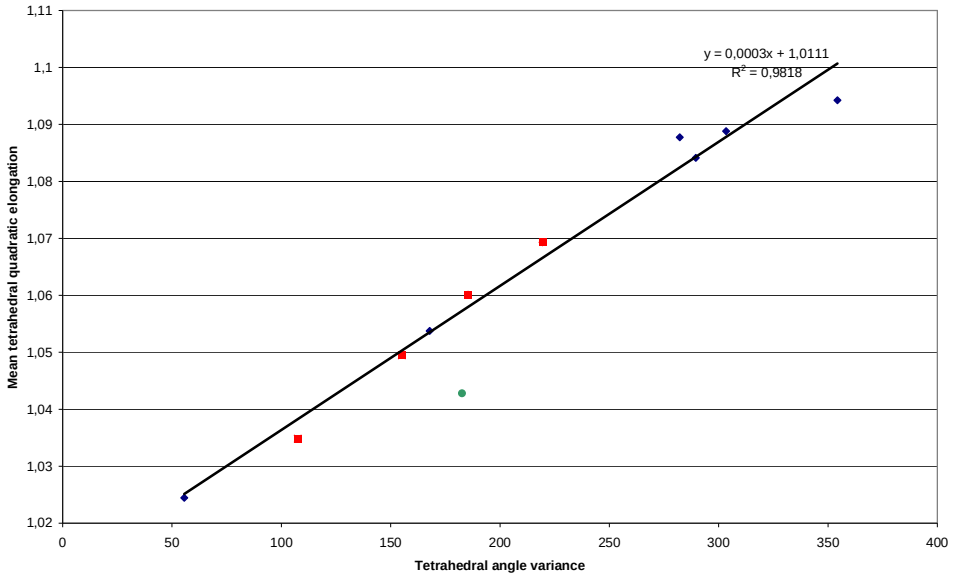

Fig. 31. Data correlation for tetracoordinated silanethiolates

where we observe that tri-*tert*-butoxysilanethiolate complexes (represented in the graph by red squares) are generally less distorted than their alkyl- and aryl- substituted counterparts (blue rombs in the graph). Most of the points correlate very well to a straight line (R^2=0,9818), the only exception being [Fe($SSiPh_3$)$_2$(PEt_3)] (green dot in the graph), whose PEt_3 ligands may impose a higher steric impediment, distorting the angles more than expected. The point corresponding to [Fe($SSiPh_3$)$_2$(PEt_3)] was not taken into account for building the tendency line.

5.B.1.3. Pentacoordinated complexes

Alkyl-substituted phenylthiolates are bulky ligands that have proved useful in the synthesis of tricoordinated thiolates of iron, such as the homoleptic trigonal planar [Fe(SC_6H_2-2,4,6-$^t Bu_3$)$_3$]$^-$ (refcode: YOMPIZ; see section 2.3.3)[197] and related heteroleptic compounds (*e.g.* [Fe(SC_6H_2-2,4,6-$^t Bu_3$)$_2${NC_5H_4-2-CH($SiMe_3$)$_2$}], refcode: YUMWAE)[259]. The size of the 2,4,6-tri-*tert*-butylphenylthiolato ligand is comparable to that of the tri-*tert*-butoxysilanethiolate moiety, therefore, would it be possible to use the latter as a source for tricoordinated silanethiolates of iron(II)?

Regrettably, it does not seem to be the case. The presence of nearby oxygen atoms offers iron an immediate resource for redistributing its charge: the greater polarizability of oxygen allows the formation of a formal bond between these atoms, an ability which turns alkoxysilanethiolates into potential chelating ligands. Chelation is known and has already been documented for other transition metal trialkoxysilanethiolates. More specifically, V, Co, Mn, Cd, Hg, Cr and Zn tri-*tert*-butoxysilanethiolates[30,40,41,232,237,260-265], have demonstrated to possess this ability. Therefore, it is understood that for our complexes $[Fe\{SSi(O^tBu)_3\}_2(\beta\text{-pic})]$ **[VII]**, $[Fe\{SSi(O^tBu)_3\}_2(\gamma\text{-pic})]$ **[VIII]**, and $[Fe\{SSi(O^tBu)_3\}_2(3,5\text{-lut})]$ **[IX]** the conditions for chelation are fulfilled, forming pentacoordinated metal complexes.

Also, a graph of the mean values of quadratic elongation vs. the angle variance can be plotted. Here it is compulsory to discuss and define what reference is more appropriate as an ideal polyhedron. Despite one could think that the ligands around the metal center try to adopt the closest form to a sphere, this is mostly true for homoleptic complexes. When we introduce several different kinds of ligands, the strength with which they are attracted to the metal center may vary depending on their nature. Thus, we observed that for the complexes that used their O-atoms for chelation, the Fe-O bonds were longer than the Fe-S or the Fe-N and that all of them fitted better to a regular trigonal bipyramid model where all the edges of the bipyramid have the same distance, but the ideal center-to-vertex distances calculated this way differ depending if it is an apical or an equatorial vertex. However, complex **[VI]** is an exception to this and fits slightly better in a model where the ideal polyhedron is an irregular trigonal bipyramid with equal center-to-vertex distances.

Nevertheless, **[VI]** still fits well in the regular trigonal bipyramid model and therefore, it is our model of choice. The following graph is plotted according to it:

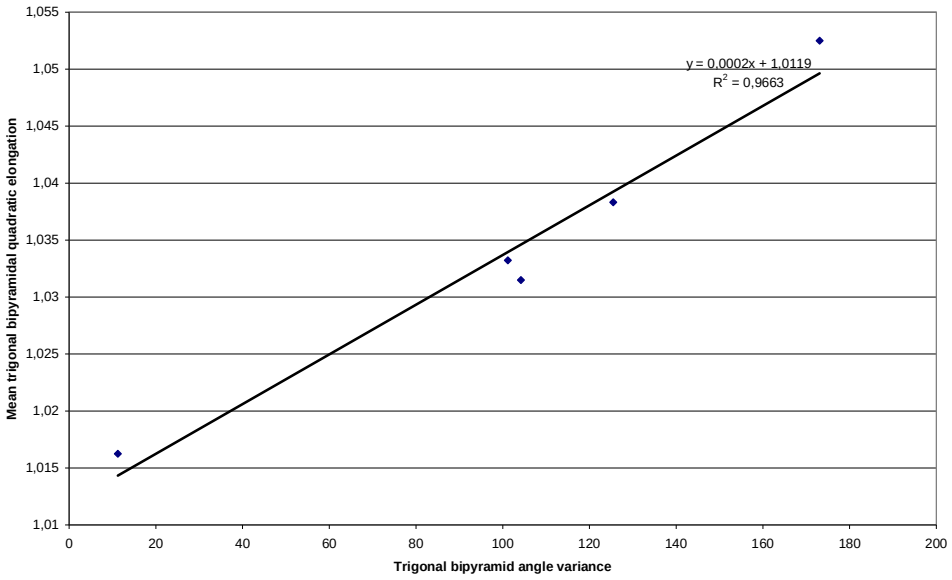

Fig. 32. Data correlation for pentacoordinated silanethiolates.

As it has been stressed before, the complexes of iron containing both alcohol and thiolate ligands are extremely rare and **[VI]** is one of the few examples known.

Previously, we thought that only two possibilities existed for mononuclear silanethiolates of iron(II): either the chelating pentacoordinated trigonal bipyramid structure with just one N-donor ligand or the most typical tetrahedral geometry with two N-donor ligands. However, the formation of **[VI]** is not completely unexpected since its Mn(II) homologue $[Mn\{SSi(O^tBu)_3\}_2(\alpha\text{-pic})(MeOH)_2]$ (refcode: XEZPAU) attains basically the same structure. Also, **[VI]** can be compared to $[Zn\{SSi(OBu^t)_3\}_2(2,4\text{-lut})(NH_3)]$ (refcode: WOWQII) as both heterocyclic coligands present a methyl group in the α- position[39]. The steric hindrance provided by this group seems to rearrange the molecular orbitals of the structure in such a manner that avoids the chelation via the oxygen atoms, but allows for smaller molecules to establish a bond (in the cases mentioned, NH_3 and MeOH enter as coligands).

From the structural point of view, **[VI]** can be considered to possess an intermediate geometry between those of the other picoline complexes and **[I]**. Much like **[VII]** and **[VIII]**, only an N-donor ligand is present in **[VI]**. The similitude with **[I]** stems not only from the presence of the methanol moieties, but also from the two H-bonds linking each of them to the closest O-atom of one silanethiolate's *tert*-butoxy groups.

Table 15. Selected distances (Å) and angles (°)	**$[Fe\{SSiR_3\}_2(\alpha\text{-pic})(MeOH)_2]$ [VI]**	**$[Mn\{SSiR_3\}_2(\alpha\text{-pic})(MeOH)_2]$ [XEZPAU]**
M-N	2.123(4)	2.174(5)
M-S(1)	2.366(15)	2.440(1)
M-S(2)	2.370(15)	-
S(1)-Si(1)	2.069(2)	2.072(1)
Si(1)-O(1)	1.653(4)	1.655(3)
Si(1)-O(2)	1.629(4)	1.628(3)
Si(1)-O(3)	1.625(4)	1.626(3)
S(2)-Si(2)	2.068(2)	-
Si(2)-O(4)	1.618(4)	-
Si(2)-O(5)	1.651(4)	-
Si(2)-O(6)	1.629(4)	-
M-O(7)*	2.242(4)	2.257(3)
M-O(8)	2.241(4)	-
N-M-S(1)	121.89(15)	122.00(1)
N-M-S(2)	121.80(15)	-
N-M-O(7)*	85.19(17)	84.6(1)
N-M-O(8)	85.49(17)	-
S(1)-M-S(2)	116.31(5)	116.04(4)
Si(1)-S(1)-M	112.04(7)	111.60(5)
Si(2)-S(2)-M	112.02(7)	-
O(7)-M-S(1)*	91.96(11)	92.54(8)
O(7)-M-S(2)*	93.06(10)	93.13(8)
O(8)-M-S(1)	93.11(11)	-
O(8)-M-S(2)	91.71(11)	-
O(7)-M-O(8)	170.67(14)	169.30(1)
$\langle\lambda\rangle$	1.01625301	
$\boldsymbol{\sigma^2}$	11.2332625	

R=^{t}BuO

* In case of the Mn homologue, the corresponding O(7) and O(8) atoms are marked as O(4) and O(5) respectively.

In both complexes, the H-bonds are notably short:

Table 16	**[Fe{SSi(O^{t}Bu)$_3$}$_2$(α-pic)(MeOH)$_2$] [VI]**	**[Mn{SSi(O^{t}Bu)$_3$}$_2$(α-pic)(MeOH)$_2$] [XEZPAU]**
O1	1.943	1.829
O5	1.915	1.829

The lack of symmetry extends to the parameters of the crystalline cell:

Table 17	**[Fe{SSi(O^{t}Bu)$_3$}$_2$(α-pic)(MeOH)$_2$] [VI]**	**[Mn{SSi(O^{t}Bu)$_3$}$_2$(α-pic)(MeOH)$_2$] [XEZPAU]**
Space group	Triclinic, P -1	Monoclinic, C 2/c
Cell length a (Å)	9.2486(2)	15.7587(10)
Cell length b (Å)	9.2611(8)	9.6671(6)
Cell length c (Å)	29.5478(19)	29.6646(16)
Cell angle α	81.645º(10)	90º
Cell angle β	81.674º(7)	99.046
Cell angle γ	62.64º	90º
Cell volume (Å^3)	2215.09	4462.93
Cell formula units Z	2	4
Measurement temperature (K)	Room temperature	100
R factor	7.54%	8.72%

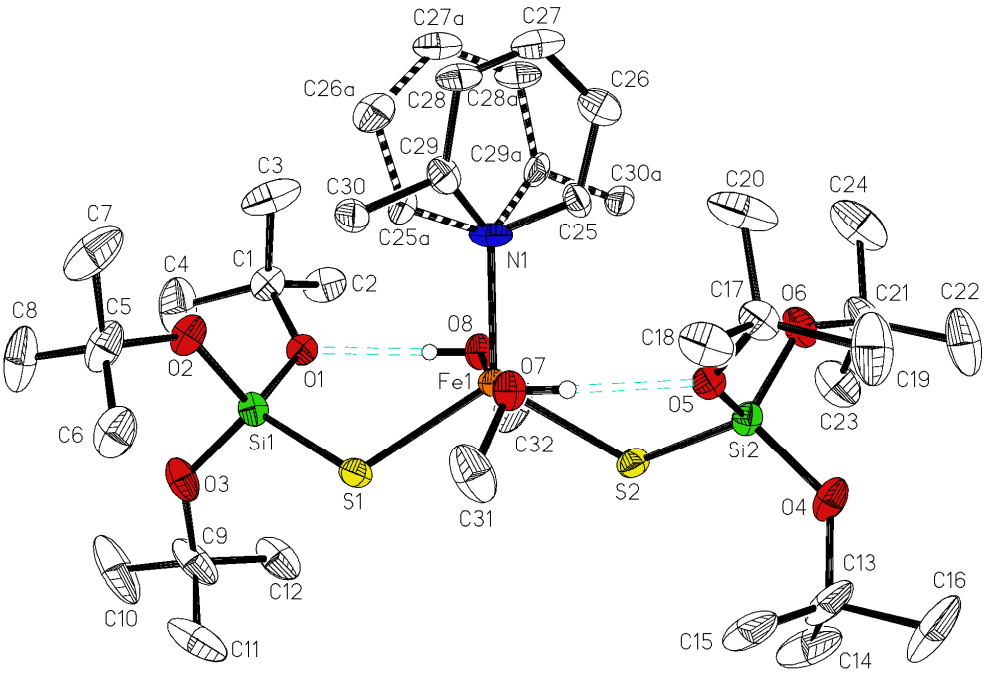

Fig. 33. Structure of [VI]. Notice two intramolecular hydrogen bonds and the alternance in the position of the α-picoline ligand even within the same crystal. Thermal ellipsoids 30%.

Table 18. Selected distances(Å) and angles(º)	**[Fe{SSi(O^{t}Bu)$_3$}$_2$(β-pic)] [VII]**	**[Mn{SSi(O^{t}Bu)$_3$}$_2$(β-pic)] [XEZPEY]**
M-N	2.112(2)	2.170(2)
M-S(1)	2.330(8)	2.412(6)
M-S(2)	2.329(8)	2.409(6)
S(1)-Si(1)	2.078(11)	2.075(8)
Si(1)-O(1)	1.665(2)	1.672(2)
Si(1)-O(2)	1.625(2)	1.626(2)
Si(1)-O(3)	1.616(2)	1.624(2)
S(2)-Si(2)	2.075(10)	2.070(7)
Si(2)-O(4)	1.659(2)	1.671(1)
Si(2)-O(5)	1.629(2)	1.628(2)
Si(2)-O(6)	1.623(2)	1.626(2)
M···O(1)	2.363(19)	2.373(2)
M···O(4)	2.377(19)	2.366(1)
N(1)-M-S(1)	115.42(8)	115.21(5)
N(1)-M-S(2)	110.91(7)	109.74(5)
S(1)-M-S(2)	133.66(3)	135.02(2)
Si(1)-S(1)-M	86.02(3)	85.37(2)
Si(2)-S(2)-M	86.34(3)	85.46(2)
O(1)···M-S(1)	76.79(5)	75.57(4)
O(4)···M-S(2)	76.50(5)	75.55(4)
O(1)···M···O(4)	178.53(7)	177.99(5)
M-S(1)-Si(1)-O(1)	-3.70(1)	3.58(6)
M-S(2)-Si(2)-O(4)	0.30(1)	0.11(6)
$\langle\lambda\rangle$	1.03831434	
$\boldsymbol{\sigma^2}$	125.478775	

Table 19	**[Fe{SSi(O^{t}Bu)$_3$}$_2$(β-pic)] [VII]**	**[Mn{SSi(O^{t}Bu)$_3$}$_2$(β-pic)] [XEZPEY]**
Space group	Monoclinic, P 2_1/c	Monoclinic, P 2_1/c
Cell length a (Å)	8.55120(10)	8.5154(5)
Cell length b (Å)	25.3305(6)	25.3692(14)
Cell length c (Å)	18.6288(4)	18.6967(7)
Cell angle α	90º	90º
Cell angle β	95.845º(2)	95.581º(4)
Cell angle γ	90º	90º
Cell volume (Å^3)	4014.13	4019.88
Cell formula units Z	4	4
Measurement temperature (K)	120	100
R factor	4.96%	4.83%

Table 20. Selected distances(Å) and angles(º)	**[Fe{SSi(O^{t}Bu)$_3$}$_2$(γ-pic)] [VIII]**		**[Mn{SSi(O^{t}Bu)$_3$}$_2$(γ-pic)] [XEZPIC]**
	Fe1	**Fe2**	
M-N	2.092(2)	2.091(2)	2.196(5)
M-S(1)	2.332(7)	2.321(7)	2.423(2)
M-S(2)	2.331(7)	2.326(8)	2.420(2)
S(1)-Si(1)	2.074(10)	2.077(10)	2.066(2)
Si(1)-O(1)	1.663(19)	1.657(19)	1.657(4)
Si(1)-O(2)	1.625(19)	1.632(19)	1.603(5)
Si(1)-O(3)	1.617(19)	1.618(18)	1.609(5)
S(2)-Si(2)	2.077(9)	2.076(10)	2.069(2)
Si(2)-O(4)	1.660(19)	1.660(19)	1.665(3)
Si(2)-O(5)	1.624(18)	1.620(2)	1.611(3)
Si(2)-O(6)	1.629(18)	1.632(2)	1.616(4)
M···O(1)	2.316(17)	2.394(18)	2.372(4)
M···O(4)	2.388(17)	2.377(19)	2.378(3)
N(1)-M-S(1)	114.83(6)	111.89(6)	106.80(1)
N(1)-M-S(2)	114.23(6)	116.93(6)	107.40(1)
S(1)-M-S(2)	130.79(3)	131.17(3)	145.71(6)
Si(1)-S(1)-M	85.19(3)	86.60(3)	85.11(7)
Si(2)-S(2)-M	86.39(3)	86.28(3)	85.37(7)
O(1)···M-S(1)	77.22(5)	76.42(5)	75.10(1)
O(4)···M-S(2)	76.42(5)	76.56(5)	74.95(9)
O(1)···M···O(4)	175.91(6)	174.37(6)	167.50(1)
M-S(1)-Si(1)-O(1)	-5.32(7)	2.93(7)	-4.50(2)
M-S(2)-Si(2)-O(4)	-2.55(7)	3.80(7)	-7.70(1)
$\langle\lambda\rangle$	1.0332	1.0314	
σ^2	101.160	104.20625	

Table 21	**[Fe{SSi(O^{t}Bu)$_3$}$_2$(γ-pic)] [VIII]**	**[Mn{SSi(O^{t}Bu)$_3$}$_2$(γ-pic)] [XEZPIC]**
Space group	Monoclinic, P 2_1/c	Orthorhombic, P b c n
Cell length a (Å)	11.2321(3)	21.9424(14)
Cell length b (Å)	25.6730(6)	14.9752(9)
Cell length c (Å)	28.5656(7)	26.1160(16)
Cell angle α	90º	90º
Cell angle β	91.190º(2)	90º
Cell angle γ	90º	90º
Cell volume (Å^3)	8235.45	8581.5
Cell formula units Z	8	8
Measurement temperature (K)	120	100
R factor	4.27%	10.32%

[Fe{SSi(O^{t}Bu)$_3$}$_2$(3,5-lut)] **[IX]** displays a distorted trigonal bipyramidal structure with both oxygen atoms occupying the apical positions and the single 3,5-lutidine ring together with the silanethiolate moieties populating the equatorial plane.

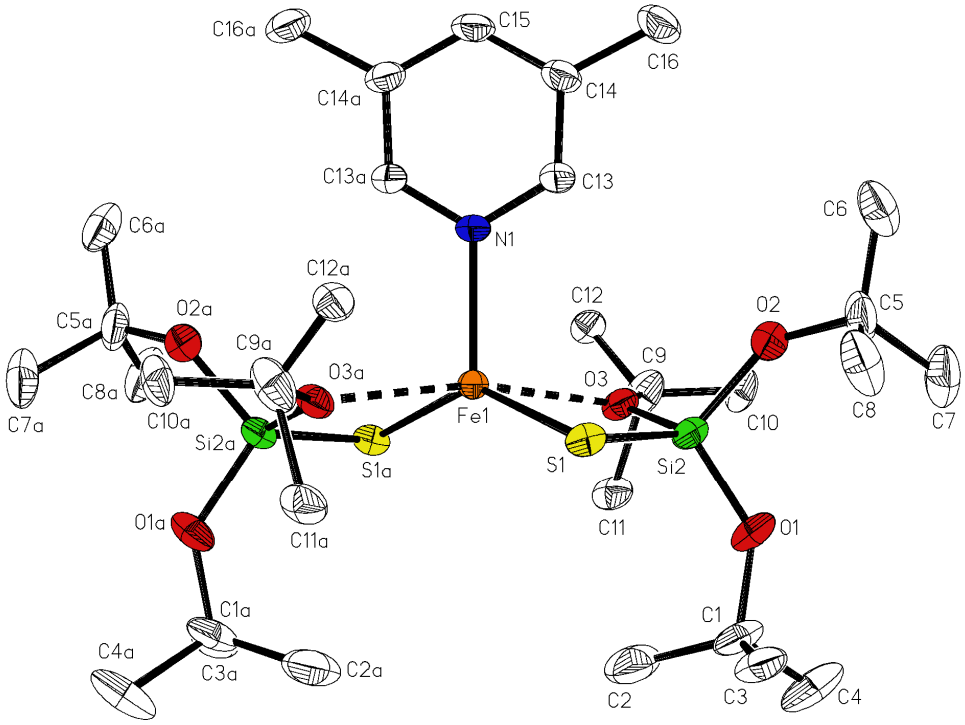

Fig. 34. Structure of [IX]. Notice the chelation provided by oxygen atoms (O3 and O3a). Thermal ellipsoids 30%.

It is significant that the closest compound in respect to **[IX]** that appears in the CCDC database, is the rather unrelated dithiolate $[Fe(S_2C_2Et_2)_2(py)](Et_4N)$ (refcode: UCECEL)[266].

More successful was the search for other transition metal silanethiolates with 3,5-lutidine as the coligand: two trialkoxysilanethiolates $[Co\{Si(O^tBu)_3\}_2(3,5\text{-lut})]$ and $[Zn\{SSi(O^tBu)_3\}_2(3,5\text{-lut})]$ (refcodes: IDADUM and HAYSAC respectively) appear to present isomorphism[34,265] with **[IX]**, and a third, $[Cd\{SSi(O^tBu)_3\}_2(3,5\text{-lut})]$ (refcode: VEGHAR), displays a similar geometry[267] although it belongs to a different space group. It is remarkable that all the trialkoxysilanethiolates functionalized their oxygen atoms to provide chelation and adopted a pentacoordinated triangular bipyramidal structure. This contrasts with the only alkylsilanethiolate found with 3,5-lutidine as the coligand: $[Zn(SSiMe_3)_2(3,5\text{-lut})_2]$ (refcode:RAPZAK)[268] which presents two main differences with regards to trialkoxysilanethiolates. First, as it lacks a suitable electronegative atom such as the O atom of the *tert*-butoxy group, it is unable to chelate. Second, the Me_3SiS^- ligands offer considerably less steric hindrance than the bulky $(^tBuO)_3SiS^-$. As a result, the complex $[Zn(SSiMe_3)_2(3,5\text{-lut})_2]$ adopts a tetrahedral geometry.

It is worth noting that a silanethiolate exists that uses 2,4-lutidine as a coligand. It is the tetrahedral [Zn{SSi(OBu^t)$_3$}$_2$(2,4-lut)(NH$_3$)] (refcode – WOWQII)[39], which does not share many characteristics with the complexes containing 3,5-lutidine, but instead is more useful to explain why chelation is not produced in complex **[VI]**. The details of [Fe{SSi(O^{t}Bu)$_3$}$_2$(3,5-lut)] compared to its closest relatives can be appreciated in the table below:

Table 22	**[Fe{SSiR$_3$}$_2$(L)] [IX]**	**[Co{SSiR$_3$}$_2$(L)] [IDADUM]**	**[Zn{SSiR$_3$}$_2$(L)] [HAYSAC]**	**[Cd{SSiR$_3$}$_2$(L)] [VEGHAR]**
Space group	C2/c	C2/c	C2/c	P2$_1$/c
Cell length a (Å)	14.685(9)	14.814(3)	14.542(3)	14.550(6)
Cell length b (Å)	13.024(6)	13.121(3)	12.806(3)	12.887(6)
Cell length c (Å)	21.881(13)	22.181(4)	22.265(4)	23.969(9)
Cell angle α	90º	90º	90º	90º
Cell angle β	104.47º(5)	102.34º(3)	101.39º(3)	114.17º(3)
Cell angle γ	90º	90º	90º	90º
Cell volume (Å^3)	4052.00	4211.81	4064.64	4100.53
Cell formula units Z	4	4	4	4
Measurement temperature (K)	120	Room temp. (283-303)	150	120
R factor	5.17%	6.11%	3.76%	3.96%

L=3,5-lutidine. R=^{t}BuO

Table 23. Selected distances (Å) and angles (º)	**[Fe{SSiR$_3$}$_2$(L)] [IX]**	**[Co{SSiR$_3$}$_2$(L)] [IDADUM]**	**[Zn{SSiR$_3$}$_2$(L)] [HAYSAC]**	**[Cd{SSiR$_3$}$_2$(L)] [VEGHAR]**
M-N	2.134(3)	2.058(4)	2.071(3)	2.297(3)
M-S(1)	2.324(8)	2.264(10)	2.248(7)	2.434(8)
M-S(2)	-	-	-	2.435(8)
S(1)-Si(1)	2.069(13)	2.0743(13)	2.080(1)	2.084(1)
Si(1)-O(1)	1.621(2)	1.645(2)	1.646(2)	1.653(2)
Si(1)-O(2)	1.633(3)	1.605(3)	1.621(2)	1.627(2)
Si(1)-O(3)	1.657(2)	1.619(3)	1.626(2)	1.627(2)
S(2)-Si(2)	-	-	-	2.085(1)
Si(2)-O(4)	-	-	-	1.656(2)
Si(2)-O(5)	-	-	-	1.626(2)
Si(2)-O(6)	-	-	-	1.626(2)
M···O(1)	2.383(2)*	2.454(3)	2.539(2)	2.616(2)
M···O(4)	-	-	-	2.598(2)
N(1)-M-S(1)	108.77(2)	111.03(3)	110.30(7)	107.09(6)
N(1)-M-S(2)	-	-	-	105.61(6)
S(1)-M-S(2)	142.47(5)	137.94(6)	139.40(3)	147.29(3)
Si(1)-S(1)-M	86.35(4)	88.06(5)	89.57(3)	89.34(3)
Si(2)-S(2)-M	-	-	-	89.08(3)
O(1)···M-S(1)	76.41(6)	76.24(6)	75.36(4)	71.90(5)
O(4)···M-S(2)	-	-	-	72.10(5)
O(1)···M···O(4)	168.08(11)	165.40(13)	166.47(5)	169.43(6)
M-S(1)-Si(1)-O(1)	-4.63(9)*	5.11(11)	7.32(7)	-5.34(8)
M-S(2)-Si(2)-O(4)	-	-	-	-5.59(8)
$\langle\lambda\rangle$	1.05249951			
$\boldsymbol{\sigma^2}$	173.070238			

R=^{t}BuO *In this case, the chelating oxygen atom is labeled in the graphic as O(3).

The ability of methyl substituted pyridines to form the pentacoordinated complexes **[VI]**, **[VII]**, **[VIII]** and **[IX]** instead of more typical tetrahedral complexes can be attributed – at least to some extent – to the electron withdrawal provided by their methyl substituents. This seems to provoke a rearrangement of the molecular orbitals in such fashion that avoids the inclusion of a second N-donor ring into the structure. The Fe-N bond length decreases as the methyl substituent is placed at a more distant position from the nitrogen atom according to the series: α-picoline (*ortho*) > β-picoline (*meta*) > γ-picoline (*para*). This contrasts with the equivalent series for the Mn(II) homologues: γ-picoline (*para*) > α-picoline (*ortho*) > β-picoline (*meta*); as shown on Table 24. Complex **[IX]** suggests that the Fe-N bond length also increases when a second methyl substituent is added, but more data are needed and the synthesis of related complexes with different lutidines should shed some light on this subject.

Table 24. M-N average bond length (in Å) for iron and manganese complexes		
	M = Fe(II)	**M = Mn(II)**
$[M\{SSi(O^tBu)_3\}_2(\alpha\text{-pic})(MeOH)_2]$	2.123	2.174
$[M\{SSi(O^tBu)_3\}_2(\beta\text{-pic})]$	2.112	2.170
$[M\{SSi(O^tBu)_3\}_2(\gamma\text{-pic})]$	2.092	2.196

On the other hand, it is evident that for such three-ligand complexes, the structure stabilization is accomplished by the additional ligation of oxygen at the iron center and thus acquiring the coordination number 5. Due to the difference in electronegativity, it is relatively easy for the oxygen atoms to establish a bond with the iron(II) center. As it has been mentioned before, this kind of bidentate behavior of trialkoxysilanethiolates is already known for other metals but these are the first examples of such a chelation with iron. **[VI]** presents the only exception to this rule. Most probably, the methyl substituent at the *para* position of the pyridine ring is close enough to the metal to provoke either some steric impediment or some electronic repulsion (or a mixture of both effects) that avoids the oxygen atoms of the silanethiolate ligands to form a bond and instead, two methanol molecules bind to accomplish the CN=5 (a more stable solution than three ligands with CN=3). The structure of $[Zn\{SSi(OBu^t)_3\}_2(2,4\text{-lut})(NH_3)]$ seems to support this hypothesis, although in this case only a molecule of ammonia is used to stabilize the structure, yielding a tetracoordinated complex instead of a pentacoordinated one.

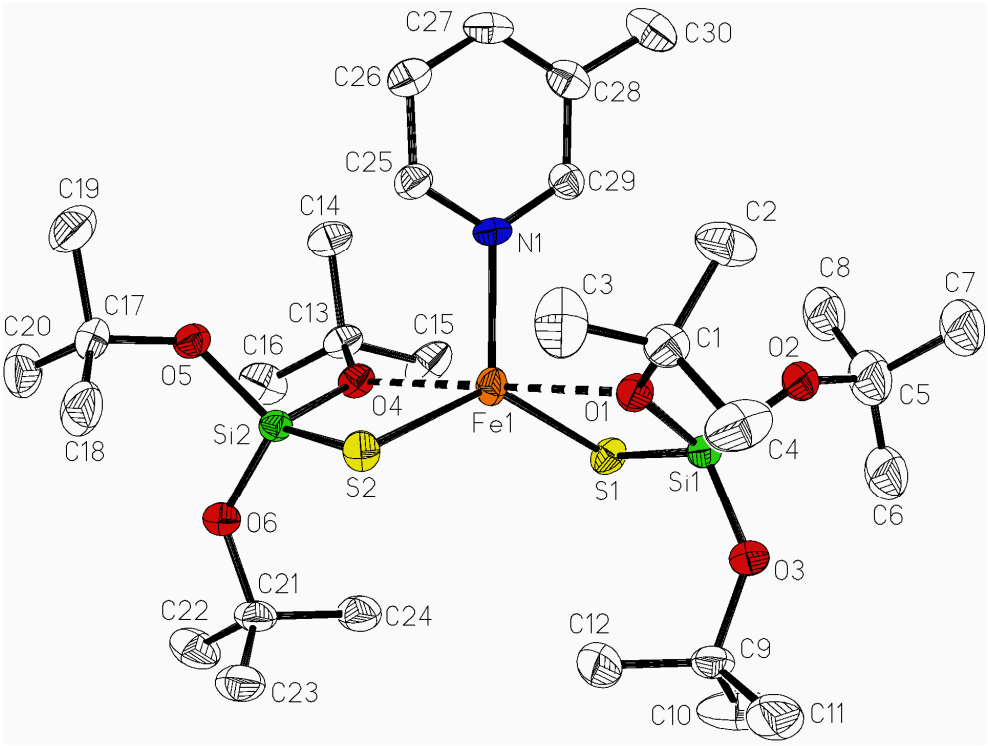

Fig 35. Structure of [VII]. Notice the chelation provided by oxygen atoms (O1 and O4). Thermal ellipsoids 50%.

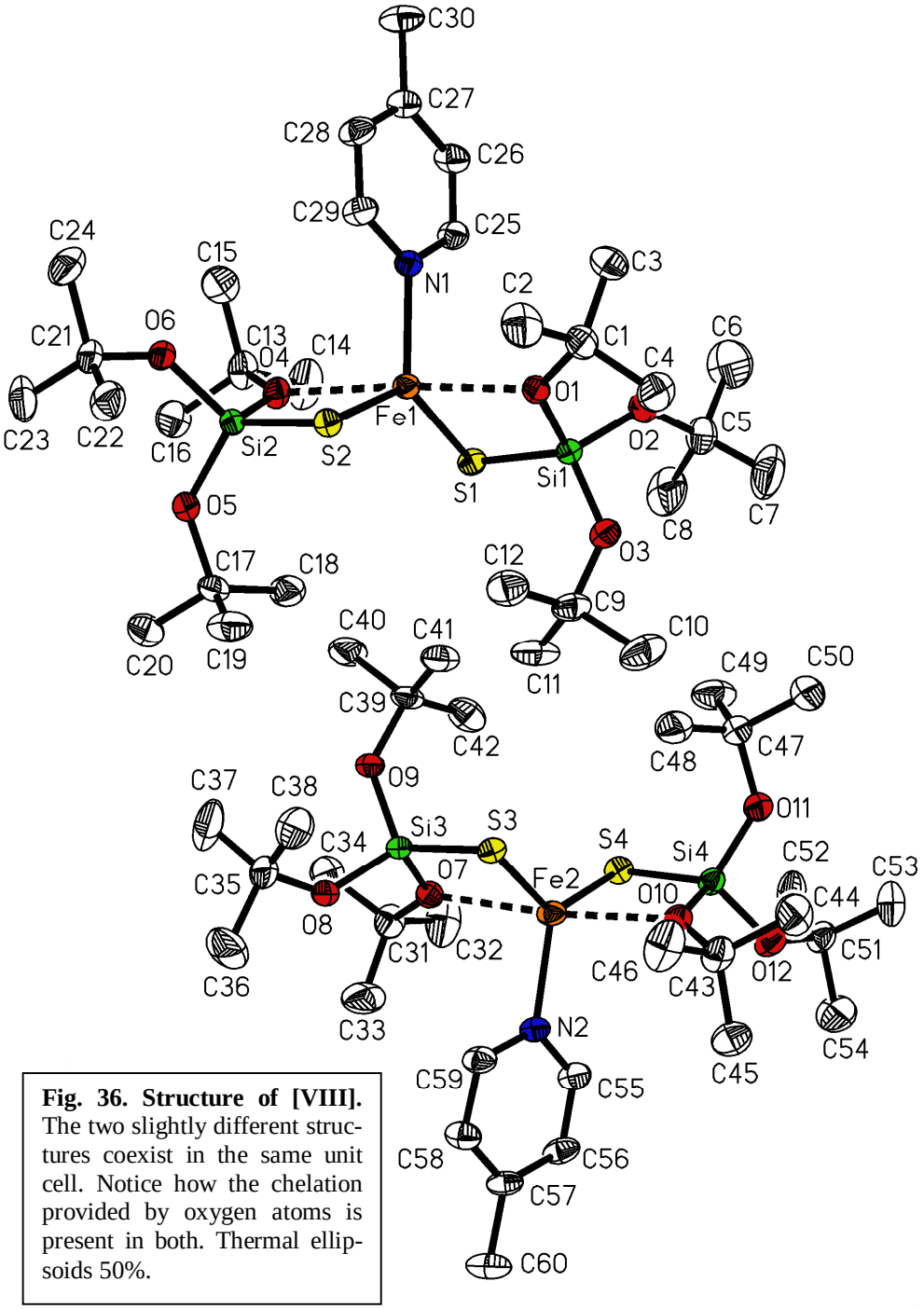

Fig. 36. Structure of [VIII]. The two slightly different structures coexist in the same unit cell. Notice how the chelation provided by oxygen atoms is present in both. Thermal ellipsoids 50%.

5.B.2. The [4Fe-4S] cubane cluster of $[Fe_4S_4\{SSi(O^tBu)_3\}_4](EtNH_4)_2$

Compound **[II]** possesses a typical 4Fe-4S distorted cubane cluster structure. **[II]** crystallizes in the form of thin, black monoclinic crystals (see table below) of considerable thermic stability. Freshly isolated samples resisted a temperature of 220ºC with no noticeable changes. **[II]** dissolves well in common solvents such as acetone, methanol, acetonitrile, tetrachloromethane and chloroform. It does not dissolve in water or isopropanol, though.

Table 25	**$[Fe_4S_4\{SSi(O^tBu)_3\}_4](EtNH_4)_2$ [II]**
Space group	Monoclinic, P 2_1/c
Cell length a (Å)	16.5476(9)
Cell length b (Å)	32.703(2)
Cell length c (Å)	16.7256(10)
Cell angle α	90º
Cell angle β	101.634º(5)
Cell angle γ	90º
Cell volume ($Å^3$)	8865.21
Cell formula units Z	4
Measurement temperature (K)	120
R factor	7.92%

This compound appears as a by-product in most reactions in which iron reacts against tri-*tert*-butoxysilanethiolate even when another ligand is involved. Its appearance is somehow surprising since there are four isolated sulfur atoms within the cluster but there is no other source of sulfur apart from the silanethiol. The mechanism why this happens has not been elucidated yet, but it is suspected to be caused by sulfur traces in the silanethiol. Figure 37 shows the structure of **[II]** with the atom labeling scheme:

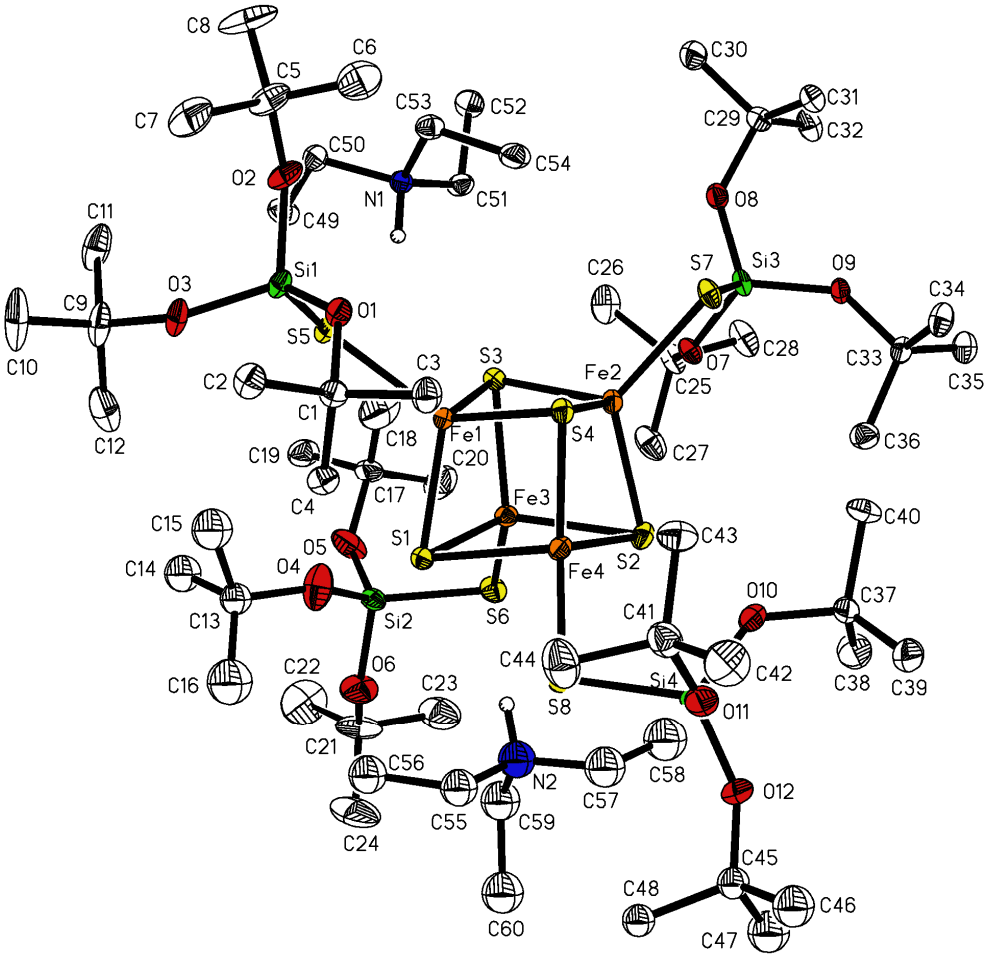

Fig. 37. Structure of [II]. The most prominent feature is the central [4Fe-4S] cluster. Only the H atoms corresponding to the cations are shown (as arbitrary spheres). Thermal ellipsoids 30%.

The structure of **[II]** is made up of three ionic compounds: the anionic $[Fe_4S_4\{SSi(O^tBu)_3\}_4]^{2-}$ that contains the cubane-type [4Fe-4S] core and two protonated amine residues (Et_3NH^+), that contribute to the electrical stability of the compound.

[II] is quite inert towards other reagents, opposed to what has been observed in other $[Fe_4S_4]^{2+}$ clusters. It is known that certain [4Fe-4S] cubane clusters react against red Se and substitute the S atoms in the core for Se either partially or totally[46,117,235], but such an activity has been impossible to reproduce for **[II]**. Nevertheless, **[II]** seems relatively unstable under the atmosphere, decomposing into the corresponding silanol $(^tBuO)_3SiOH$, elemen-

tary sulfur and iron oxides after some time. The stability of the crystals depends in great measure on their size and purity. Thus, big, pure crystals can remain practically unaltered for a few weeks. However, if the crystals are small or contain a higher quantity of impurities, the decomposition occurs after some days.

Addition of elemental sulfur seems to produce a higher yield of **[II]**, according to the equation:

$$4FeCl_2 + 10(^tBuO)_3SiS^- + 4S \longrightarrow [Fe_4S_4\{SSi(^tBuO)_3\}_4]^{2-} + 3RSSR + 8Cl^- \qquad (2)$$

But it also makes crystallization more difficult. What is more, the powder obtained in this manner is easily attacked by atmospheric oxygen and decomposes after few minutes.

Additional tests have been performed on this 4Fe-4S structure, namely FTIR and UV/Vis spectroscopy, cyclic voltammetry and some preliminary magnetic susceptibility and EPR measurements, with different results.

FTIR was successfully performed in KBr as well as directly on a solid state sample. Both samples present practically the same peaks, with the exception of the strong broad depression at 3425cm^{-1} in the hygroscopic KBr sample which corresponds to water that could not be completely removed from the pellet. Also, the equipment is more sensitive towards KBr samples, covering a broader spectra (400-4000cm^{-1}) than the one that could be attained from the microscope-coupled solid sample analysis (700-4000cm^{-1}).

As can be appreciated in the graphs pictured below, the peaks corresponding to the stretching of the C-H bond are clearly recognizable: a very strong asymmetric band at *ca.* 2973cm^{-1}, νCH_3; and a secondary peak at ~ 2870-2880cm^{-1}, νCH_3. The asymmetric medium peak for δCH_3 at ~ 1462-1470cm^{-1} is also associated to the deformation of CH_3 in *tert*-butyl groups. The tri-*tert*-butyl groups are responsible for the symmetric scissors at 1387-1363cm^{-1} and the doublet at 1207-1240cm^{-1}. The C-O bond causes a band to appear at 1190cm^{-1}. The presence of Si can be inferred from the very strong bands at 1024-1048 cm^{-1}, which arise from the valence vibrations of aliphatic Si-O-R. Strong bands at 820-802 cm^{-1} have been related to metal-oxygen interaction in cobalt complexes, thus we can attribute the bands that appear at 825-801 cm^{-1} to the interaction between iron and oxygen.

The resulting FTIR spectra are shown in the pictures below. The first spectrum (fig. 38) was obtained from a KBr pellet containing the sample while the second one (fig. 39) was registered directly from the product in crystalline state:

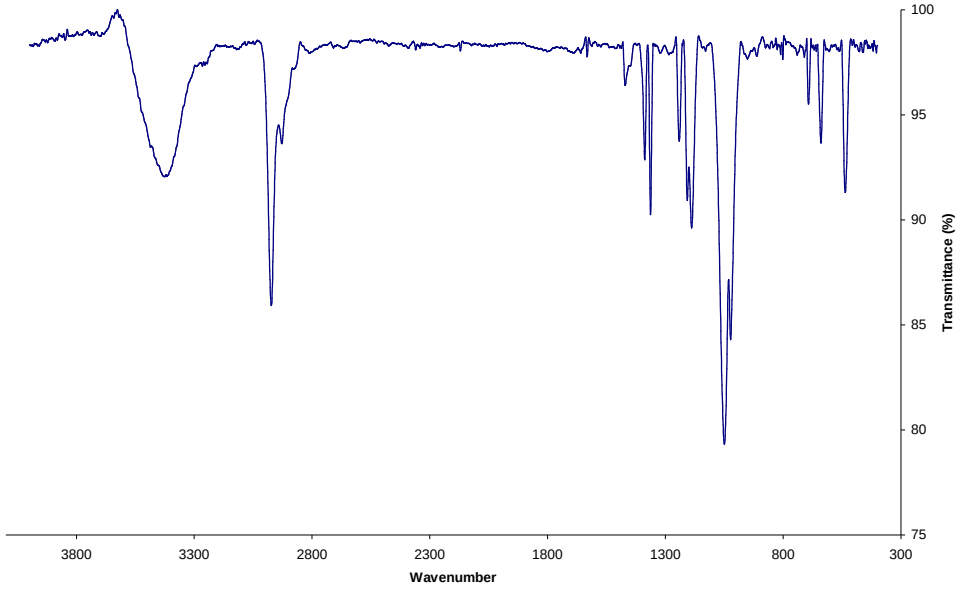

Fig. 38. IR spectrum of [II] obtained from a KBr pellet containing the sample. The broad depression at ~ 3500 cm^{-1} corresponds to residual H_2O.

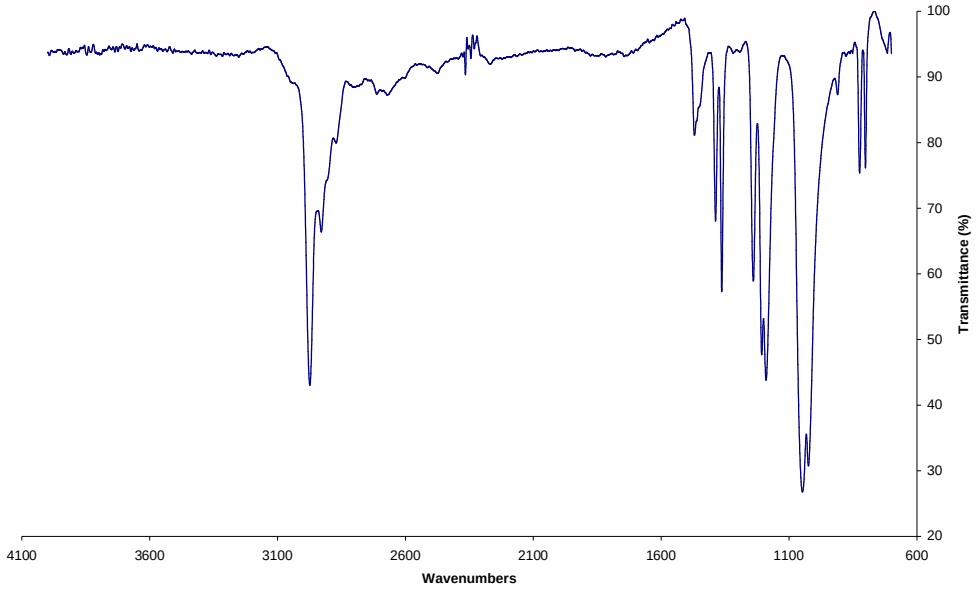

Fig. 39. IR spectrum of [II] obtained from a pure solid state sample.

UV-Vis spectroscopy was also performed as indicated in Section 4.2.3. However, the results were not very appealing. Our equipment was not ready to perform the analysis under strictly inert atmosphere and **[II]** seems to decompose much faster when in solution than in solid state and the spectra obtained were not conclusive. As a consequence, at the time the sample was put under the beam, it had already decomposed, giving incoherent results.

The magnetic susceptibility of **[II]** was measured twice and the results obtained were also not conclusive. The sample had to be delivered to another laboratory and in the meantime it could have partially decomposed, with, for example , more or less Fe(II) centers oxidized into Fe(III). This can in great measure falsify the measurements, giving erroneous or anomalous results as has indeed been observed. EPR analysis was likewise unsuccessful. Nevertheless, since an activity has been well registered, the investigations will be continued.

Cyclic voltammetry was performed in order to measure the redox activity of **[II]**. 1 mmol of **[II]** was dissolved in acetonitrile using standard Schlenk techniques to avoid oxidation. It is worth noting that acetonitrile is one of the most common solvents used in voltammetry when dealing with [4Fe-4S] clusters. The resulting plot is shown in fig. 40 on the next page. So far, this is a preliminary result, since we did not have enough material readily available to repeat the measurements. A relatively big quantity of high purity crystals are needed in order to perform the experiments and crystallization process is very slow, thus it requires a long time to obtain more materials for a new measurement.

In any case, the preliminary data obtained for the potential peak corresponding to the $[Fe_4S_4]^{2+/1+}$ reduction in the first cycle are promising since they agree well with the values found in the bibliography for similar [4Fe-4S] clusters[112,118,269-271] in acetonitrile. In general, complexes of the $[Fe_4S_4(L)_4]^{2-}$ kind, have been found to present simple one-electron reversible reductions and irreversible multielectron oxidations[269]. In our case, the graphic corresponding to the first cycle suggests irreversible redox couples at $E_{1/2}$ = -0.93 V for $[Fe_4S_4]^{2+/1+}$ and at $E_{1/2}$ = -1.28 V for $[Fe_4S_4]^{1+/0}$. Further polarization causes potential shift toward more cathodic potentials, probably produced by the decomposition of the material, which would explain the perceptibly divergent graphic corresponding to the second cycle.

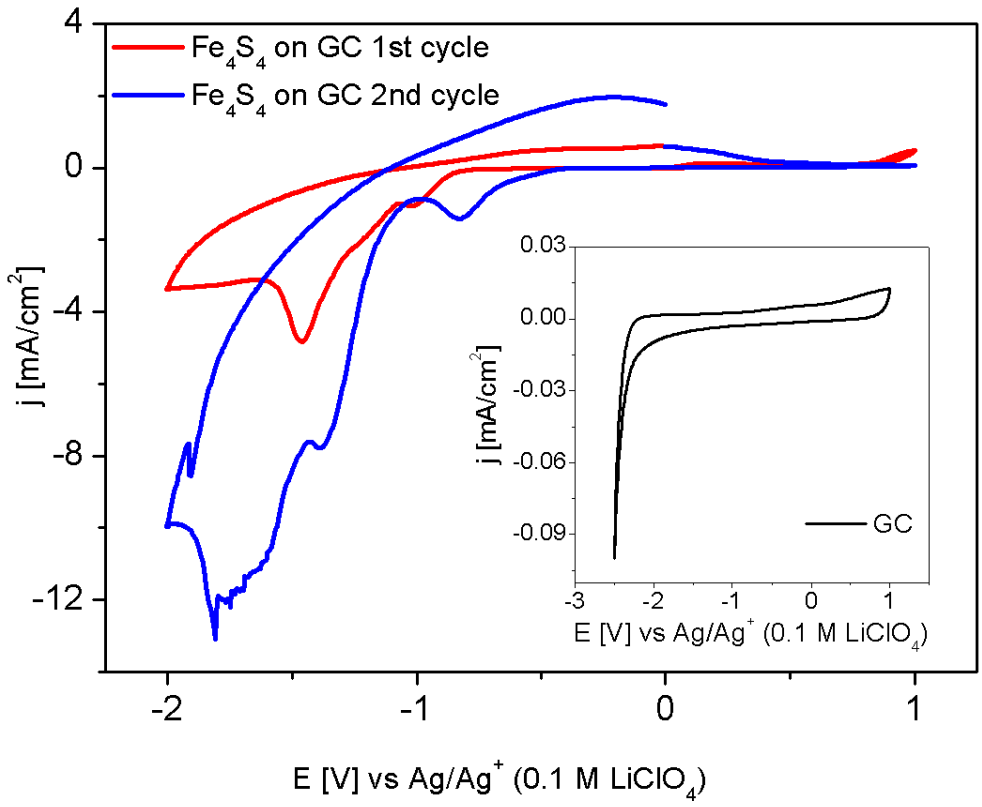

Fig. 40. Cyclic voltammogram curves of Fe_4S_4 (50 mV/s) showing irreversible one-electron reduction. The inset shows cyclic voltammetry curve of GC electrode (sweep rate 50 mV/s). Measurements were obtained in 0.1 M $LiClO_4$ in MeCN electrolyte

	1st cycle		2nd cycle	
	E_p (V)	$E_{p/2}$ (V)	E_p (V)	$E_{p/2}$ (V)
$[Fe_4S_4]^{2+/1+}$	-1.02	-0.93	-0.82	-0.71
$[Fe_4S_4]^{1+/0}$	-1.46	-1.28	-1.39	-1.25

Table 26. Redox potentials of $[Fe_4S_4]^{2+}$ clusters in acetonitrile

On the geometry of the [4Fe-4S] clusters

When dealing with [4Fe-4S] clusters we often find them referred to as "cubane clusters" or "cubanes". These terms are in most cases nothing else than a euphemism to describe vaguely cuboidal shapes. With the only exception of Sydora's complex [(^{t}Bu$_3$SiCC)Fe(μ-SSi^{t}Bu$_3$)]$_4$ (refcode: OHOKIF), which suffers a minimal deviation from a perfect cube, most of the [4Fe-4S] clusters are better described as two concentric tetrahedra, hence a *stella octangula*[272].

In several [4Fe-4S] clusters there is a significant degree of distortion introduced by the $\bar{4}$ (**4-bar**) contraction[273,274]. This effect causes that four of the Fe-S bonds are either abnormally shorter (compressed) or larger (elongated) than the other 8. The **4-bar** contraction can be explained in an analogous manner to the Jahn-Teller effect, but applied to the multicentric [4Fe-4S] cluster (which can be better visualized as two parallel rhomboidal [2Fe-2S] subclusters with a rotation of ~ 90º with respect to each other). For instance, in case of compressed clusters, it is the antiferromagnetic coupling between the electronic spin of the subclusters that causes them to move toward each other along a perpendicular axis. However, the same authors found no correspondence between the spin state and the **4-bar** contraction[273].

Therefore, if it is not recommendable to make use of the parameters that describe a cube, and the values we can easily obtain are not reliable as a measure of the **4-bar** contraction, what can we do in order to assess the distortion of a [4Fe-4S] cluster? In 2003, Fee *et al.* introduced a method and some tools[274] to quantitatively evaluate the distortion of these structures. Certainly, their method deserves credit by its simplicity. Given any $[Fe_4S_4(L)_4]^n$ complex, we can establish three distorted tetrahedra defined by the four Fe atoms, by the four S atoms of the cluster and by the four terminal atoms of the L ligands, respectively. As four points not in a plane are circumscribed inside one and only one sphere, each tetrahedron defines one such circumsphere. If we now calculate the circumcenter (CC) of each sphere, the problem of assessing the distortion of 12 points in space is reduced to evaluating the distortion of 3 points and the divergence between the three circumradii. In order to simplify and standardize the calculations, the origin of coordinates is arbitrarily chosen as the circumcenter of the iron tetrahedron (CC_{Fe} = (0, 0, 0)).

Fee *et al.* warn that the calculations cannot be provided by general algebraic methods since these produce sometimes unstable results when taking the error in account. Thus, they released an informatic tool, the java program ClusterGeom, that performs the necessary calculations including the propagation of the error from an input .pdb or .cif file. The output is given not only as Cartesian coordinates, but also in geospherical coordinates and Hammer-Aitoff projection coordinates. The Hammer-Aitoff projection[275] is quite common in cartography as a method to represent a spherical shape (*i.e.* the Earth) on a plane.

Following, we present the values of the radii, circumcenters, and the divergence between radii for several $[Fe_4S_4(SR)_4]^{2-}$ clusters found in the CCDC Database. We are also taking into account the values of an ideal cluster provided by Fee *et al.* in their article for comparison. The parameters corresponding to the iron, sulfur and terminal thiolate sulfur tetrahedra are indicated by the subindexes (Fe, S or SG, respectively). As stems from table 27, **[II]** is noticeably distorted respect to other clusters. See Annex C for more detailed data.

Reference code	r_{Fe}	r_S	r_{SG}	CC_S-CC_{Fe}	CC_{SG}-CC_{Fe}	Δr_{Fe-S}	Δr_{S-SG}
IDEAL	1.65	2.25	3.95	0	0	0.6	1.7
[II]	1.697	2.208	3.956	0.017	0.025	0.511	1.748
MEAN	1.681	2.207	3.933	0.0181	0.014	0.526	1.727

Table 27. Parameters of the defining circumspheres for synthetic cubane clusters.

From the analysis of this set of data, we obtain the following conclusions:

1) The circumcenters CC_S and CC_{SG} present a moderate shift respect the origin of coordinates (CC_{Fe}).

2) The radius corresponding to the iron tetrahedron circumsphere (r_{Fe}) is significantly longer than the corresponding value for an ideal cluster and also longer than the average.

3) The value of the radius of the sulfur tetrahedron circumsphere (r_S) is on the average for clusters in this oxidation state, but is much shorter than the r_S of an ideal cluster.

4) The circumradius of the thiolate sulfur circumsphere (r_{SG}) is close to the ideal value but is longer than expected according to the average.

5) The divergence between r_{Fe} and r_S is lower than the average and significantly lower than the ideal value.

6) The divergence between r_S and r_{SG} is higher than the average value and significantly higher than the divergence in a perfect cluster.

7) The measurement temperature has been taken into account; but it does not seem to exert much influence on the distortion of the cube. Lower temperatures do not guarantee a lower degree of distortion.

5.B.3. Homoleptic octahedral complexes of iron(II)

Heterocyclic N-donor compounds with a ring composed of a number of carbon atoms different from 6 did not achieve the intended heteroleptic silanethiolates. Instead, two of these ligands formed very stable homoleptic complexes: $[Fe(N\text{-meimid})_6]Cl_2.2H_2O$ **[XI]** and $[Fe(phen)_3]Cl_2.6MeOH$ **[XII]**. The structural data of these complexes were published[240,241] in Acta Crystallographica Sect. E.

5.B.3.1. $[Fe(N\text{-meimid})_6]Cl_2.2H_2O$

The imidazole ring is ubiquitous in biological systems. As the terminal group of histidines, it can be found playing a role in such heterogeneous systems as vitamin B_{12}, Fe-Ni nitrogenase, hemoglobin, myoglobin or cytochrome c[276]. In view of this, octahedral homoleptic complexes of iron with imidazole ligands have been postulated as models for such biological sites and some examples can be found on the CCDC database[276-279].

As has been commented before, we have accomplished the synthesis of one such adduct, $[Fe(N\text{-meimid})_6]Cl_2.2H_2O$ **[XI]**. According to the bibliography, a related tetrahydrate is already known[280,281], $[Fe(imid)_6]Cl_2.4H_2O$ (refcode: AXAKIT). **[XI]** is also isostructural with its Co(II), Ni(II) and Ru(II) homologues[282-284].

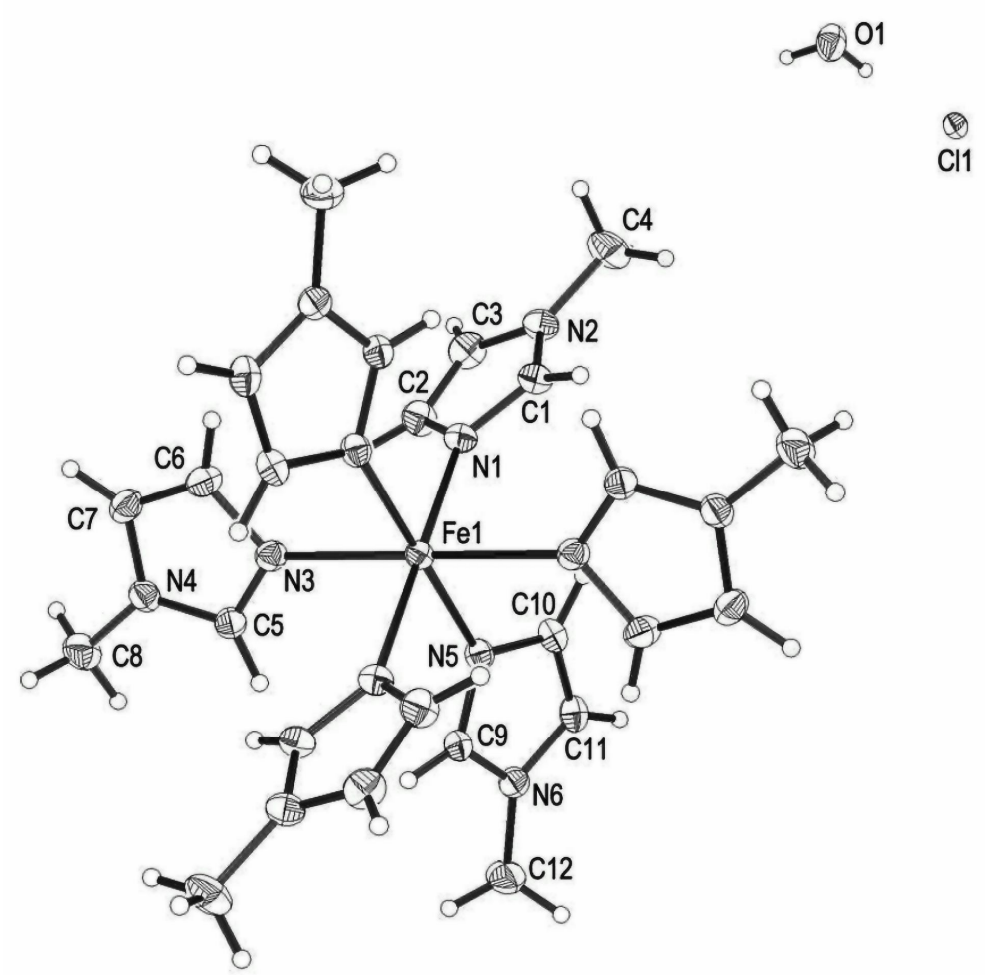

Fig. 41. The structure of the components of [XI]. Thermal ellipsoids 50% (arbitrary spheres for the H atoms). Unlabelled atoms are generated by the symmetry code (-x, -y, -z).

A closer look to the cationic part, reveals that the Fe atom occupies an inversion centre and three independent 1-methylimidazole ligands generate a distorted octahedral environment with N—Fe—N angles close to 90º while the opposite imidazole rings lie in the same plane. The M—N bonds in **[XI]** are the longest found in the four isomorphous compounds, which follow the order Fe > Co > Ni> Ru.

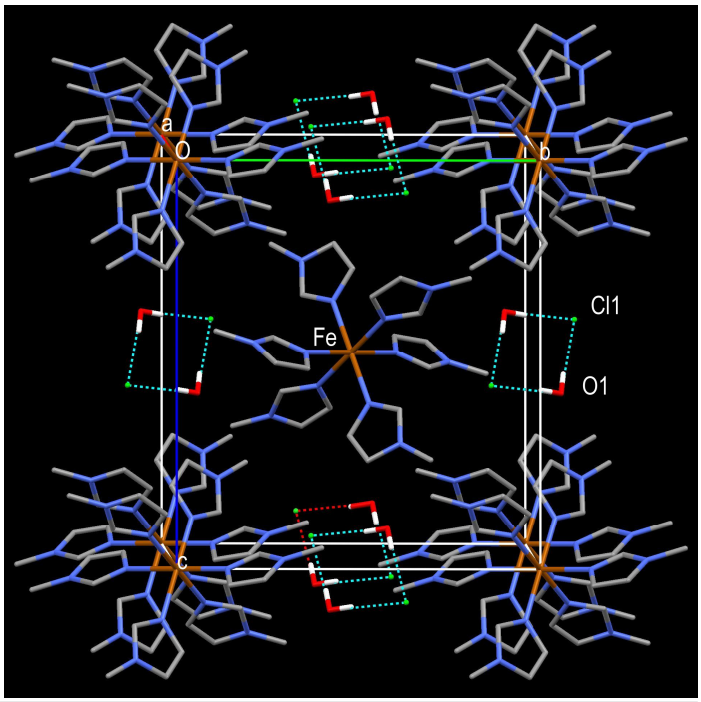

Fig. 42. A packing diagram of [XI] viewed along the a axis. H atoms (except water) have been omitted. Dashed lines indicate hydrogen bonds.

[XI] is formally composed of two ions. The cationic part is composed of an iron atom, octahedrally coordinated by six N-methylimidazole ligands. An anionic O—H···Cl hydrogen-bonded assembly formed by two chloride ions and two water molecules completes this structure. The most striking feature of this structure is the way the anionic assemblies arrange in a planar fashion as rhomboids as can be appreciated in fig. 42. In contrast, the tetrahydrate $[Fe(imid)_6]Cl_2.4H_2O$ ([AXAKIT]) combines the anionic clusters of several unit cells via additional H-bonds to form pseudo-planar hexagonal assemblies that extend infinitely over a plane[280-281].

5.B.3.2. $[Fe(phen)_3]Cl_2.6MeOH$

Metal complexes with 1,10-phenanthroline as a ligand are well known, but structures of these where the $[Fe(phen)_3]^{2+}$ cation is accompanied by simple (X^-) halide counter-ions are surprisingly scarce. Only two examples were found in the CCDC database: a dihydrate nitrobenzene solvate[285] and a dihydrate[286], where the water molecules and iodide ions form chains through hydrogen bonds, (refcodes: CEMPEP and TPHOLF, respectively). In both cases, the anions and solvent molecules are located between the layers formed by the metal complex cations.

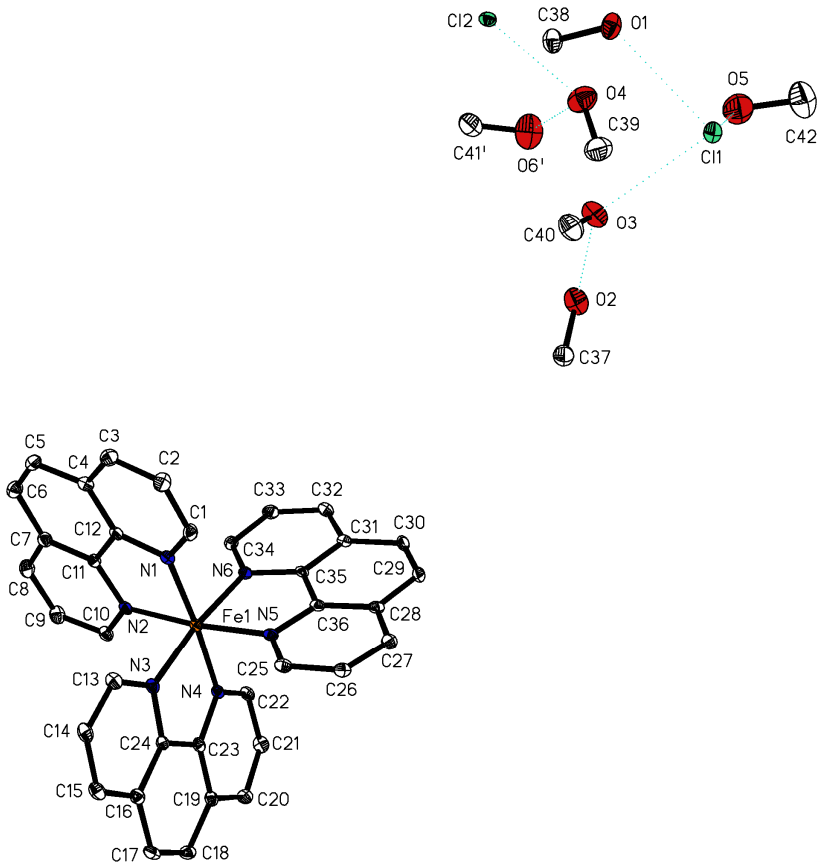

Fig. 43. The asymmetric unit of [XII], showing 50% probability displacement ellipsoids. H atoms have been omitted for clarity.

[XII] incorporates six molecules of methanol in the asymmetric unit (Fig. 43). The coordination of the Fe(II) ion in the discrete complex cation $[Fe(phen)_3]^{2+}$ is almost perfect octahedral, with cis N—Fe—N angles approaching 90º and all Fe—N bond lengths spanning a small range (Table 1), which compares well with those observed in the above-quoted solvated iodides (1.96–1.99 Å).

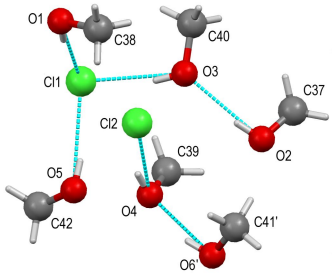

Fig. 44. Detail of the H-bonded $[Cl(MeOH)_4]^-$ and $[Cl(MeOH)_2]^-$ clusters. Dashed lines represent O···O and O···Cl contacts.

All methanol molecules interact through hydrogen bonds, either with Cl^- anions or with another methanol molecule within the asymmetric unit. As expected, the O—H···Cl contacts are longer than O—H···O, by ca 0.2–0.4 Å. These interactions lead to the formation of

two well separated anionic clusters, both with methanol molecules – $[Cl(MeOH)_2]^-$, with an O—H···O—H···Cl interaction, and $[Cl(MeOH)_4]^-$, where one Cl^- ion interacts simultaneously with three methanol molecules (Fig. 44). The anions are packed within the crystal structure without the formation of any obvious layers, and are ordered as rods along the [100] axis (Fig. 45).

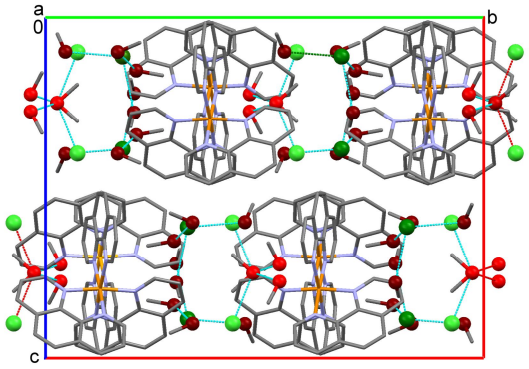

Fig. 45. A packing diagram for [XII], viewed along the [100] axis. Dashed lines indicate O···O and O···Cl contacts in hydrogen bonds. For clarity, H atoms have been omitted and C atoms are shown as sticks. The spheres represent hydrogen-bond partners within $[Cl(MeOH)_4]^-$ (darker) and $[Cl(MeOH)_2]^-$ (lighter) assemblies.

Note:

Some of the results in the present work were preliminary presented in different form at the following conferences:

1. **L. Aparici Plaza;**
   New Fe(II) silanethiolate complexes
   Sesja Sprawozdawcza Studium Doctoranckiego,
   Wydzial Chemyczny Politechniki Gdanskiej, 2006; materiały, 39.

2. **L. Aparici Plaza, K. Baranowska, B. Becker;**
   First trialkoxysilanethiolates of iron
   XLIX Zjazd PTChem oraz SITPChem,
   Gdańsk, 2006; materiały S. 87.

3. **L. Aparici Plaza, K. Baranowska, B. Becker;**
   Silanethiolates of Fe(II) with auxiliary N-donor ligands. Synthesis and structure of bis(tri-*tert*-butoxysilanethiolato)(3,5-lutidine)iron(II)
   50 Jubileuszowy Zjazd PTChem oraz SITPChem,
   Toruń 2007. Materiały, S. 103.

4. **L. Aparici Plaza;**
   Silanethiolates of Fe(II) with auxiliary N-donor ligands
   Sesja Sprawozdawcza Studium Doctoranckiego,
   Wydzial Chemyczny Politechniki Gdanskiej, 2007; materiały, 49.

5. **L. Aparici Plaza, K. Baranowska, B. Becker;**
   Trialkoxysilanethiolates of iron(II) with auxilary N-donor ligands
   49 Konwersatorium Krystalograficzne : Sesja Naukowa PTK;
   Wrocław 2007, Materiały, S. 202-203.

6. **L. Aparici Plaza, K. Baranowska, B. Becker;**
   Silanethiolates of Fe(II). Synthesis and structure of bis(tri-*tert*-butoxysilanethiolato) tetra(methanol)iron(II)
   50 Konwersatorium Krystalograficzne i II Sesja Naukowa PTK;
   Wrocław, 26-28 VI 2008, Materiały, S. 64

7. **L. Aparici Plaza, A.P. Nowak, K. Baranowska, A. Lisowska-Oleksiak, B. Becker;**
   Synthesis and properties of the cubane type cluster $[Fe_4S_4\{SSi(O^tBu)_3\}_4](Et_3NH)_2$
   XVIth International Winter School on Coordination Chemistry;
   Karpacz, Poland, 8-12 December 2008, Proceedings, S. 128.

6 CONCLUSIONS

The silanethiolate ligand does not exist in nature. However, it already has shown to make possible a range of geometries and coordination modes that rival those of their relatives, the organic thiolates. In this work, we have provided new methods for the synthesis of silanethiolates making use of tri-*tert*-butoxysilanethiol. The resulting tri-*tert*-butoxysilanethiolates are the first alkoxysilanethiolates of iron ever synthesized. We can classify the new complexes according to several factors, such as coordination number and geometry, crystallographic space group or nuclearity.

A total of 10 new silanethiolates of iron have been synthesized for the first time. Of these, 9 of them are mononuclear disilanethiolates of iron(II) and the other contains the mixed-oxidation state cluster $[Fe_4S_4]^{2+}$, which formally implies that two of the iron atoms are in the +2 oxidation state and the other two in the +3 oxidation state. However, in reality all iron atoms behave identically as possessing a +2.5 oxidation state.

All the mononuclear trialkoxysilanethiolates of iron(II) have been isolated in crystalline form. The crystals are colorless or pale yellow. They are characterized by their high instability and are easily oxidized, which makes the use of Schlenk techniques imperative. They also show a low degree of symmetry, with all compounds crystallizing in monoclinic and triclinic space groups. Thus, **[I]**, **[III]**, **[V]**, and **[VI]** are triclinic, all crystallizing in the P-1 space group, **[IV]** and **[IX]** crystallize in the monoclinic C2/c space group, **[VII]** and **[VIII]**

belong to the monoclinic $P2_1/c$ group and **[X]** is the only member of the $P2_1/n$ monoclinic space group.

The use of N-donor heterocyclic bases as the coligands has provided very satisfactory results. Single rings (pyridine, piperidine and morpholine) readily react to form ditri-*tert*-butoxysilanethiolates of iron(II) with tetrahedral geometry, including two N-donor rings. If methyl- or dimethyl-pyridines (β-, γ-picoline, 3,5-lutidine) are used, the ligation of a second ring is avoided and we allow for chelation of the alkoxysilanethiolate moieties through the O-atoms of their *tert*-butoxy groups. However, if the methyl substituent is found in the α-position of the ring (α-picoline), providing a significantly higher steric hindrance, it seems that the molecular orbitals rearrange in a fashion that hinders the chelation but allows for additional small molecules to stablish a bond to iron. Surprisingly, the use of bigger, more sterically hindered N-donor rings derivated from pyridine, as well as the use of smaller 5-membered heterocyclic imidazole rings does not provide a route for heteroleptic trialkoxysilanethiolates containing both kinds of ligands. Instead, homoleptic complexes containing only the N-donor ligand have been isolated.

The use of tmeda as the coligand yields a tetrahedral disilanethiolate of iron(II) which can be compared to the existent $[Fe(SSiPh_3)_2(tmeda)].CH_2Cl_2$, synthesized by Komuro *et al*[44]. Although both complexes share a similar tetrahedral structure, Komuro reports that his compound is stable under normal conditions, while we have proved that **[X]** is not only sensitive to oxygen, but also it decomposes in solution under an inert atmosphere after few days.

So far, no homoleptic trialkoxysilanethiolate of iron(II) has been isolated.

We have successfully used the Robinson-Gibbs-Ribbe method[242] for determining and analyzing the level of distortion of our complexes. Despite its limitations, this method is fast, simple and reliable for the geometries analyzed. Also, plotting the mean quadratic elongation vs. the angle variance revealed helpful when explaning certain geometric distortions. However, in a few cases we lacked enough values to attain satisfactory conclusions; therefore we recommend further work with silanethiolates of iron in order to obtain more data.

As a result of the application of this method, we obtained that the distortion of tetrahedral silanethiolates of iron(II) follows the trend:

$[CpFe(SSiPh_3)(CO)_2]$ > $[Fe(SSiPh_3)_2(tmeda)].CH_2Cl_2$ > $[Fe(SSi^tBu_3)_2(THF)_2]$ > $[CpFe(SSi^tBu_3)(CO)_2]$ > $[Fe\{SSi(O^tBu)_3\}_2(tmeda)]$ > $[Fe\{SSi(O^tBu)_3\}_2(pip)_2]$ > $[Fe(SSiPh_3)_2(Et_3P)_2]$ > $[Fe(SSiPh_3)_2(^tBupy)_2]$ > $[Fe\{SSi(O^tBu)_3\}_2(morph)_2]$ > $[Fe(SSiPh_3)_2(CH_3CN)_2]$

And with the exception of $[Fe(SSiPh_3)_2(Et_3P)_2]$, all of them fit well on the regression line:

$\langle\lambda\rangle$ =0,0003$\boldsymbol{\sigma}^2$ + 1,0111

Likewise, the distortion of bipyramidal silanethiolates of iron(II) can be ordered according to the trend:

[Fe{SSi(O^{t}Bu)$_3$}$_2$(3,5-lut)] > [Fe{SSi(O^{t}Bu)$_3$}$_2$(β-pic)] > [Fe{SSi(O^{t}Bu)$_3$}$_2$(γ-pic)] > [Fe{SSi(O^{t}Bu)$_3$}$_2$(α-pic)(MeOH)$_2$]

With all points fitting reasonably well in the line

$\langle\lambda\rangle$ =0,0002$\boldsymbol{\sigma}^2$ + 1,0119

To sum up, silanethiolates of iron(II), despite not abundant, already display a heterogeneous and varied set of coordination modes. In our case, we encountered tetrahedral, trigonal bipyramidal and octahedral geometries (CN = 4, 5, and 6 respectively).

Future work should focus on the use of reaction (1) as the basis for the synthesis of new mononuclear silanethiolates of iron(II). N-donor heterocyclic bases have already proved useful as coligands in the synthesis of new complexes of this kind. It would be interesting to investigate the application of different coligands and see how well the resulting complexes fit in the $\langle\lambda\rangle$ vs. $\boldsymbol{\sigma}^2$ graph according to the Robinson-Gibbs-Ribbe method.

Also it would be of interest from the point of view of biomimicry to test the use of porphines as the coligands. Despite the use of big polycyclic ligands derivated from pyridine has proved fruitless, the fact that only one porphine is allowed at a time suggests that either one or two silanethiolate moieties could enter the structure in distal and proximal positions. Furthermore, given the properties of heme groups, it is possible that iron(III) complexes are produced this way. In any case, such a complex would provide a model for certain cytochromes based in silanethiolates, and could be compared to existent models based in organic thiolates .

Models for biological [Fe_4S_4] centers are directly synthesized from organic thiols; in some cases, additional work is required in order to develop a determined model. For instance, redox operations based in electrochemical treatments are used to produce clusters of different oxidation states. We have successfully synthesized the $[Fe_4S_4]^{2+}$ cluster, for the first time from the direct reaction of silanethiol with an iron(II) or an iron(III) salt. When compared to analogue reactions with thiols, it is puzzling that no additional source of sulfur is required for the reaction to take place. So far we have not found a successful explanation for this fact.

Magnetic susceptibility measurements on samples of **[II]** were not conclusive and further investigations are necessary. EPR and also Mössbauer spectra should be registered as well. Since a huge amount of literature data exists for typical [4Fe-4S] clusters derived from organic thiols, this quite uncommon trialkoxysilanethiolate derivative may be of interest.

Also, **[II]** was submitted for a cyclic voltammetry test and it seems to possess redox activity like most other synthetic [4Fe-4S] clusters, although still more experiments are needed to confirm this fact. If this is corroborated, then redox treatment of complex **[II]** could produce derivatives of this cluster with different oxidation states.

It would also be recommendable to study the use of **[II]** as a reagent to synthesize heterometallic clusters which could provide novel models for mixed-metal-sulfur metalloproteins such as nitrogenases or hydrogenases or could demonstrate catalytic activity.

7 SUMMARY

Mononuclear iron(II) thiolates and [4Fe-4S] cubane clusters are well known in bioinorganic chemistry, as they play an important role in biocatalysis. The former are related to the structures of monometallic iron-sulfur proteins such as ferredoxins and rubredoxins, while the latter are present in certain ferredoxins as well as in more complex metalloproteins such as hydrogenase and nitrogenase. Due to their redox activity, [4Fe-4S] clusters are involved in the storage and delivery of electrons in a number of metalloproteins, acting as nanocapacitors.

For several years, organic thiolate complexes have been successfully used to model some of these sites either structurally or functionally. In the present work, we adopt a purely inorganic approach to the modeling of these sites by making use of silanethiolates as ligands.

In general, silanethiolates can be considered as the silicon analogues of organic thiolates. However, they are much more labile than thiolates and therefore have to be handled under very controlled conditions: generally a water and oxygen-free environment is the most apropriate. Nevertheless, some of these handicaps can be overcome with the use of tri-*tert*-butoxysilanethiol, the only silanethiol known not to undergo hydrolysis under normal conditions.

Metal silanethiolates are commonly obtained by the direct reaction of the silanethiol with the metal salt in presence of triethylamine. Several examples are already known, but so far little attention has been paid to iron. We aimed to shed some light into this neglected area. As a result, during the course of our investigations, we have demonstrated that iron(II) chlorides react readily with silanethiol to yield silanethiolates. In total, we have isolated and

characterized – to a different extent – 10 new silanethiolates of iron: $[Fe\{SSi(O^tBu)_3\}_2(MeOH)_4]$ **[I]**, $[Fe_4S_4\{SSi(O^tBu)_3\}_4](Et_3NH)_2$ **[II]**, $[Fe\{SSi(O^tBu)_3\}_2(py)_2]$ **[III]**, $[Fe\{SSi(O^tBu)_3\}_2(pip)_2]$ **[IV]**, $[Fe\{SSi(O^tBu)_3\}_2(morph)_2]$ **[V]**, $[Fe\{SSi(O^tBu)_3\}_2(\alpha\text{-pic})(MeOH)_2]$ **[VI]**, $[Fe\{SSi(O^tBu)_3\}_2(\beta\text{-pic})]$ **[VII]**, $[Fe\{SSi(O^tBu)_3\}_2(\gamma\text{-pic})]$ **[VIII]**, $[Fe\{SSi(O^tBu)_3\}_2(3,5\text{-lut})]$ **[IX]**, and $[Fe\{SSi(O^tBu)_3\}_2(tmeda)]$ **[X]**.

This family of complexes is characterized by the heterogeneous structures and coordination numbers of its members. Thus, we have identified octahedral (**[I]**), tetrahedral (**[III]**, **[IV]**, **[V]** and **[X]**) and bipyramidal (**[VI]**, **[VII]**, **[VIII]** and **[IX]**) iron(II) silanethiolates with coordination numbers ranging from 4 to 6, as well as an interesting [4Fe-4S] cubane-type cluster (**[II]**). It is worth noting that this is the first time that coordination numbers 5 and 6 are ever reported for iron(II) silanethiolates. Also, **[II]** is the first [4Fe-4S] cluster obtained from a direct reaction using this kind of ligands.

Additionally, in the course of our experiments we have isolated two new homoleptic iron(II) complexes, $[Fe(N\text{-meimid})_6]Cl_2.2H_2O$ **[XI]** and $[Fe(phen)_3]Cl_2.6MeOH$ **[XII]**, which are both characterized by their interesting hydrogen bond arrangements at the anionic sites.

We have encountered that the synthesis of silanethiolates of iron(II) as well as determining their structure and properties is difficult and challenging, since these complexes are extremely unstable and very sensitive to oxygen, which requires them to be handled with extreme caution. Despite their intrinsic instability, their structure could be determined with great accuracy by X-ray methods. Still, **[II]** demonstrated to be more robust than its mononuclear relatives, which allowed us to perform some additional tests.

As a novelty, we introduce a set of mathematic and informatic tools to assess the distortion of silanethiolates of iron. On one hand, we applied the Robinson-Gibbs-Ribbe method for measuring the distortion of mononuclear coordination complexes as a tool to classify our compounds and to provide an appropriate framework for them. On the other, the program ClusterGeom developed by Fee *et al.* helped us evaluate the degree of distortion in the [4Fe-4S] cluster of **[II]**.

To sum up, in the present work we offer reliable methods to obtain heteroleptic iron(II) silanethiolates, and a [4Fe-4S] cluster. We describe their structure and present some of their features, stressing their relationship with common bioinorganic centers. Finally, we provide some tools to evaluate the structural distortion of these complexes.

8 STRESZCZENIE

Monometaliczne tiolany żelaza(II) i klastery [4Fe-4S] o budowie typu kubanu są dobrze znane w chemii bionieorganicznej, gdyż związki tego typu pełnią ważną rolę w biokatalizie. Pierwsze z nich są odpowiednikami monometalicznych białek żelazowo-siarkowych takich jak ferredoksyny i rubredoksyny, te drugie znaleźć można zarówno w niektórych ferredoksynach, jak i w bardziej złożonych metalloproteinach, takich jak hydrogenaza czy nitrogenaza. Aktywność redoksowa sprawia, że klastery [4Fe-4S] wchodzące w skład wielu metaloprotein są angażowane w procesy magazynowania i dostarczania elektronów, spełniając rolę nanokondensatorów.

Od kilkunastu lat kompleksy tiolanowe są stosowane do modelowania takich centrów enzymatycznych, przy czym próbuje się odwzorować ich funkcję, względnie strukturę. Obecnie przedstawiana praca prezentuje czysto nieorganiczne podejście do tego zagadnienia – jako ligandy zostały użyte silanotiolany.

Silanotiolany metali są zazwyczaj otrzymywane w bezpośredniej reakcji silanotiolu z solą metalu w obecności odpowiedniego akceptora. Znanych jest już sporo przykładów takich związków, ale jak dotąd niewiele uwagi poświęcono żelazu. Naszym zamiarem było uzupełnienie danych w ramach tego słabo poznanego obszaru. W rezultacie, w trakcie badań wykazaliśmy, że chlorek żelaza(II) reaguje z tri-*tert*-butoksysilanotiolem w obecności trietyloaminy. Zależnie od zastosowanych warunków (rozpuszczalnik, dodatkowy reagent) zostało otrzymanych, wyizolowanych i scharakteryzownych (w różnym stopniu) – 10 nowych tri-*tert*-butoksysilanotiolanów żelaza: $[Fe\{SSi(O^tBu)_3\}_2(MeOH)_4]$ **[I]**, $[Fe_4S_4\{SSi(O^tBu)_3\}_4](Et_3NH)_2$ **[II]**, $[Fe\{SSi(O^tBu)_3\}_2(py)_2]$ **[III]**, $[Fe\{SSi(O^tBu)_3\}_2(pip)_2]$ **[IV]**, $[Fe\{SSi(O^tBu)_3\}_2(morph)_2]$ **[V]**, $[Fe\{SSi(O^tBu)_3\}_2(\alpha$-

pic)$(MeOH)_2$] **[VI]**, [Fe{SSi(O^tBu)$_3$}$_2$(β-pic)] **[VII]**, [Fe{SSi(O^tBu)$_3$}$_2$(γ-pic)] **[VIII]**, [Fe{SSi(O^tBu)$_3$}$_2$(3,5-lut)] **[IX]**, and [Fe{SSi(O^tBu)$_3$}$_2$(tmeda)] **[X]**. Są to nie tylko nowe związki (a więc także nowe silanotiolany), ale przede wszystkim pierwsze, kiedykolwiek otrzymane związki kompleksowe żelaza, w których podstawowym ligandem jest reszta wywodząca się od kwasu monotioortokrzemowego $(HO)_3SiSH$.

Przedstawiciele tej rodziny kompleksów reprezentują różne typy strukturalne i różne są też liczby koordynacyjne odpowiednich centrów metalicznych. Zidentyfikowane zostały silanotiolany żelaza(II) oktaedryczne (**[I]**), tetraedryczne (**[III]**, **[IV]**, **[V]** i **[X]**) oraz typu bipiramidy trygonalnej (**[VI]**, **[VII]**, **[VIII]** i **[IX]**) z liczbami koordynacyjnymi od 4 do 6, jak również otrzymano interesujący klaster [4Fe-4S] o strukturze typu kubanu (**[II]**). Warto nadmienić, że jak dotąd tiolany żelaza, w których liczba koordynacyjna Fe wynosiłaby 5 lub 6 nie były znane.

W trakcie prac eksperymentalnych zostały także wyizolowane dwa nowe homoleptyczne związki żelaza(II), [Fe(N-meimid)$_6$]Cl_2.$2H_2O$ **[XI]** i [Fe(phen)$_3$]Cl_2.6MeOH **[XII]**. Obydwa charakteryzują się ciekawą aranżacją wiązań wodorowych w części anionowej.

Stwierdziliśmy, że synteza silanotiolanów żelaza(II) jak również badania ich struktury i właściwości są trudne i wymagające wiele od eksperymentatora. Związki te są bardzo nietrwałe i niezmiernie wrażliwe na działanie tlenu co sprawia, że praca z nimi wymaga najwyższej uwagi. Mimo tej, charakterystycznej dla nich wrażliwości, ich struktura została określona z dużą dokładnością za pomocą analizy rentgenostrukturalnej. W porównaniu do otrzymanych związków monometalicznych **[II]** okazał się być trwalszym, co umożliwiło wykonanie dodatkowych badań.

Pewną nowością w badaniach silanotiolanów jest zastosowanie narzędzi matematycznych, pozwalających na ocenę zaburzeń struktury związków. Do pomiaru zaburzeń w kompleksach monometalicznych zastała użyta metoda Robinsona-Gibbsa-Ribbego, narzędzie, które może ułatwić klasyfikację otrzymywanych związków. Z kolei Program ClusterGeom, opracowany przez Fee, *et al.* pozwolił ocenić zakres zaburzeń w przypadku klastera [4SFe-4S] obecnego w związku kompleksowym **[II]**.

Podsumowując, w przedkładanej pracy zawarto opis dogodnych metod otrzymywania heteroleptycznych silanotiolanów żelaza i klastera [4Fe-4S]. Opisano ich budowę i niektóre właściwości, wskazując na relacje jakie je łączą z typowymi centrami bionieorganicznymi. Całość uzupełniono o narzędzia pozwalające na ocenę zaburzeń w strukturze badanych kompleksów.

9 ACKNOWLEDGEMENTS

Any attempt to provide a complete account of all the people that have influenced and supported me through the years will probably reveal futile and unfair, always at the risk of commiting some flagrant omisions. Despite I have tried limiting the present text to those people who have had the most direct influence on this work since I moved to Poland; I cannot forget some people who have continuosly supported me in spite of the distance.

First and foremost, I would like to thank my supervisor, prof. dr. hab. Barbara Becker for believing in my proposal. Were it not for her exceptional view of the world, I would not have moved to Poland and none of this would have been accomplished. She is for me an inspiration and a source of knowledge. Words will never be enough to describe my gratitude.

Following, a special thanks to my parents. They brought me to life, sacrificed much to properly educate my brother and me and always offered inconditional support to both of us. Also, my gratitude for providing economic support whenever it was needed –given the short-sighted politics of certain governments–. I hope that this work adds to the pride you feel for your children.

From a technical point of view, I have to thank dr. Andrzej P. Nowak and dr. hab. Anna Lisowska-Oleksiak, of the Department of Chemical Technology at Gdańsk University of Technology for performing the electrochemical measurements of

$[Fe_4S_4\{SSi(O^tBu)_3\}_4](Et_3NH)_2$; to prof. dr. hab. J. Jezierska and dr. L. Jerzykiewicz of the University of Wroclaw for the magnetic susceptibility and EPR measurements; and to dr. Katarzyna Baranowska of the Department of Inorganic Chemistry at GUT for the X-ray measurements and resolution of the structures.

Likewise, my gratitude goes to the rest of the members of the Department of Inorganic Chemistry at GUT for being so kind and gentle and having enough patience to teach me and discuss problems in spite of the hurdles that language represented at the very beginning. Their comments and criticism were unvaluable in order to produce the present work.

In addition, I would like to thank my brother for being my best friend and supporter. I want to give him credit for the special graphic treatment he provided to some of the images in this work. The cover deserves a special mention, since it is based on one of his photographs.

In a more personal note, I cannot forget to mention mgr. Ewa Jurkiewicz and the members of the Koło Języka Hiszpańskiego, who amazed me by their passion for the Spanish language and culture. I felt proud to collaborate at their cultural meetings and to learn from them. Also, they were kind enough to dedicate some of their time and efforts to make my stay in Poland more comfortable.

Additionally, I would like to point out the good work and the devotion to foreign students of the members of ESN Gdansk, which provided guidance during the first years of my stay in Poland. They always found time to assess me on different matters and their advice provided extraordinarily valuable.

Finally, all of my love and gratitude to Edyta Kolenos for her patience, care and comprehension.

10 ANNEXES

ANNEX A

The following list resumes all published (as of 2009) syntheses of iron silanethiolates in chronological order:

a) Komuro *et al.* (2002)[44]:

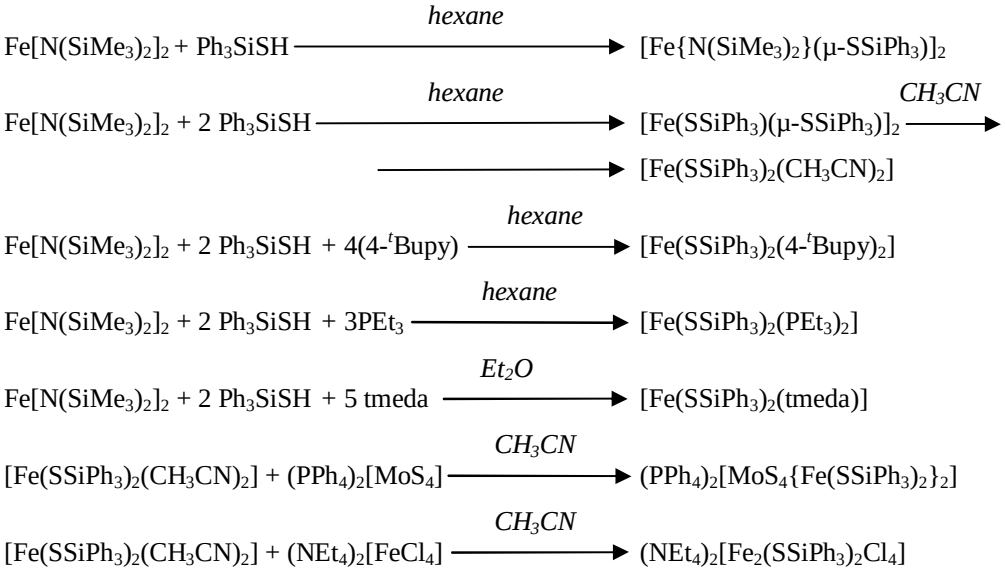

b) Sydora *et al.* (2003)[45]:

$$2[\{(Me_3Si)_2N\}_2Fe] + 4^tBu_3SiSH \xrightarrow{C_6H_6} [(^tBu_3SiS)Fe]_2(\mu\text{-}SSi^tBu_3)_2] + 4(Me_3Si)_2NH$$

$$NaSSi^tBu_3(thf)_{1.48} + FeCl_2(thf)_2 \xrightarrow{THF} [\{Cl_2Fe\}(\mu\text{-}SSi^tBu_3)_2\{FeCl(thf)\}]Na$$

$$NaSSi^tBu_3(thf)_{1.68} + FeBr_2(thf)_2 \xrightarrow{THF} [\{Br_2Fe\}(\mu\text{-}SSi^tBu_3)_2\{FeBr(thf)\}]Na$$

$$NaSSi^tBu_3(thf)_{1.68} + FeI_2(thf)_2 \xrightarrow{THF} cis[\{I(thf)Fe\}_2(\mu\text{-}SSi^tBu_3)_2]$$

$$[\{Cl_2Fe\}(\mu\text{-}SSi^tBu_3)_2\{FeCl(thf)\}]Na \xrightarrow{C_6H_6} [Fe(\mu\text{-}Cl)(\mu\text{-}SSi^tBu_3)]_{12}(C_6H_6)_n$$

$$NaSSi^tBu_3(thf)_{1.40} + FeBr_2(thf)_2 \xrightarrow{THF/C_6H_6} [Fe(\mu\text{-}Br)(\mu\text{-}SSi^tBu_3)]_{12}(C_6H_6)_n$$

$$NaSSi^tBu_3(thf)_{1.56} + FeI_2(thf)_2 \xrightarrow{THF/C_6H_6} [Fe(\mu\text{-}I)(\mu\text{-}SSi^tBu_3)]_{14}(C_6H_6)_n$$

$$[Fe(\mu\text{-}Cl)(\mu\text{-}SSi^tBu_3)]_{12}(C_6H_6)_n + LiCCSSi^tBu_3(OEt_2)_{0.28} \xrightarrow{C_6H_6} [\{(^tBu_3SiCC)Fe(\mu\text{-}SSi^tBu_3)\}_4(C_6H_6)_3]$$

c) Holm *et al.* (2003)[46]:

$$[Fe_4S_4(PPr^i{}_3)_4](BPh_4) + (Ph_4P)(SSiPh_3) \xrightarrow{THF/CH_3CN} [Fe_4S_4(PPr^i{}_3)_3(SSiPh_3)] \xrightarrow{THF} [Fe_8S_8(PPr^i{}_3)_4(SSiPh_3)_2]$$

d) Kovacs *et al.* (2003)[47]:

$$[CpFe(CO)_2(THF)]BF_4 + LiSSiPh_3.Et_2O \xrightarrow{CH_2Cl_2} CpFe(CO)_2SSiPh_3$$

$$[CpFe(CO)_2(THF)]BF_4 + NaSSi^iPr_3 \xrightarrow{CH_2Cl_2} CpFe(CO)_2SSi^iPr_3$$

e) Komuro *et al.* (2004)[48]:

$$[Li(tmeda)SSiMe_2Bu^t]_2 + Fe(CH_3CN)_2(CF_3SO_3)_2 \xrightarrow{hexane} [Fe(SSiMe_2Bu^t)_2(tmeda)]$$

f) Vela *et al.* (2005)[50]:

$$[L^{tBu}FeF] + Me_3SiSSSiMe_3 \xrightarrow{toluene} [L^{tBu}FeSSiMe_3]$$

g) Sydora *et al.* (2006)[49]:

$$[\{(^{t}Bu_3SiS)Fe\}_2(\mu\text{-}SSi^{t}Bu_3)_2] \xrightarrow{THF} 2[(^{t}Bu_3SiS)_2Fe(THF)_2]$$

h) Kückmann *et al.* (2007)[51]:

$$NaSSi^{t}Bu_3 + [\{CpFe(CO)_2\}(thf)]BF_4 \xrightarrow{CH_2Cl_2} [\{CpFe(CO)_2\}SSi^{t}Bu_3]$$

ANNEX B

The crystallographic data of the complexes presented in this work are summarized here.

	[I]	**[II]**
Chemical formula	$C_{28}H_{70}FeO_{10}S_2Si_2$	$C_{60}H_{140}Fe_4N_2O_{12}S_8Si_4$
Molecular mass ($g \cdot mol^{-1}$)	742.99	1673.98
Crystallographic system	Triclinic	Monoclinic
Space group	P -1	P $2_1/c$
Crystal shape / color	Prismatic / yellow	Block / black
Crystal size (mm)	0.36x0.165x0.158	0.17985x0.11194x0.03647
a (Å)	8.7569(11)	16.5476(9)
b (Å)	9.277(2)	32.703(2)
c (Å)	14.8123(15)	16.7256(10)
α (º)	94.689(16)	90
β (º)	100.554(10)	101.634(5)
γ (º)	116.327(14)	90
V ($Å^3$)	1042.0(3)	8865.2(9)
Z	1	4
D_{cal} ($g \cdot cm^{-3}$)	1.184	1.254
Temperature (K)	120(2)	120(2)
μ(MoKα) (mm^{-1})	0.563	0.932
θ range	2.49-25.05	2.49-25.05
Range of h, k and l	-10<h<10 -11<k<11 -17<l<17	-19<h<19 -38<k<37 -15<l<19
F(000)	404	3592
R_{int}	0.0669	0.0792
N(refl. Total)	3638	15645
N(refl. observed)	3041	13324
Criterion of significance	I>2σ(I)	I>2σ(I)
N(parameters)	208	850
S/F^2 (goodness-of-fit)	1.048	1.116
R_1, $w_2(F^2>2\sigma(F^2))$	0.0669, 0.2240	0.0792; 0.1593
$\rho\Delta_{min}$, $\rho\Delta_{max}$ (e/A^3)	-0.431; 0763	-0.566; 1.499

	[III]	**[IV]**
Chemical formula	$C_{34}H_{64}FeN_2O_6S_2Si_2$	$C_{34}H_{76}FeN_2O_6S_2Si_2$
Molecular mass ($g \cdot mol^{-1}$)	773.12	785.12
Crystallographic system	Triclinic	Monoclinic
Space group	?	C 2/c
Crystal shape / color	Prism/colorless	Prism / light brown
Crystal size (mm)		0.49315×0.16672×0.08385
a (Å)	9.2457(7)	36.668(5)
b (Å)	9.3228(11)	10.0244(14)
c (Å)	28.558(2)	28.173(3)
α (º)	89.946(8)	90
β (º)	89.956(6)	119.197(13)
γ (º)	60.297(6)	90
V ($Å^3$)	2138.1(3)	9040(2)
Z	1	8
D_{cal} ($g \cdot cm^{-3}$)	1.009	1.154
Temperature (K)	120(2)	120(2)
μ(MoKα) (mm^{-1})	0.552	0.517
θ range	2.14-25.05	2.50-25.05
Range of h, k and l	-10<h<10 -11<k<11 -34<l<25	-43<h<43 -11<k<11 -32<l<31
F(000)	744	3424
R_{int}	0.0533	0.0737
N(refl. total)	7309	7806
N(refl. observed)	6376	6667
Criterion of significance	I>2σ(I)	I>2σ(I)
N(parameters)	442	442
S/F^2 (goodness-of-fit)	1.178	1.064
R_1, $w_2(F^2>2\sigma(F^2))$	0.2359; 0.5402	0.0585; 0.1348
$\rho\Delta_{min}$, $\rho\Delta_{max}$ (e/A^3)	-2.168; 3.158	-0.409; 0.972

	[V]	**[VI]**
Chemical formula	$C_{32}H_{72}FeN_2O_8S_2Si_2$	$C_{30}H_{59}FeNO_6S_2Si_2$
Molecular mass ($g \cdot mol^{-1}$)	789.07	705.93
Crystallographic system	Triclinic	Triclinic
Space group	P -1	P -1
Crystal shape / color	Plate / pale yellow	yellow
Crystal size (mm)	0.18×0.14×0.02	
a (Å)	9.8189(4)	9.2486(2)
b (Å)	13.9198(5)	9.2611(8)
c (Å)	16.2354(8)	29.5478(10)
α (º)	88.178(3)	81.645(10)
β (º)	80.903(4)	81.674(7)
γ (º)	81.497(3)	62.64
V ($Å^3$)	2166.93(16)	2215.0(2)
Z	2	2
D_{cal} ($g \cdot cm^{-3}$)	1.209	1.058
Temperature (K)	120(2)	293(2)
μ(MoKα) (mm^{-1})	0.543	0.521
θ range	2.56-27.50	2.49-25.05
Range of h, k and l	-12<h<12 -18<k<18 -15<l<21	-11<h<11 -9<k<11 -35<l<35
F(000)	856	760
R_{int}	0.022	0.0264
N(refl. total)	9853	7738
N(refl. observed)	8512	6398
Criterion of significance	$I>2\sigma(I)$	$I>2\sigma(I)$
N(parameters)	442	500
S/F^2 (goodness-of-fit)	1.078	1.373
R_1, $w_2(F^2>2\sigma(F^2))$	0.0375; 0.0917	0.0764; 0.1886
$\rho\Delta_{min}$, $\rho\Delta_{max}$ (e/A^3)	-0.254; 0.721	-0.595; 0.467

	[VII]	**[VIII]**
Chemical formula	$C_{30}H_{61}FeNO_6S_2Si_2$	$C_{30}H_{61}FeNO_6S_2Si_2$
Molecular mass ($g \cdot mol^{-1}$)	707.95	707.95
Crystallographic system	Monoclinic	Monoclinic
Space group	P $2_1/c$	P $2_1/c$
Crystal shape / color	Prism / yellow	Prism / yellow
Crystal size (mm)	0.378x0.289x0.133	0.36x0.32x0.26
a (Å)	8.5512(10)	11.2321(3)
b (Å)	25.3305(6)	25.6730(6)
c (Å)	18.6288(4)	28.5656(7)
α (º)	90	90
β (º)	95.845(2)	91.190(2)
γ (º)	90	90
V ($Å^3$)	4014.13(14)	8235.4(4)
Z	4	8
D_{cal} ($g \cdot cm^{-3}$)	1.171	1.142
Temperature (K)	120(2)	120(2)
μ(MoKα) (mm^{-1})	0.575	0.561
θ range	1.95-25.05	2.09-25.05
Range of h, k and l	-10<h<10 -30<k<29 -19<l<21	-11<h<13 -30<k<29 -34<l<26
F(000)	1528	3056
R_{int}	0.0239	0.0212
N(refl. total)	7040	14469
N(refl. observed)	5961	11651
Criterion of significance	$I>2\sigma(I)$	$I>2\sigma(I)$
N(parameters)	396	826
S/F^2 (goodness-of-fit)	1.099	1.127
R_1, $w_2(F^2>2\sigma(F^2))$	0.0482; 0.131	0.0427; 0.1096
$\rho\Delta_{min}$, $\rho\Delta_{max}$ (e/A^3)	-0.877; 2.576	-0.380; 0.575

	[IX]	**[X]**
Chemical formula	$[Fe\{SSi(O^tBu)_3\}_2(C_7H_9N)]$	$C_{30}H_{70}FeN_2O_6S_2Si_2$
Molecular mass ($g \cdot mol^{-1}$)	721.97	731.03
Crystallographic system	Monoclinic	Monoclinic
Space group	C 2/c	P 2_1/n
Crystal shape / color	Prism / colorless	Prism / colorless
Crystal size (mm)	0.14x0.07x0.03	0.28x0.23x0.18
a (Å)	14.6847(9)	18.3612(8)
b (Å)	13.0237(6)	9.2138(4)
c (Å)	21.8811(13)	24.6405(10)
α (º)	90	90
β (º)	104.470(5)	94.549(4)
γ (º)	90	90
V ($Å^3$)	4052.0(4)	4155.5(3)
Z	4	4
D_{cal} ($g \cdot cm^{-3}$)	1.183	1.168
Temperature (K)	120(2)	120(2)
μ(MoKα) (mm^{-1})	0.571	0.558
θ range	1.92-25.05	2.23-25.50
Range of h, k and l	-16<h<17 -15<k<15 -22<l<26	-20<h<22 -10<k<11 -29<l<29
F(000)	1560	1592
R_{int}	0.029	0.0458
N(refl. total)	3591	7728
N(refl. observed)	2884	5607
Criterion of significance	$I>2\sigma(I)$	$I>2\sigma(I)$
N(parameters)	268	410
S/F^2 (goodness-of-fit)	1.151	0.898
R_1, $w_2(F^2>2\sigma(F^2))$	0.0517; 0.1358	0.0744; 0.2161
$\rho\Delta_{min}$, $\rho\Delta_{max}$ (e/A^3)	-0.662; 0.811	-1.317; 2.890

	[XI]	**[XII]**
Chemical formula	$C_{24}H_{40}Cl_2FeN_{12}O_2$	$C_{42}H_{48}Cl_2FeN_6O_6$
Molecular mass ($g \cdot mol^{-1}$)	655.43	859.61
Crystallographic system	Monoclinic	Orthorhombic
Space group	P 2_1/n	P b c a
Crystal shape / color	Prism / colorless	Prism / red
Crystal size (mm)	0.26031x0.15539x0.03445	
a (Å)	8.0205(7)	23.6859(5)
b (Å)	13.2884(12)	18.4567(4)
c (Å)	14.9438(14)	18.5616(4)
α (º)	90	90
β (º)	98.138(8)	90
γ (º)	90	90
V ($Å^3$)	1576.7(2)	8114.5(3)
Z	2	8
D_{cal} ($g \cdot cm^{-3}$)	1.381	1.407
Temperature (K)	120(2)	120(2)
μ(MoKα) (mm^{-1})	0.691	0.559
θ range	2.73-25.04	2.04-25.05
Range of h, k and l	-9<h<9 -13<k<15 -17<l<17	-24<h<28 -21<k<21 -22<l<21
F(000)	688	3600
R_{int}	0.0288	0.0307
N(refl. total)	2736	7110
N(refl. observed)	2614	5339
Criterion of significance	I>2σ(I)	I>2σ(I)
N(parameters)	198	544
S/F^2 (goodness-of-fit)	1.085	1.096
R_1, $w_2(F^2>2\sigma(F^2))$	0.0346; 0.0863	0.0455; 0.1055
$\rho\Delta_{min}$, $\rho\Delta_{max}$ (e/A^3)	-0.285; 0.399	-0.262; 0.669

ANNEX C

Parameters of the defining circumspheres for synthetic [4Fe-4S] clusters, including data for an ideal cluster and the mean values. The complexes are referenced by their CCDC code.

Reference code	r_{Fe}	r_S	r_{SG}	CC_S-CC_{Fe}	CC_{SG}-CC_{Fe}	Δr_{Fe-S}	Δr_{S-SG}
IDEAL	1.650	2.250	3.950	0.000	0.000	0.600	1.700
[II]	1.697	2.208	3.956	0.017	0.025	0.511	1.748
BZMSFE	1.682	2.208	3.931	0.009	0.009	0.526	1.723
CACLAU	1.673	2.203	3.914	0.026	0.011	0.530	1.711
CATTOG	1.688	2.214	3.936	0.014	0.014	0.526	1.722
CATTUM	1.686	2.208	3.934	0.000	0.000	0.522	1.726
CEQYAY	1.688	2.202	3.946	0.000	0.000	0.514	1.744
CESSEY	1.668	2.210	3.912	0.004	0.009	0.542	1.702
CESSUO	1.675	2.203	3.922	0.000	0.011	0.528	1.719
CESXED	1.674	2.213	3.918	0.019	0.016	0.539	1.705
DAZDIR	1.683	2.201	3.946	0.000	0.000	0.518	1.745
EMULED	1.689	2.205	3.962	0.020	0.013	0.516	1.757
FAGREK	1.692	2.200	3.954	0.010	0.011	0.508	1.754
FEMJAI	1.676	2.213	3.923	0.024	0.007	0.537	1.710
FEMJAI01	1.675	2.202	3.921	0.028	0.005	0.527	1.719
FEMJAI02a	1.667	2.211	3.909	0.027	0.035	0.544	1.698
FEMJAI02b	1.666	2.203	3.907	0.052	0.015	0.537	1.704
FESBAS10	1.687	2.205	3.936	0.009	0.006	0.518	1.731
FESTPH	1.675	2.211	3.921	0.012	0.026	0.536	1.71
HETSFE	1.671	2.212	3.924	0.053	0.024	0.541	1.712
JAQTIF	1.677	2.212	3.905	0.024	0.008	0.535	1.693
JATVOQ	1.676	2.209	3.921	0.015	0.006	0.533	1.712
KEYWAM	1.678	2.217	3.911	0.000	0.000	0.539	1.694
KEYWUG	1.706	2.207	3.953	0.032	0.036	0.501	1.746
KIXDEA	1.699	2.201	3.952	0.000	0.000	0.502	1.751
LUZDOZ	1.676	2.207	3.941	0.052	0.025	0.531	1.734
NATFOD	1.685	2.211	3.948	0.026	0.017	0.526	1.737
NIWSANa	1.697	2.200	3.973	0.033	0.030	0.503	1.773
NIWSANb	1.696	2.200	3.973	0.033	0.031	0.504	1.773
OBINIX	1.682	2.214	3.938	0.013	0.010	0.532	1.724
PATJIA	1.690	2.212	3.936	0.018	0.043	0.522	1.724
PUGSOZ	1.670	2.197	3.931	0.000	0.000	0.527	1.734
SUVWOV	1.665	2.201	3.900	0.000	0.000	0.536	1.699
TUBHED	1.669	2.202	3.944	0.028	0.015	0.533	1.742
MEAN	1.681	2.207	3.933	0.0181	0.014	0.526	1.727

ANNEX D

Following, we present the values of the M-S bond for different silanethiolates which were used in the present work for the elaboration of figures 23, 24 and 25. The data have been ordered according to the coordination number of the complexes. The complexes are referenced by their CCDC code.

a) Tetracoordinated complexes

Li silanethiolates		
Reference code	**M-S distances (in Å)**	
JESRIJ	2.481	2.493
mean Li-S	2.487	

Ti silanethiolates		
Reference code	**M-S distances (in Å)**	
IYUDIP-a	2.413	2.436
IYUDIP-b	2.414	2.439
IYUDOV	2.439	2.444
mean Ti-S	2.431	

V silanethiolates			
Reference code	**M-S distances (in Å)**		
DUVLEL	2.242	2.243	2.250
mean V-S	2.245		

Cr silanethiolates		
Reference code	**M-S distances (in Å)**	
MIRVEP	2.408	2.408
mean Cr-S	2.408	

Mn silanethiolates		
Reference code	**M-S distances (in Å)**	
CEZYOW	2.454	2.454
CEZZAJ	2.408	2.429
LUGPIM	2.380	2.389
mean Mn-S	2.419	

Fe silanethiolates		
Reference code	**M-S distances (in Å)**	
EKIJEN	2.320	
RIDJIY	2.345	
LUGNOQ	2.293	2.323
LUGNUW	2.303	2.304
LUGPEI	2.321	2.326
YECRII	2.271	2.289
LUGPAE	2.304	2.311
[III]	2.301	2.300
[IV]	2.335	2.352
[V]	2.309	2.346
[X]	2.313	2.283
mean Fe-S	2.312	

Co silanethiolates			
Reference code	**M-S distances (in Å)**		
IDADOG	2.285	2.273	
IDAFAU	2.316	2.294	
CERNIX	2.297	2.305	
IDAFEY	2.278	2.306	
WUGTOH	2.310	2.312	
WUGTUN	2.298	2.300	
WUGVAV	2.278	2.318	2.329
IDADEW	2.280	2.280	
IYUDAH	2.266	2.266	
LUGPOS	2.271	2.277	
YIDNIJ	2.297	2.297	
PODNEC	2.272	2.303	
WOFREP	2.278	2.301	
mean Co-S	2.292		

Ni silanethiolates		
Reference code	**M-S distances (in Å)**	
IYUDUB	2.232	2.250
IYUFAJ	2.246	2.253
LUGPUY	2.271	2.276
mean Ni-S	2.255	

Cu silanethiolates	
Reference code	**M-S distances (in Å)**
MAQCIQ	2.397
QEYGEG	2.402
QICTOM	2.371
mean Cu-S	2.390

Zn silanethiolates		
Reference code	**M-S distances (in Å)**	
REWJAE	2.247	2.296
WOWQEE	2.285	2.293
WOWQOO	2.294	2.295
WOWQII	2.286	2.298
AREJEM	2.288	2.312
AREJOW	2.270	2.270
RAPYOX-a	2.142	2.163
RAPYOX-b	2.156	2.156
RAPZAK	2.100	2.105
PODNIG	2.281	2.301
WOFRAL	2.276	2.307
mean Zn-S	2.246	

Ru silanethiolates	
Reference code	**M-S distances (in Å)**
KODQUP	2.461
mean Ru-S	2.461

Cd silanethiolates		
Reference code	**M-S distances (in Å)**	
SESLAE	2.465	2.482
GIFQAO	2.491	2.491
mean Cd-S	2.482	

Ga silanethiolates			
Reference code	**M-S distances (in Å)**		
NEMJOE	2.233	2.245	2.252
mean Ga-S	2.243		

Pt silanethiolates	
Reference code	**M-S distances (in Å)**
UFEGUW	2.350
mean Pt-S	2.350

Hg silanethiolates		
Reference code	**M-S distances (in Å)**	
DUDDAH	2.316	2.316
mean Hg-S	2.316	

Mean M-S for all tetracoordinated silanethiolates = 2.315 Å

b) pentacoordinated complexes

V silanethiolates		
Reference code	**M-S distances (in Å)**	
VIHPIL	2.329	2.337
mean V-S	2.333	

Mn silanethiolates		
Reference code	**M-S distances (in Å)**	
CEHZEV	2.428	2.428
RENBUI	2.438	2.479
CEZYUC	2.416	2.451
mean Mn-S	2.443	

Fe silanethiolates		
Reference code	**M-S distances (in Å)**	
[VI]	2.366	2.370
[VII]	2.330	2.329
[VIII]a	2.332	2.331
[VIII]b	2.321	2.326
[IX]	2.324	2.324
mean Fe-S	2.335	

Co silanethiolates		
Reference code	**M-S distances (in Å)**	
IDADIA	2.265	2.272
IDADUM	2.264	2.264
YOYNIJ	2.268	2.268
GEPVED	2.287	2.287
mean Co-S	2.272	

Zn silanethiolates		
Reference code	**M-S distances (in Å)**	
AREJAI	2.263	2.266
AREJIQ	2.264	2.271
PEDWEB	2.258	2.267
HAYSAC	2.428	2.428
REWHUW	2.249	2.249
mean Zn-S	2.294	

Cd silanethiolates		
Reference code	**M-S distances (in Å)**	
VEGHAR	2.434	2.435
mean Cd-S	2.435	

Mean M-S for all pentacoordinated silanethiolates = 2.333 Å

c) hexacoordinated complexes

Mn silanethiolates		
Reference code	**M-S distances (in Å)**	
CEHZIZ	2.567	2.567
RENBOC	2.498	2.498
mean Mn-S	2.533	

Co silanethiolates		
Reference code	**M-S distances (in Å)**	
WOWQAA	2.291	2.301
mean Co-S	2.296	

Cd silanethiolates		
Reference code	**M-S distances (in Å)**	
VERXIA	2.522	2.522
mean Cd-S	2.522	

Fe silanethiolates		
Reference code	**M-S distances (in Å)**	
[I]	2.517	2.517
mean Fe-S	2.517	

Mean M-S for all hexacoordinated silanethiolates = 2.480 Å

Annex E

Values of the angle variances and the mean quadratic elongations for the known silanethiolates of iron(II). These data have been used in the elaboration of the graphs plotted in Fig. 31 and Fig. 32.

Tetracoordinated Fe(II) silanethiolates	σ^2	$\langle\lambda\rangle$
[III]	155.109	1.049
[IV]	185.385	1.060
[V]	107.479	1.035
[X]	219.400	1.069
EKIJEN	354.335	1.094
RIDJIY	282.193	1.088
LUGNOQ	55.600	1.024
LUGNUW	167.869	1.054
LUGPEI	303.373	1.089
YECRII	289.557	1.084
LUGPAE	182.649	1.043

Pentacoordinated Fe(II) silanethiolates	σ^2	$\langle\lambda\rangle$
[VI]	11.233	1.016
[VII]	125.479	1.038
[VIII]-a	101.160	1.033
[VIII]-b	104.206	1.031
[IX]	173.070	1.052

11 BIBLIOGRAPHY

1. T. A. Wertime *Science* **v30, 182** (1973) 875
2. N. H. Gale and Z. A. Stos-Gale *Science* **v2, 216** (1982) 11
3. R. M. Rowlett *Science* **v12, 161** (1968) 123
4. J. A. Babor and J. Ibarz *Química General Moderna* 7ª ed. Ed. Martín, S.A.(1964) 799
5.Inorganic Chemistry. Holleman-Wiberg. Academic Press 2001 pp 1430-1431
6. A. D. Little *Ind. Eng. Chem.* **v18, 5** (1926) 444
7. E. G. Hill *Ind. Eng. Chem.* **v27, 6** (1935) 611
8. A. S. Cushman *J. Ind. Eng. Chem.* **v7, 11** (1915) 934
9. J. A. Babor and J. Ibarz *Química General Moderna* 7ª ed. Ed. Martín, S.A. (1964) 804
10. R. S. Tour *Ind. Eng. Chem.* **v12, 9** (1920) 844
11. A. Hellman, E. J. Baerends, M. Biczysko, T. Bligaard, C. H. Christensen, D. C. Clary, S. Dahl, R. van Harrevelt, K. Honkala, H. Jonsson, G. J. Kroes, M. Luppi, U. Manthe, J. K. Nørskov, R. A. Olsen, J. Rossmeisl, E. Skúlason, C. S. Tautermann, A. J. C. Varandas and J. K. Vincent *J. Phys. Chem. B* **v110, 36** (2006) 17719
12. C. L. Parker *Ind. Eng. Chem.* **v5, 5** (1913) 440
13. C. J. H. Jacobsen *Chem. Commun.* **12** (2000) 1057
14. A. F. Holleman, E. Wiberg *Inorganic Chemistry* N. Wiberg (Ed.), Academic Press (2001) 1447
15. A. F. Holleman, E. Wiberg *Inorganic Chemistry* N. Wiberg (Ed.), Academic Press (2001) 1445
16. R. Zboril, M. Mashlan and D. Petridis *Chem. Mater.* **v14, 3** (2002) 969
17. Z. Liu, D. Zhang, S. Han, C. Li, B. Lei, W. Lu, J. Fang, and C. Zhou *J. Am. Chem. Soc.* **v127, 1** (2005) 6

18. K. Woo, J. Hong, S. Choi, H. W. Lee, J. P. Ahn, C. S. Kim and S. W. Lee *Chem. Mater.* **v16, 14** (2004) 2814
19. D. E. Kony *Egypt. J. Solids* **v27, 2** (2004) 285
20. V. Hlavacek and J. A. Puszynski *Ind. Eng. Chem. Res*. **v35, 2** (1996) 349
21. J. A. Kohn and D. W. Eckart *J. Phys. Chem.* **v67, 4** (1963) 957
22. D. Cruickshank *Journal of the European Ceramic Society* **v23, 14** (2003) 2721
23. N. W. Grimes *Physics in Technology* **v6, 1** (1975) 22
24. M. Winter and R. J. Brodd *Chem. Rev.* **v104, 10** (2004) 4245
25. C. Wadia, A. P. Alivisatos and D. M. Kammen *Environ. Sci. Technol.* **v42, 6** (2009) 2072
26. I. Bertini, H. B. Gray, E. I. Stiefel and J. S. Valentine *Biological Inorganic Chemistry: Structure & Reactivity* University Science Books (2007) 51
27. I. Bertini, H. B. Gray, E. I. Stiefel and J. S. Valentine *Biological Inorganic Chemistry: Structure & Reactivity* University Science Books (2007) 46
28. P. V. Rao and R. H. Holm *Chem Rev*. **v104, 2** (2004) 527
29. W. Wojnowski, M. Wojnowski, K. Peters, E. M. Peters and H. G. von Schnering *Z. anorg. Allg. Chem.* **v531**(1985) 147
30. W. Wojnowski, M. Wojnowski, H. G. von Schnering and M. Noltemeyer *Z. anorg. Allg. Chem.* **v531**(1985) 153
31. W. Wojnowski, M. Wojnowski, K. Peters and E. M. Peters *Z. anorg. Allg. Chem.* **v535**(1986) 31
32. A. Herman and W. Wojnowski *Struct. Chem.* **v3, 3** (1992) 239
33. B. Becker, A. Zalewska, A. Konitz and W. Wojnowski *Z.Anorg. Allg. Chemie* **v627** (2001) 271
34. B. Becker, A. Zalewska, A. Konitz and W. Wojnowski *Polyhedron* **v20** (2001) 2567
35. B. Becker, A. Pladzyk, A. Konitz and W. Wojnowski *Appl.Organometal. Chem.* **v16, 9** (2002) 517
36. B. Becker, K. Radacki and W. Wojnowski *J. Organometal. Chem.* **v521** (1996) 39
37. B. Becker , A. Dołega, A. Konitz and W. Wojnowski *Polyhedron* **v20** (2001) 949
38. A. Dołega, A. Ciborska, J. Chojnacki, M. Walewski and W. Wojnowski *Thermochimica Acta* **v429** (2005) 103
39. B. Becker, A. Dołęga, A. Konitz, L. Swinder and W. Wojnowski *Z.Anorg. Allg. Chem.* **v627** (2001) 280
40. A. Dołęga , B. Becker, J. Chojnacki, A. Konitz and W. Wojnowski *Inorganica Chimica Acta* **v357** (2004) 461
41. A. Kropidłowska, J. Chojnacki and B. Becker *Inorg. Chem. Comm.* **v9** (2006) 383
42. J. Chojnacki, B. Becker, A. Konitz and W. Wojnowski *Z. Anorg. Allg. Chem.* **v626** (2000) 2173
43. B. Becker, K. Baranowska, J. Chojnacki and W. Wojnowski *Chem.Commun*. **v28** (2004) 620
44. T. Komuro, H. Kawaguchi and K. Tatsumi *Inorg. Chem.* **v41** (2002) 5083
45. O. L. Sydora, P. T. Wolczanski and E. B. Lobkovsky *Angew. Chem. Int.* **v42** (2003) 2685
46. H. C. Zhou and R. H. Holm *Inorg. Chem.* **v42** (2003)11
47. I. Kovacs, F. Belanger-Gariepy and A. Shaver *Inorg. Chem.* **v42** (2003) 2988
48. T. Komuro, T. Matsuo, H. Kawaguchi and K. Tatsumi *Dalton Trans*. **10** (2004) 1618
49. O. L. Sydora, T. P. Henry, P. T. Wolczanski, E. B. Lobkovsky, E. Rumberger and D. N. Hendrickson *Inorg. Chem.* **v45** (2006) 609

50. J. Vela, J. M. Smith, Y. Yu, N. A. Ketterer, C. J. Flaschenriem, R. J. Lachicotte and P. L. Holland *J. Am.Chem. Soc.* **v127** (2005) 7857
51. T. I. Kückmann, F. Dornhaus, M. Bolte, H. W. Lerner, M. C. Holthausen and M. Wagner *Eur. J. Inorg Chem.* **14** (2007) 1989
52. J. J. R. Frausto da Silva and R. J. P. Williams *The Biological Chemistry of the Elements: The Inorganic Chemistry of Life* 1st Ed. Oxford University Press (1991) 12
53. I. Bertini, H. B. Gray, E. I. Stiefel and J. S. Valentine *Biological Inorganic Chemistry: Structure & Reactivity* University Science Books (2007) 8
54. I. Bertini, H. B. Gray, E. I. Stiefel and J. S. Valentine *Biological Inorganic Chemistry: Structure & Reactivity* University Science Books (2007) 12
55. R. Crichton *Inorganic biochemistry of iron metabolism* 2nd Ed., Wiley (2001) 2
56. A. F. Holleman, E. Wiberg *Inorganic Chemistry* N. Wiberg (Ed.), Academic Press (2001) 484
57. E. I. Ochiai *Bioinorganic Chemistry* 2nd Ed. Academic Press (2008) 38
58. A. F. Holleman, E. Wiberg *Inorganic Chemistry* N. Wiberg (Ed.), Academic Press (2001) 1431
59. A. F. Holleman, E. Wiberg *Inorganic Chemistry* N. Wiberg (Ed.), Academic Press (2001) 1440
60. S. J. Lippard and J. M. Berg *Principles of bioinorganic chemistry* University Science Books (1994) 21
61. J. J. R. Frausto da Silva and R. J. P. Williams *The Biological Chemistry of the Elements: The Inorganic Chemistry of* Life 1st Ed. Oxford University Press (1991) 39
62. R. H. Holm, P. Kennepohl and E. I. Solomon *Chem. Rev.* **v96** (1996) 2239
63. A. F. Holleman, E. Wiberg *Inorganic Chemistry* N. Wiberg (Ed.), Academic Press (2001) 1438
64. I. Bertini, H. B. Gray, E. I. Stiefel and J. S. Valentine *Biological Inorganic Chemistry: Structure & Reactivity* (2007) 243
65. L. B. Dugad, G. N. La Mar, L. Banci and I. Bertini *Biochemistry* **v29** (1990) 2263
66. R. Crichton *Inorganic biochemistry of iron metabolism* 2nd Edition, Wiley (2001)
67. J. J. R. Frausto da Silva and R. J. P. Williams *The Biological Chemistry of the Elements: The Inorganic Chemistry of Life* 2nd Ed. Oxford University Press (2001) 7
68. E. I. Ochiai *J. Chem. Educ.* **v63** (1986) 942
69. I. Bertini, H. Gray, S. Lippard and J. S. Valentine *Bioinorganic Chemistry* (1994) 3
70. G. I. Likhtenstein, A. I. Kotelnikov, A. W. Kulikov, L. A. Syrtsova, V. R. Bogatyrenko, A. I. Melnikov, E. N. Frolov and A. I. Berg *Int. J. Quant.Chem* **v16, 3** (2004) 419
71. C. E. Forde, Ph.D. Thesis – *Modelling biological iron* (1997) 1
72. I. Bertini, H. B. Gray, E. I. Stiefel and J. S. Valentine *Biological Inorganic Chemistry: Structure & Reactivity* University Science Books (2007) 443
73. C. Huber and G. Wächtershäuser *Science* **v281** (1998) 670
74. H. Ogino, S. Inomata and H. Tobita *Chem. Rev.* **v98** (1998) 2093
75. R. A. Henderson *Chem. Rev.* **v105** (2005) 2365
76. S. C. Lee and R. H. Holm *Chem. Rev.* **v104** (2004) 1135
77. L. Que, Jr., M. A. Bobrik, J. A. Ibers and R. H. Holm *J. Am.Chem. Soc.* **v96** (1974) 13
78. R. J. M. Klein Gebbink, S. I. Klink, M. C. Feiters and R. J. M. Nolte *Eur. J. Inorg. Chem.* **2** (2000) 253
79. S. Groysman and R. H. Holm *Biochemistry* **v48, 11** (2009) 2310
80. A. V. Coelho, P. Matias, V. Fulop, A. Thompson, A. Gonzalez and M. A. Carrondo *J. Biol. Inorg. Chem.* **v2** (1997) 680

81. A. Fish, T. Danieli, I. Ohad, R. Nechushtai and O. Livnah *J. Mol. Biol.* **v350** (2005) 599
82. C. Frazao, D. Aragao, R. Coelho, S. S. Leal, C. M. Gomes, M. Teixeira and M. A. Carrondo *FEBS Lett.* **582** (2008) 763
83. D. Coucouvanis *Acc. of Chem Res.* **v24** (1991) 1
84. B. S. Snyder, M. S. Reynolds, I. Noda and R. H. Holm *Inorg. Chem.* **v27**(1988) 595
85. B. S. Snyder and R. H. Holm *Inorg. Chem.* **v27** (1988) 2339
86. H. Kalyvas and D. Coucouvanis *Inorg. Chem.* **v45** (2006) 8462
87. K. S. Hagen, A. D. Watson and R. H. Holm *J. Am. Chem. Soc.* **v105** (1983) 3905
88. J. F. You, B. S. Snyder, G. C. Papaefthymiou and R. H. Holm *J. Am. Chem. Soc*. **v112** (1990)1067
89. S. C. Lee and R. H. Holm *Proc. Natl. Acad. Sci*. **v100** (2003) 3595
90. Y. Zhang and R. H. Holm *J. Am. Chem. Soc.* **v125** (2003) 3910
91. J. L. Zuo, H. C. Zhou and R. H. Holm *Inorg. Chem.* **v42** (2003) 4624
92. R. Panda, Y. Zhang, C. C. McLauchlan, P. V. Rao, F. A. Tiago de Oliveira, E. Münck and R. H. Holm, *J. Am. Chem. Soc.* **v126** (2004) 6448
93. R. Panda, C. P. Berlinguette, Y. Zhang and R. H. Holm, *J. Am. Chem. Soc.* **v127** (2005) 11092
94. J. Sun, C. Tessier and R. H. Holm *Inorg. Chem.* **v46** (2007) 2691
95. H. B. Kraatz and N. Metzler-Nolte *Concepts and models in bioinorganic chemistry* Wiley-VCH (2006) 400
96. A. F. Holleman, E. Wiberg *Inorganic Chemistry* N. Wiberg (Ed.), Academic Press (2001) 1456
97. G. N. L. Jameson, E. M. Walters, W. Manieri, P. Schümann, M. K. Johnson and B. Hanh Huynh *J. Am. Chem. Soc*. **v125** (2003) 1146
98. L. M. Lawson Daku, J. Pecaut, A. Lenormand-Foucaut, B. Vieux-Melchior, P. Iveson and J. Jordanov *Inorg. Chem.* **v42** (2003) 6824
99. P. S. Yoon, J. Rawlings, W. H. Orme-Johnson and H. F. DeLuca *Biochemistry* **v19** (1980) 2172
100. C. W. Carter, Jr. J. Kraut, S. T. Freer, R. A. Alden, L. C. Sieker, E. Adman and L. H. Jensen., *Proc. Natl Acad Sci* **v69** (1972) 3526
101. G. H. Stout, S. Turley, L. C. Sieker and L. H. Jensen *Proc. Natl. Acad. Sci* **v85** (1988)1020
102. C. D. Stout *J. Biol. Chem* **v263** (1988) 9256
103. L. C. Sieker, E. Adman and L. H. Jensen *Nature* **v235** (1971) 40
104. T. A. Scott and R. H. Holm *Inorg. Chem.* **v47** (2008) 3426
105. J. W. Raebiger, C. A. Crawford, J. Zhou and R. H. Holm *Inorg. Chem.* **v36** (1997) 994
106. J. Huang, C. Goh and R. H. Holm *Inorg. Chem.* **v36** (1997) 356
107. Y. Deng, Q. Liu, C. Chen, Y. Wang, Y. Cai, D. Wu, B. Kang, D. Liao and J. Cui *Polyhedron* **v16** (1997) 4121
108. S. M. Malinak, K. D. Demadis and D. Coucouvanis *J. Am. Chem. Soc*. **v117** (1995) 3126
109. W. H. Armstrong, P. K. Mascharak and R. H. Holm *Inorg. Chem.* **v21** (1982) 1699
110. P. K. Mascharak, G. C. Papaefthymiou, W. H. Armstrong, S. Foner,R. B. Frankel and R. H. Holm *Inorg. Chem.* **v22** (1983) 2851
111. P. K. Mascharak, W. H. Armstrong, Y. Mizobe and R. H. Holm *J. Am. Chem. Soc.* **v105** (1983) 475
112. M. A. Bobrik, E. J. Laskowski, R. W. Johnson, W. O. Gillum, J. M. Berg, K. O. Hodgson and R. H. Holm *Inorganic Chemistry* **v17** (1978) 1402

113. J. G. Reynolds and R. H. Holm *Inorg. Chem.* **v20** (1981) 1873
114. H. Ogino, H. Tobita, K. Yanagisawa, M. Shimoi and C. Kabuto *J. Am. Chem. Soc.* **v109** (1987) 5847
115. S. Rutchik, S. Kim and M. A. Walters *Inorg. Chem.* **v27** (1988) 1513
116. J. M. McConnachie and J. A. Ibers *Inorg. Chem.* **v30** (1991) 1770
117. S. B. Yu, G. C. Papaefthymiou and R. H. Holm *Inorg. Chem.* **v30** (1991) 3476
118. C. Zhou and R. H. Holm *Inorg. Chem.* **v36** (1997) 4066
119. R. Hauptmann, R. Kliss, J. Schneider and G. Henkel *Z. anorg. allg. Chem.* **v624** (1998) 1927
120. A. Kern, C. Näther and F. Tuczek *Inorg. Chem.* **v43** (2004) 5011
121. J. M. Moulis, J. Meyer and M. Lutz *Biochemistry* **v23** (1984) 6605
122. J. L. Breton, J. A. Farrar, M. C. Kennedy, H. Beinert and A. J. Thomson *Biochem. J.* **v311** (1995) 197
123. J. W. Peters, M. H. B. Stowell, S.M. Soltis, M.G. Finnegan, M.K. Johnson and D.C. Rees *Biochemistry* **v36** (1997) 1181
124. B. K. Burgess and D. J. Lowe *Chem. Rev.* **v96** (1996) 2983
125. B. A. MacKay and M. D. Fryzuk *Chem. Rev.* **v104** (2004) 385
126. B. K. Burgess *Chem. Rev.* **v90** (1990) 1377
127. J. B. Howard and D. C. Rees *Chem. Rev.* **v96** (1996) 2965
128. R. R. Eady *Chem. Rev.* **v96** (1996) 3013
129. F. A. Tezcan, J. T. Kaiser, D. Mustafi, M. Y. Walton, J. B. Howard and D. C. Rees *Science* **v309** (2005) 1377-1380
130. A. F. Holleman, E. Wiberg *Inorganic Chemistry* N. Wiberg (Ed.), Academic Press (2001) 605
131. J. W. Peters, W. N. Lanzilotta, B. J. Lemon and L. C. Seefeldt *Science* **v282** (1998) 1853
132. C. Tard and C. J. Pickett *Chem. Rev.* **v109** (2009) 2245
133. S. Ogo, T. Kabe, K. Uehara, B. Kure, T. Nishimura, S. C. Menon, R. Harada and S. Fukuzumi *Science* **316** (2007) 585
134. I. Bertini, H. B. Gray, E. I. Stiefel and J. S. Valentine *Biological Inorganic Chemistry: Structure & Reactivity* University Science Books (2007) 403
135. S. Gao, J. Fan, S. Sun, X. Peng, X. Zhao and J. Hou *Dalton Trans.* (2008) 2128
136. F. Gloaguen, J. D. Lawrence, T. B. Rauchfuss, M. Bénard and M. M. Rohmer *Inorg. Chem.* **v41** (2002) 6573
137. J. Evans and C. J. Pickett *Chem. Soc. Rev.* **v32** (2003) 268
138. S. Shima, O. Pilak, S. Vogt, M. Schick, M. S. Stagni, W. Meyer-Klaucke, E. Warkentin, R. K. Thauer and U. Ermler *Science* **v321** (2008) 572
139. A. F. Holleman, E. Wiberg *Inorganic Chemistry* N. Wiberg (Ed.), Academic Press (2001) 56
140. A. F. Holleman, E. Wiberg *Inorganic Chemistry* N. Wiberg (Ed.), Academic Press (2001) 503
141. J. A. Babor, J. Ibarz *Química General Moderna* 7ª ed. Ed. Martín, S.A.(1964) 571
142. A. F. Holleman, E. Wiberg *Inorganic Chemistry* N. Wiberg (Ed.), Academic Press (2001) 505
143. J. A. Babor, J. Ibarz *Química General Moderna* 7ª ed. Ed. Martín, S.A.(1964) 572
144. A. F. Holleman, E. Wiberg *Inorganic Chemistry* N. Wiberg (Ed.), Academic Press (2001) 515
145. J. A. Babor, J. Ibarz *Química General Moderna* 7ª ed. Ed. Martín, S.A.(1964) 570

146. H. Hart, L. E. Craine, D. J. Hart *Química Orgánica* 9ª Ed McGraw Hill 208
147. H. Hart, L. E. Craine, D. J. Hart *Química Orgánica* 9ª Ed McGraw Hill 229
148. H. Zhang, C. Romero, and S. Baldelli *J. Phys. Chem. B* **v109** (2005) 15520
149. K. Aramaki *Corros. Sci.* **v41** (1999) 1715
150. A. Labande, J. Ruiz and D. Astruc *J. Am. Chem. Soc.* **v124** (2002) 1782
151. M. Brust, M. Walker, D. Bethell, D. J. Schiffrin and R. Whyman *J. Chem. Soc. Chem. Commun.* **1994**, 801.
152. M. Brust, J. Fink, D. Bethell, D. J. Schiffrin and C. Kiely, *Chem. Commun.* (1995) 1655
153. Y. Y. Luk, M. L. Tingey, D. J. Hall, B. A. Israel, C. J. Murphy, P. J. Bertics and N. L. Abbott *Langmuir* **v19** (2003) 1671
154. J. H. Reif *Science* **v296** (2002) 478
155. J. M. Tour *Acc. Chem. Res.* **v33** (2000) 791
156. B. Becker, A. Radacki, A. Konitz and W. Wojnowski *Z. Anorg. Allg. Chem* **v621** (1995) 904
157. J. Chojnacki, B. Becker, A. Konitz, M. J. Potrzebowski and W. Wojnowski *J. Chem. Soc. Dalton Trans.* (1999) 3063
158. S. J. Lippard and J. M. Berg *Principles of bioinorganic chemistry* University Science Books (1994) 27
159. I. G. Dance *Polyhedron* **5** (1986) 1037
160. E. R. Roland, E. C. Walborsky, J. C. Dewan and R. R. Schrock *J. Am. Chem. Soc.* **v107** (1985) 5795
161. T. Nguyen, A. Panda, M. M. Olmstead, A. F. Richards, M. Stender, M. Brynda, and P. P. Power *J. Am. Chem. Soc* **v127** (2005) 8545
162. D. L. King and L. Li *Catal. Tod.* **v116** (2006) 526
163. A. E. Fenwick, P. E. Fanwick, and I. P. Rothwell *Organometallics* **v22, 3** (2003) 535
164. E. R. T. Tiekink *Bioinorg. Chem. Appl.* **v1, 1** (2003) 53
165. S. Groysman and R. H. Holm *Inorg. Chem.* **v48** (2009) 621
166. E. Block, M. Gernon, H. Kang, G. Ofori-Okai and J. Zubieta, *Inorg. Chem.* **v28** (1989) 1263
167. K. Tang, M. Aslam, E. Block, T. Nicholson and J. Zubieta, *Inorg. Chem.* **v26** (1987) 1488
168. C. E. Forde, Ph.D. Thesis – *Modelling biological iron* (1997) 6
169. K. M. Miller and C. E. Strouse *Inorg.Chem.* **v23** (1984) 2395
170. K. M. Miller and C. E. Strouse *Acta Crystallogr.,Sect .C: Cryst. Struct. Commun.* **C40** (1984) 1324
171. M. Schappacher, L. Ricard, J. Fischer, R. Weiss, E. Bill, R. Montiel-Montoya, H. Winkler and A. X. Trautwein *Eur. J. Biochem.* **v168** (1987) 419
172. N. Ueyama, N. Nishikawa, Y. Yamada, T. Okamura and A. Nakamura *Inorg. Chim. Acta* **v283** (1998) 91
173. S. C. Tang, S. Koch, G. C. Papaefthymiou, S. Foner, R. B. Frankel, J. A. Ibers and R. H. Holm *J.Am.Chem.Soc.* **v98** (1976) 2414
174. N. Ueyama, N. Nishikawa, Y. Yamada, T. Okamura and A. Nakamura *J.Am.Chem.Soc.* **v118** (1996) 12826
175. N. Ueyama, N. Nishikawa, Y. Yamada, T. Okamura, S. Oka, H. Sakurai and A. Nakamura *Inorg.Chem.* **v37** (1998) 2415
176. M. P. Byrn and C. E. Strouse *J.Am.Chem.Soc.* **v113** (1991) 2501
177. N. Xu, D. R. Powell, L. Cheng, G. B. Richter-Addo *Chem.Commun.* (2006) 2030

178. C. H. Chen, Y. S. Chang, C. Y. Yang, T. N. Chen, C. M. Lee and W. F. Liaw *Dalton Trans.* (2004) 137
179. D. Sellmann, K. P. Peters and F. W. Heinemann *Eur. J. Inorg. Chem.* (2004) 581
180. G. Henkel, H. Strasdeit, W. Simon and B. Krebs *Inorg. Chim. Acta* **v76** (1983) 207
181. T. Mashiko, C. A. Reed, K. J. Haller, M. E. Kastner and W. R. Scheidt *J. Am. Chem. Soc*. **v103** (1981) 5758
182. S. A. Koch, L. E. Maelia and M. Millar *J. Am. Chem. Soc*. **v105** (1983) 5944
183. L. E. Maelia, M. Millar and S. A. Koch *Inorg. Chem.* **v31** (1992) 4594
184. M. Millar, S. A. Koch and R. Fikar *Inorg. Chim. Acta* **v88** (1984) 15
185. M. Millar, J. F. Lee, T. O'Sullivan, S. A. Koch and R. Fikar *Inorg. Chim. Acta* **v243** (1996) 333
186. K. Beisheng and C. Jinhua *Jiegou Huaxue (Chin. J. Struct. Chem.)* **v4** (1985) 119
187. Z. Nagy-Magos, L. Marko, A. Szakacs-Schmidt, G. Gervasio, E. Belluso and S. F. Kettle *Bull. Soc. Chim. Belg.* **v100** (1991) 445
188. J. J. Ellison, K. Ruhlandt-Senge and P. P. Power *Angew. Chem., Int. Ed.* **v33** (1994) 1178
189. T. C. Harrop, Datong Song and S. J. Lippard *J. Am. Chem. Soc.* **v128** (2006) 3528
190. E. Delgado, B. Donnadieu, S. Garcia and F. Zamora *J. Organomet. Chem.* **v649** (2002) 21
191. K. Bose, J. Huang, B. S. Haggerty, A. L. Rheingold, R. J. Salm and M. A. Walters *Inorg. Chem.* **v36** (1997) 4596
192. W. F. Liaw, C. Kim, M. Y. Darensbourg and A. L. Rheingold *J. Am. Chem. Soc.* **v111** (1989) 3591
193. S. A. Wander, J. H. Reibenspies, J. S. Kim and M. Y.Darensbourg *Inorg. Chem.* **v33** (1994) 1421
194. M. M. Kubicki, P. Oudet, C. Martin and C. Barre *J. Chem. Soc., Dalton Trans.* (1995) 3699
195. R. N. Mukherjee, A. J. Abrahamson, G. S. Patterson, T. D. P. Stack and R. H. Holm *Inorg.Chem.* **v27** (1988) 2137
196. L. D. Field, W. J. Shaw and P. Turner *Chem.Commun.* (2002) 46
197. F. M. MacDonnell, K. Ruhlandt-Senge, J. J. Ellison, R. H. Holm and P. P. Power *Inorg.Chem.* **v34** (1995) 1815
198. I. Pierre *J. Prakt. Chem.* **v41** (1847) 342
199. C. Friedel and A. Landeburg *Compt. rend.* **v64** (1867) 1295
200. W. Wojnowski *Zeszyty naukowe Politechniki Gdańskiej, Chemia XXII* **v172** (1971) 1
201. J. Pikies and W. Wojnowski *J. Organometal. Chem* **v386** (1990) 305
202. W. Wojnowski, K. Peters, E. M. Peters and H. G. Von Schnering *Z. Kristallogr.* **v174** (1986) 305
203. E. W. Felcyn and W. Wojnowski *Z. Anorg. Allg. Chem.* **v554** (1987) 197
204. B. Becker and W. Wojnowski *Synth. React. Inorg. Met.-Org. Chem* **v12, 5** (1982) 565
205. W. Wojnowski and M. Wojnowska *Z. Anorg. Allg. Chem* **v397** (1973) 69
206. W. Wojnowski and R. Piękoś *Z. Anorg. allg. Chem.*(1962) 189
207. W. Wojnowski and M. Wojnowska *Z. Anorg. Allg. Chem* **v389** (1972) 302
208. T. Tanabe, N. Takeda and N. Tokitoh *Eur. J. Inorg. Chem.* (2007) 1225
209. W. Wojnowski *Roczniki chem* **v38** (1964) 1262
210. M. Wojnowska and W. Wojnowski *Z. Anorg. Allg. Chem.* **v403** (1974) 179
211. J. Chojnacki *J. Mol. Struct: THEOCHEM* **v862** (2008) 112
212. B. Becker and W. Wojnowski *J. Chromatogr.* **v219** (1989) 302

213. W. Wojnowski *Z. Anorg. Allg. Chem.* **403** (1974) 186
214. W. Wojnowski and K. Przyjemska-Szydlik *Z. Anorg. Allg. Chem.* **424** (1976) 273
215. K. Przyjemska , W. Wojnowski *Z. Anorg. Allg. Chem.* **551** (1987) 203
216. J. Pikies, K. Przyjemska , W. Wojnowski *Z. Anorg. Allg. Chem.* **551** (1987) 209
217. J. Pikies, W. Wojnowski *Phosphorus, Sulfur and Silicon*, **78** (1993) 133
218. S. Konieczny and W. Wojnowski *Z. Anorg. Allg. Chem* **v562** (1988) 153
219. S. Konieczny, K. Wrzesien and W. Wojnowski *J. Organomet. Chem.* **v446** (1993) 73
220. T.Ostdick and P.A. McCusker *Inorg. Chem.* **v6** (1967) 98
221. W. E. Newton and E.G. Rochow *Inorganica Chimica Acta* **v4** (1970) 133
222. J. Chojnacki *Polyhedron* **v27** (2008) 969
223. W. Wojnowski, M. Wojnowski, K. Peters, E. M. Peters and H. G. von Schnering *Z. Anorg. Allg. Chem.* **v530** (1985) 79
224. P. A. Shapley, H. C. Liang and N. C. Dopke *Organometallics* **v*20*** (2001) 4700
225. W. Wojnowski, K. Peters, E. M. Peters and H. G. Von Schnering *Z. Kristallogr.* **v174** (1986) 297
226. E. Jesionka, K. Baranowska and W. Wojnowski *Phosphorus, Sulfur, and Silicon* **v184** (2009)
227. E. Jesionka, J. Chojnacki and W. Wojnowski *Acta Cryst.* **v62**(2006) 1982
228. T. Komuro, T. Matsuo, H. Kawaguchi, and K. Tatsumi *Inorg. Chem.* **v42** (2003) 5340
229. B. Kasterka, J. Chojnacki, W. Wojnowski and J.F. Biernat *Chem. Anal.* **v38** (1993) 287
230. J. Chojnacki, B. Kasterka, W. Wojnowski and J.F. Biernat *Chem. Anal.* **v41** (1996) 347
231. A. Kropidłowska, J.Chojnacki and B. Becker *Polyhedron* **v25, 10** (2006) 2142
232. A. Kropidłowska, J.Chojnacki and B. Becker *J. Inorg. Biochem.* **101** (2007) 578
233. A. Kropidłowska, J.Chojnacki and B. Becker *Inorg. Chim. Acta* **360** (2007) 2363
234. G. Christou and C. D. Garner *J. Chem. Soc., Dalton Trans.* (1979) 1093
235. A. Kern, C. Nather, F. Studt and F. Tuczek, *Inorg. Chem.* **v43** (2004) 5003
236. A. Pladzyk and K. Baranowska *Acta Crystallogr. Sect. E: Struct. Rep. Online* **v62** (2006) 2602
237. A. Dolega, K. Baranowska, J. Gajda, S. Kazmierski and M. J. Potrzebowski *Inorg. Chim. Acta ,* **v360** (2007) 2973
238. B.Becker, W.Wojnowski, K.Peters, E.-M.Peters, H.G.Von Schnering *Polyhedron,* **v11** (1992) 613
239. A.Kropidlowska, I.Turowska-Tyrk, B.Becker *Acta Crystallogr. ,Sect. E: Struct. Rep. Online* ,**62** (2006) m3407
240. L. Aparici Plaza, K. Baranowska and B. Becker *Acta Cryst. Sect E: Struct Reports Online* **v63** (2007) 1537
241. L. Aparici Plaza, K. Baranowska and B. Becker *Acta Cryst. Sect E: Struct Reports Online* **v62** (2006) 2077
242. K. Robinson, G. V. Gibbs and P. H. Ribbe *Science* **v172** (1971) 567
243. M. E. Fleet *Miner. Mag.* **v40** (1976) 531
244. B. Moubaraki, B. A. Leita, G. J. Halder, S. R. Batten, P. Jensen, J. P. Smith, J. D. Cashion, C. J. Kepert, J. F. Létard and K. S. Murray *Dalton Trans.* **(**2007) 4413
245. P. Guionneau, M. Marchivie, G. Bravic, J. F. Létard and D. Chasseau, *Top. Curr. Chem.* **v234** (2004) 97
246. E. M. Makovicky and T. Balić-Žunić *Acta Cryst. Sect. B: Struct. Sci.* **v54** (1998) 766
247. I. D. Brown *Acta Cryst. Sect. B: Struct. Sci.* **v62** (2006) 692

248. E. Lalik *J. Appl. Cryst.* **v38** (2005) 152
249. K. D. Colins, "Cayley-Menger Determinant." From *MathWorld*--A Wolfram Web Resource, created by E. W. Weisstein http://mathworld.wolfram.com/Cayley-MengerDeterminant.html
250. F. Jackson and E. W. Weisstein "Tetrahedron." From *MathWorld*--A Wolfram Web Resource. http://mathworld.wolfram.com/Tetrahedron.html
251. www.scilab.org Copyright © 1989-2007. INRIA ENPC. Scilab is a trademark of INRIA.
252. E. W. Weisstein "Octahedron." From *MathWorld*--A Wolfram Web Resource. http://mathworld.wolfram.com/Octahedron.html
253. E. W. Weisstein "Dipyramid." From *MathWorld*--A Wolfram Web Resource. http://mathworld.wolfram.com/Dipyramid.html
254. E. W. Weisstein "Triangular Dipyramid." From *MathWorld*--A Wolfram Web Resource. http://mathworld.wolfram.com/TriangularDipyramid.html
255. E. W. Weisstein "Variance." From *MathWorld*--A Wolfram Web Resource. http://mathworld.wolfram.com/Variance.html
256. A. Chavez, L. Que Jr. and W. B. Tolman, *Chem. Commun.* (2001) 111
257. S. E. McMullen and K. S. Hagen *Acta Crystallogr. Sect.C:Cryst.Struct.Commun.* **v58** (2002) 48
258. H. Oshio, E. Ino, T. Ito and Y. Maeda *Bull. Chem. Soc. Jpn.* **v68** (1995) 889
259. H. K. Lee, B. S. Luo, T. C. W. Mak and W. P. Leung *J. Organomet. Chem.* **v489** (1995) 71
260. F. Preuss, M. Steidel and R. Exner *Z. Naturforsch., B: Chem. Sci.* **v45** (1990) 1618
261. A. Kropidlowska, J. Chojnacki, J. Golaszewska and B. Becker *Acta Crystallogr., Sect. E: Struct. Rep. Online* **v62** (2006) 2260
262. A. Ciborska, K. Baranowska, W. Wojnowski (2007) *Acta Crystallogr., Sect. E: Struct. Rep.Online* ,**v63,**m1239
263. A. Ciborska, K. Baranowska, W. Wojnowski (2007) *Acta Crystallogr., Sect.E: Struct. Rep. Online*, **v63,** m2972
264. A. Dolega, M. Wieczerzak and K. Baranowska *Acta Crystallogr. Sect.E: Struct. Rep.Online* **v63** (2007) 1774
265. A. Dolega, A. Konitz, E. Baum and W. Wojnowski *Acta Crystallogr. Sect.E: Struct. Rep. Online* **v61** (2005) 2582
266. S. Friedle, D. V. Partyka, M. V. Bennett and R. H. Holm *Inorg.Chim.Acta* **v359** (2006) 1427
267. A. Dolega, J. Chojnacki, A. Konitz, W. Komuda and W. Wojnowski *Acta Crystallogr.,Sect.E:Struct.Rep. Online* **v62** (2006) 636
268. M. W. DeGroot and J. F. Corrigan *Organometallics* **v24** (2005) 3378
269. M. G. Kanatzidis, D. Coucouvanis, A. Simopoulos, A. Kostikas, and V. Papaefthymiou *J. Am. Chem. Soc.* **107** (1985) 4925
270. N. Ueyama, Y. Yamada, T. Okamura, S. Kimura, and A. Nakamura *Inorg. Chem.* 35 (1996) 6473
271. Chaoyin Zhou, James W. Raebiger, Brent M. Segal, R.H. Holm *Inorganica Chimica Acta* **300–302** (2000) 892–902
272. Weisstein, Eric W. "Stella Octangula." From *MathWorld*--A Wolfram Web Resource. http://mathworld.wolfram.com/StellaOctangula.html
273. M. J. Carney, G. C. Papaefthymiou, K. Spartalian, R. B. Frankel, and Richard H. Holm *J. Am. Chem. Soc.*, v**110** (1988) 6084

274. J. A. Fee, J. M. Castagnetto, D. A. Case, L. Noodleman, C. D. Stout, R. A. Torres *J. Biol. Inorg. Chem.* **8** (2003) 519
275. Weisstein, Eric W. "Hammer-Aitoff Equal-Area Projection." From MathWorld--A Wolfram Web Resource. http://mathworld.wolfram.com/Hammer-AitoffEqual-AreaProjection.html
276. G. Carver, P. L. W. Tregenna-Piggott, A.-L. Barra, A. Neels, and J. A. Stride *Inorganic Chemistry*, Vol. 42, No. 18, (2003) 5771
277. J. A. García-Vázquez, J. Romero, A. Sousa-Pedrares, A. Sousa, A. D. Garnovskii, and D. A. Garnovskii *J. of Chem. Crys.*, **v30, 1** (2000) 23
278. D. S. Marlin, M. M. Olmstead, and P. K. Mascharak *Inorganic Chemistry*, **v42, 5** (2003) 1681
279. D. S. Jacob, V. Kahlenberg, K. Wurst, L. A. Solovyov, I. Felner, L. Shimon, H. E. Gottlieb, and A. Gedanken *Eur. J. Inorg. Chem.* (2005) 522
280. F.-F. Jian, Q.-X. Wang, P.-P. Sun, K. Jiao *Wuji Huaxue Xueba (Chin. J. Inorg. Chem.)* **20** (2004) 581
281. F.-F. Jian, Y.-P. Tong, H.-L. Xiao, Q.-X. Wang, K. Jiao *Jiegou Huaxue (Chin. J. Struct Chem.)* **23** (2004) 979
282. A. Marzotto, A. Bianchi, G. Valle and D. A. Clemente *Acta Cryst.* **C45** (1989) 582
283. W.-H. Wang, X.-Y. Su, Z.-H. Mao, J.-S. You, and R.-G. Xie *Acta Cryst.* **E62** (2006) m445
284. M. J. Clarke, V. M. Bailey, P. E. Doan, C. D. Hiller, K. J. LaChance-Galang, H. Daghlian, S. Mandal, C. M. Bastos, and D. Lang *Inorg. Chem.* **35** (1996) 4896
285. T. Fujiwara, E. Iwamoto and Y. Yamamoto *Inorg. Chem.* **v23** (1984) 115
286. L. Johansson, M. Molund and A. Oskarsson *Inorg. Chim. Acta*, **v31** (1978) 117
287. G. M. Sheldrick *Acta Crystallogr. Sect. A: Found. Crystallogr.* **v64** (2008) 112
288. L. J. Farrugia *J. Appl. Cryst* **30** (1997) 565
289. C. F. Macrae, P. R. Edgington, P. McCabe, E. Pidcock, G. P. Shields, R. Taylor, M. Towler and J. van de Streek *J. Appl. Cryst.* 39 (2006) 453
290. L. J. Farrugia *J. Appl. Cryst.* 32 (1999) 837